The role of hydraulic strategies in understanding the response of fynbos to drought

by

Robert Paul Skelton

Thesis Presented for the Degree of

DOCTOR OF PHILOSOPHY

in the Department of Biological Sciences

UNIVERSITY OF CAPE TOWN

August 2014

Abstract

This dissertation is an investigation into the relevance of the hydraulic framework (*sensu* McDowell et al., 2008) in understanding the response of diverse communities to drought. This framework distinguishes species that respond to dehydration by rapidly decreasing stomatal conductance (g_s) (isohydric), thereby maintaining relatively constant midday minimum water potential, from those that maintain relatively high g_s (anisohydric), thereby maintaining carbon assimilation albeit at the cost of hydraulic dysfunction. However, currently, the importance of the hydraulic framework in explaining drought response in diverse communities is poorly understood. Drought-related plant mortality is of particular concern in South Africa's fynbos biome, a global biodiversity hotspot. This Mediterranean-type region is predicted to experience an increase in drought, with unknown consequences for the endemic flora. We asked whether drought affected this diverse ecosystem in a predictable manner and if these patterns fit with existing frameworks of plant drought-mortality mechanisms.

To answer these questions, we conducted several related studies investigating the hydraulic strategies of diverse fynbos functional types. The first was a long-term field study aimed at quantifying environmental variability and the physiological response of three co-occurring species representing three diverse functional types. The species were *Protea repens* (L.) L. (Proteaceae), a large, deep-rooted overstory shrub, *Erica monsoniana* L.f. (Ericaceae), a small, shallow-rooted shrub and *Cannomois congesta* Mast. (Restionaceae), a reed-like graminoid. We measured key functional traits, including water potential, vulnerability to cavitation, gas exchange and sapflow to examine the response of these species to naturally occurring seasonal drought. From detailed physiological investigations of diverse fynbos species, we were able to report highly contrasting hydraulic regulation strategies. Our second investigation was a novel trait-based framework for assessing the vulnerability of species to drought. We used the concept of safety margins to develop new measures of carbon limitation and hydraulic failure. We used the difference between the water potential at stomatal closure (P_{g12}) and the minimum seasonal water potential as a proxy for carbon limitation, and that between the water potential at 50% loss of conductivity in the stem and P_{g12} as a proxy for stomatal limitation of cavitation. Finally, we incorporated novel modifications into a soil-plant-atmosphere continuum model to simulate transpiration and

water potential and used this to predict the response of fynbos functional types to drought events.

There was strong agreement between our long-term field-based measurements and both the trait framework and the model. Ericoid response was consistent with anisohydric regulation, while proteoid response was consistent with isohydric regulation. Proteoids appear to avoid hydraulic failure and carbon limitation by maintaining relatively high minimum seasonal water potential (P_{min}). Ericoid species varied in vulnerability and seasonal percentage loss of conductivity, resulting in two distinct predictions of mortality within this functional type. The restioid response was poorly captured by the current hydraulic framework. Surprisingly, predawn water potential of *C. congesta* remained relatively high, despite a lack of stomatal closure and shallow rooting. We provide evidence that this species experiences large losses of conductivity, but refills conduits regularly by taking up rainfall or atmospheric cloud moisture and dew. This result was consistent with our analysis of functional traits and showed that shallow-rooted restioids have a combination of high vulnerability to embolism, low P_{g12} and low P_{min} that makes them vulnerable to hydraulic failure. Our model also described the transpiration and water potential of *C. congesta* accurately when dew was included.

In combination, our results highlight that the hydraulic framework is highly relevant in understanding the response of fynbos to drought. Our detailed physiological investigation and model simulations allow us to describe contrasting hydraulic strategies and make predictions about the future response of fynbos communities to drought.

Acknowledgements

First and foremost I would like to thank my primary advisor, Dr. Adam West. I have benefitted tremendously from his guidance and without his input this dissertation would not have been possible. He has been an excellent mentor and patient teacher throughout my journey. I would like to thank him for stimulating my thoughts, piquing my interest in plant physiology and prodding me in the right direction when I needed it most or when I veered off track. I look forward to many shared collaborations in the future.

Secondly, I would like to thank the many other academic contributors to my thesis. These people have assisted and taught and prodded and pushed me. Professor Todd Dawson from the University of California at Berkeley deserves special mention. I learnt and was inspired from several interactions with him during the past few years. I have also benefitted tremendously from interacting with various people from the University of Cape Town Biological Sciences Department.

I was fortunate to receive funding from the South African Environmental Observation Network Fynbos Node. Nicky Allsopp was instrumental in this and for this I am grateful. I also received funding from the University of Cape Town.

My family has been incredible throughout my life's journey. Dad and Mom, throughout my time at UCT, you've been remarkably supportive and encouraging. Thanks for all the sacrifices on my behalf and for allowing me to pursue an interest in science. Thanks for always putting education first in my life. I appreciate that you've had to make many personal sacrifices in aid of my journey and for this I am forever indebted to you. You embrace my lunacy with an open ear, an open heart and an open mind and for this I love you with all my heart. You inspire me to do more than I think I can and you are my pillars of strength. I love and respect you both.

My siblings have always been an inspiration to me. They stimulated and pushed and supported me. John and Bridge and Sarah and Dale, I look forward to sharing many more happy moments together in the future.

The hardest tasks are made easier when you have the support of great friends. I am indebted to many people for support and guidance and friendship. Saul Nachman deserves particular

mention for providing me with tremendous proofing advice. His keen eye for detail added a tremendous amount to the dissertation. All mistakes that remain are mine.

Last, but certainly not least, Julia Harris provided me with constant love and support. She displayed incredible level headedness in tumultuous times and stuck by me even when I neglected her to work on my thesis late into the night. She made those tough times bearable. To be friends with the one you love is truly special and I hope this continues for many years. Now we can finally open that bottle of champagne that's been sitting in our fridge for the past few months!

Table of contents

Chapter One: Introduction

Protracted periods of soil or atmospheric water deficit are characteristic features of arid and semi-arid ecosystems. In these regions, water limitation places a major constraint on primary productivity and, if severe enough, may cause plant mortality (Austin *et al.*, 2004; Sevanto *et al.*, 2013). Predictions for climate change scenarios are that drought will increase in frequency and severity for large parts of the world (Hartmann, 2011; Field *et al.*, 2014) and, already, widespread drought-induced tree die-off in response to global-change-type events has been reported for woodlands in the North American south-west (Breshears *et al.*, 2005; Allen *et al.*, 2010; Choat *et al.*, 2012). These drought events are likely to have major consequences for plant community composition and landscape-level processes (Breshears *et al.*, 2005; Betts *et al.*, 2007; Adams *et al.*, 2010; Hartmann, 2011; Anderegg *et al.*, 2013). Current predictions of how plant communities may respond to drought and future climate change scenarios are frequently based on bioclimatic modelling (Midgley *et al.*, 2002) or dynamic global vegetation models (Cramer *et al.*, 2001; Scheiter & Higgins, 2009). These models usually have limited experimental support and rely on several assumptions, including exclusive climatic control of species or ecosystem distribution. They often do not allow for diverse responses to drought events and lack a mechanistic basis. Diverse communities that are regularly exposed to drought are likely to contain a great variety of drought survival strategies (West *et al.*, 2012), rendering broad generalisations inappropriate and even potentially misleading (Hoffman *et al.*, 2009). To more accurately predict changes in arid and semi-arid ecosystems it is necessary to attain an improved understanding of the mechanisms underlying the diversity of plant response during drought events.

A framework for describing plant water-regulation strategies and making predictions as to how such strategies are likely to impact plant survival under drought conditions has been developed (Zimmermann, 1983; Campbell, 1985; Tyree & Sperry, 1988; Jones & Sutherland, 1991; Sperry *et al.*, 1998; Sperry, 2000; McDowell *et al.*, 2008). This hydraulic framework incorporates the physical properties of water movement through soils and plants as well as physiological differences between species (Campbell, 1985; Jones & Sutherland, 1991; Sperry *et al.*, 2002; McDowell *et al.*, 2008). Central to it is an understanding of plant-water relations and transpiration rate (E) based on Darcy's Law, which relates to the flow of a fluid in a porous medium:

$$E_w = k\,(P) \times (P_s - P_l - h\,\rho_w\,g) \qquad \text{(Eq. 1.1)}$$

where k is the hydraulic conductance of the soil-plant-atmosphere continuum as a function of water potential (P), h is the height of the water column, ρ_w is the density of water and g is the acceleration due to gravity (Campbell, 1985). For as long as k remains constant, E is proportional to the water-potential gradient in the soil-plant-atmosphere continuum. However, E generates tension in the water column as water is pulled from the soil to the site of evapotranspiration. As xylem pressures fall below a critical value, known as P_e, cavitation (i.e. a phase change from liquid water to vapour) may occur (Tyree & Sperry, 1988). If water potentials continue to decline, these air bubbles can nucleate and form emboli, which reduce hydraulic conductance. Alternatively, embolism may also be caused directly by air entry into the xylem vessels, a process known as "air-seeding" (Tyree & Sperry, 1988). When E exceeds a threshold (E_{crit}) whole-plant conductance falls to zero as a result of widespread embolism at some point within the continuum. As soil moisture declines during drought events, hydraulic failure occurs at progressively lower values of E (Sperry *et al.*, 1998).

The physiological and morphological response of plants to drought varies between species and takes place over multiple timescales. Long-term responses, covering periods of months to years, include adjustments to reduce water loss and demand, increase water absorption or decrease the vulnerability to cavitation (Chaves *et al.*, 2003). Examples of these processes include reductions in growth and flowering (West *et al.*, 2012), downregulation of metabolic demand (Chaves *et al.*, 2002), leaf shedding (Tyree *et al.*, 1993), increases in the root- to shoot-area ratio (Ewers *et al.*, 2000) and production of vessels with increased resistance to cavitation (Maherali *et al.*, 2004). Over relatively short periods, such as days to months, species may perform physiological adjustments that result in similar homeostatic effects. The primary short-term adjustment in many species is to reduce stomatal conductance by closing stomata (Jones & Sutherland, 1991; Blackman *et al.*, 2009), but species vary in their sensitivity and degree of closure. In this regard, species adopt a strategy along a continuum between two extreme hydraulic regulation strategies: isohydry and anisohydry. Isohydric species are defined as those that close their stomata rapidly in response to drought and, consequently, maintain relatively high water potentials (Jones & Sutherland, 1991; McDowell *et al.*, 2008). Anisohydric species continue to display relatively high stomatal conductance with the onset of drought and hence experience declining water potentials (McDowell *et al.*, 2008). Isohydric species ensure relatively large safety margins between realised E and E_{crit} and thus avoid dramatic loss of hydraulic conductivity (McDowell *et al.*, 2008). This is in contrast to anisohydric species, which function with much lower safety

margins between E and E_{crit}. The benefit of such a strategy is continued carbon assimilation during periods of relatively mild drought, whereas isohydric species tend to rely more on stored carbohydrate reserves (Mitchell *et al.*, 2012; Sevanto *et al.*, 2013).

Importantly, diverse hydraulic strategies have strong implications for the predicted mechanism and timing of species death during drought (McDowell, 2011; Sevanto *et al.*, 2013). Isohydric species are less prone to hydraulic failure during drought events compared to anisohydric species (Sevanto *et al.*, 2013). However, during protracted drought events isohydric species experience sustained negative carbon balance and eventually may die from carbon starvation (McDowell, 2011; Sevanto *et al.*, 2013). Although carbon starvation is expected to be a slow process during any single drought event, depletion of carbon reserves over several drought periods may reduce a species' ability to recover and ultimately survive (Breshears *et al.*, 2009). Carbon limitation may also reduce a species' ability to defend against insect or pathogen infestation, producing a further avenue for mortality in isohydric species (Plaut *et al.*, 2012). In contrast, anisohydric species are able to acquire carbon further into drought events and are predicted to survive longer during relatively lengthy, mild drought events (Sevanto *et al.*, 2013). Mortality in these species has been shown to occur more rapidly during short, severe drought events through hydraulic failure (Mitchell *et al.*, 2012). Notably, these diverse mechanisms of mortality exemplify the importance of acquiring detailed physiological knowledge if we are to accurately predict future impacts of drought on community composition.

The primary example of where different hydraulic strategies lead to distinct patterns of mortality during a severe drought event is that of the piñon-juniper woodlands in the south-western United States (Breshears *et al.*, 2005, 2009; West *et al.*, 2007b, 2008). Here, widespread mortality of an isohydric species *Pinus edulis* resulted from sustained periods of carbon deficit, while a sympatric anisohydric species *Juniperus monosperma* largely survived (Breshears *et al.*, 2005, 2009; West *et al.*, 2007b). Globally, mortality events in a range of communities have also been shown to be consistent with this hydraulic framework (Brodribb & Cochard, 2009; Allen *et al.*, 2010; Anderegg *et al.*, 2012b, 2013; West *et al.*, 2012; Mitchell *et al.*, 2012; Zeppel *et al.*, 2013). However, there remains an urgent need to extend our understanding of the role of hydraulic strategies in determining community dynamics in biomes outside of North America and the Mediterranean basin. In particular, the importance of the hydraulic framework in highly diverse communities where trees are not the dominant

functional type deserves greater attention. The overwhelming majority of studies to date have documented the hydraulic strategies of woody tree species and the implications for mortality in tropical or temperate forest biomes (Allen *et al.*, 2010). Yet high functional diversity is likely to produce complex drought responses and have major implications for community composition. Very few studies have investigated how diverse functional types are affected during drought, despite the importance of diversity for ecosystem functionality (Díaz & Cabido, 2001).

The Cape Floristic Region (CFR) of Southern Africa, a global biodiversity hotspot, is of particular concern (Fig. 1.1). This Mediterranean-type region of *c*.90 000 km^2 contains approximately 8700 plant species of which over 68% are endemic (Linder, 2003). Current climate change models predict an increase in mean annual temperatures for the entire region and a decrease in mean annual rainfall in the western part (De Wit & Stankiewicz, 2006; Hewitson & Crane, 2006; Lumsden *et al.*, 2009; Field *et al.*, 2014). These conditions are likely to exacerbate the severity of current summer drought periods and could induce widespread mortality. Indeed, several studies from southern African biomes have documented shifts in community composition in response to recent severe drought events (Milton *et al.*, 1995; Midgley *et al.*, 2005; Foden *et al.*, 2007; Hoffman *et al.*, 2009). However, our ability to predict how mountain fynbos, a locally dominant and highly diverse vegetation type, is likely to respond is severely hampered by our limited knowledge of how diverse functional types are affected by drought (Hannah *et al.*, 2005). Predictions based on climatic-niche modelling are mostly restricted to the relatively large overstory shrubs of the Proteaceae family (Midgley *et al.*, 2002; Midgley & Thuiller, 2010) and overlook the substantial graminoid and ericoid components within the region. These three major groups have highly divergent functional traits, such as rooting depth (Higgins *et al.*, 1987), leaf size (Yates *et al.*, 2010b) and stem vulnerability to cavitation (Jacobsen *et al.*, 2009; Pratt *et al.*, 2012), making it probable that they will respond to drought in a complex manner. Detailed physiological examinations of the variety of drought responses in mountain fynbos communities are rare. Although several studies have investigated the physiological response to seasonal drought (Miller *et al.*, 1983; von Willert *et al.*, 1989; Herppich *et al.*, 1994), these were mostly of low temporal resolution and lacked a predictive framework in which to interpret their results. West et al. (2012) was the first study from the CFR to interpret its findings in terms of the hydraulic framework. Importantly, this study demonstrated that, while mountain fynbos species could be categorised as being typically anisohydric or

isohydric, there was considerable variation in the response to drought within these groups and even within families (West *et al.*, 2012). This finding underlines the importance of a more detailed understanding of diverse responses if the scientific community is to more accurately predict community responses in the future. In particular, predictions of how communities are likely to respond will benefit from (a) a better knowledge of the range of physiological responses present in a community, (b) an understanding of the major environmental drivers of plant response and (c) the identification of common response pathways determined by associations between traits and physiological responses.

The general objective of this dissertation is to further examine the importance of hydraulic strategies in determining the response to drought of highly speciose communities. I aim to build upon previous studies by asking whether functional traits of diverse species combine in a predictable manner with hydraulic strategies so as to produce predictions of drought mortality that fit within the existing framework. This knowledge will enable us to produce an improved mechanism-based understanding of the vulnerability of different fynbos species to drought events and will provide considerable insight into the role of the hydraulic framework in complex communities. Chapters Two and Three aim to explore variation in hydraulic strategies present in the CFR. Broadly, this is achieved by quantifying the detailed physiological responses to major environmental drivers of three main functional types over several successive years. Chapter Two describes methodological advances in the use of miniature external heat-ratio-method (HRM) sapflow gauges on fynbos species. It was necessary to establish that these gauges were suitable for quantifying transpiration of highly diverse functional types with varied stem morphologies. Significantly, novel findings in Chapter Two demonstrate that it was possible to capture almost continuous sapflow measurements from Restionaceae species. Continuous measurements offer the potential for detection of the dependence of species on varying or transient water sources. This is particularly relevant in highly pulsed environments, such as the CFR, where periodic campaign measurements might inadequately capture response to ephemeral events. Chapter Three aims to identify divergent physiological responses to summer drought periods and the traits that predisposed species to those strategies. Previous studies in the region have shown species to vary in influential functional traits pertinent to drought response, such as vulnerability to cavitation and rooting depth (Higgins *et al.*, 1987; Jacobsen *et al.*, 2007, 2009). However, examining these traits in isolation is not particularly useful. To understand whole-plant response to drought it is important to examine the interactions between

functional traits and physiological responses. Specific hypotheses that were tested in this chapter include that deeper-rooted, isohydric species will be more sensitive to atmospheric vapour pressure deficits compared to shallow-rooted anisohydric species. Instead, the latter are more likely to respond to changes in soil moisture and rely on either being resistant to cavitation or refilling after rainfall events. These hypotheses were tested by monitoring detailed physiological responses of diverse species from different functional types over three summers and by quantifying several important hydraulic traits in a laboratory setting. Species of the CFR display a remarkable range of solutions to the problem of long, hot and dry summers posed by a Mediterranean-type climate (Specht & Moll, 1983; Yates *et al.*, 2010b; Skelton *et al.*, 2012; Pratt *et al.*, 2012). This presents the challenge of trying to establish general but accurate predictions. A primary goal of Chapter Four is to identify potential outcomes determined by associations between traits and physiological responses. The objective of our study as detailed in Chapter Four was to develop a predictive framework based on associations between key functional traits that would enable more rapid, yet reliable, assessment of the vulnerability of diverse species. To further extend our predictive ability, Chapter Five provides results from a model developed to simulate drought events and the physiological response of diverse species. The model was developed using soil properties and diverse plant physiological responses and then parameterised using field data. The results detailed in this chapter enabled us to make predictions about the likely effect of different drought events on species with different combinations of functional traits and hydraulic strategies. In addition to providing testable hypotheses about trait combinations and pathways to mortality, our study was also explicitly designed to provide predictions of how long different species could persist under a variety of drought conditions. Finally, Chapter Six is a synthesis of the results from the four data chapters.

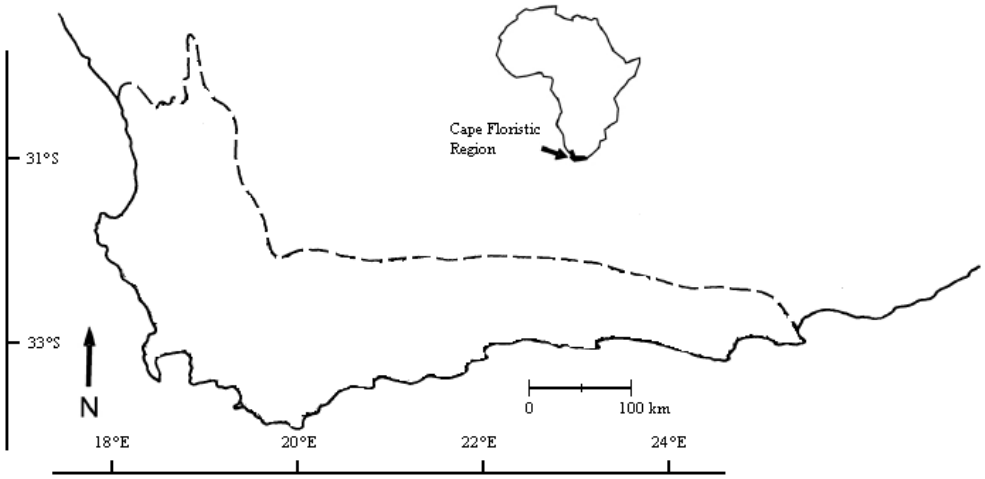

Figure 1.1: Map showing the extent of the CFR (dotted line) on the extreme south-western corner of Africa (inset).

Chapter Two: External heat pulse method allows comparative sapflow measurements in diverse functional types in a Mediterranean-type shrubland in South Africa

Functional Plant Biology (2013) **40**: 1076–1087.

Skelton, R.P.;[1] West, A.G.;[1] Dawson, T.E.[2] and Leonard, J.M.[1]

[1] University of Cape Town – Department of Biological Sciences, HW Pearson Building Upper Campus, Cape Town, Western Cape 7700, South Africa.

[2] University of California Berkeley – Department of Integrative Biology, 3060 Valley Life Sciences Building, Berkeley, CA 94720, USA.

Abstract

There has been limited application of sapflow technology to small-stemmed species and across co-existing functional types, restricting its use in diverse floras such as the Mediterranean-type shrubland in South Africa. Our main objective was to test whether sapflow may provide an alternative to traditional gas-exchange measurements, which would permit comparative evaluation of transpiration at a previously unattained temporal resolution. We tested miniature external heat-ratio-method (HRM) sapflow gauges on three co-occurring functional types with contrasting stem or culm anatomies and examined the relationship between sapflow and shoot- and leaf-level water loss in both a controlled and field environment. Our sapflow gauges captured dynamic patterns of transpiration in both settings for all three functional types. In a controlled environment, the relationship between sapflow and transpiration was linear in all three species with r^2 values ranging from 0.78 for *Cannomois congesta* Mast. (Restionaceae) to 0.96 for *Protea repens* (L.) L. (Proteaceae) and *Erica monsoniana* L.f. (Ericaceae). In the field, r^2 values were lower, ranging from 0.59 for *C. congesta* to 0.74 for *P. repens*. We discuss the efficacy and potential of this methodology to cast light on patterns of community ecology in functionally diverse shrublands by capturing continuous variation in transpiration.

Introduction

Understanding plant response to rapidly changing environmental conditions is critical for exploring community dynamics and assessing the vulnerability of communities to projected climate change (Breshears *et al.*, 2005; McDowell *et al.*, 2008; Hoffman *et al.*, 2009). Quantifying plant response to changing climatic variables requires that we have appropriate measurement tools that can be scaled to the question of interest. While traditional sapflow methodologies have proven capable of documenting high-resolution responses of trees to environmental conditions over extended time periods (Burgess *et al.*, 2000, 2001), there has been less success in achieving this for small-stemmed species and across co-existing species of varied morphology (e.g. trees, shrubs and graminoids). This has limited our ability to collect the high-temporal-resolution data on co-existing species' responses to environmental drivers necessary for evaluating the response of complex communities to climate change. This is particularly important for regions supporting exceptionally high levels of species diversity and endemism. Fynbos, the Mediterranean-type flora of South Africa's Cape Floristic Region (CFR), is a prime example of a highly speciose flora with co-existing diverse functional types. Over 8,500 species are contained within a region of *c*. 90,000 km^2 and it is one of the few global biodiversity hotspots outside the tropics. A large proportion of the exceptional species diversity can be captured by three main functional groups: the proteoid, ericoid and restioid functional types (Cowling *et al.*, 1996; Linder, 2003). Proteoids are typically large, broad-leaved overstorey shrubs. Ericoids are small-to medium-sized, fine-leaved sclerophyllous shrubs with thin (< 10 mm) stems. The largest genus of this functional type and the largest in the CFR is *Erica*, which contains over 600 endemic species. The Restionaceae is a family of over 400 reed-like, monocotyledonous species with long photosynthetic culms, typically less than 5 mm in diameter. Recent work has shown that these functional types have remarkably different hydraulic strategies which significantly impact their abilities to cope with drought and potential climate change (West *et al.*, 2012). In addition to being an area of exceptional floral diversity, the CFR is also threatened by future climate change (Midgley *et al.*, 2002; Hoffman *et al.*, 2009). Predictions are that the region will experience more concentrated rainfall events in winter, but drier summer periods (Lumsden *et al.*, 2009). To better understand the potential impact of climate change on this diversity, it is imperative to provide more detailed knowledge of plant response to environmental drivers.

Sapflow systems have been widely used to study plant-water relations and may prove to be invaluable tools for providing the required detailed physiological knowledge (Ewers & Oren, 2000; Zeppel *et al.*, 2008; Vandegehuchte & Steppe, 2012a,b). Sapflow studies afford several advantages over traditional methods of measuring transpiration, such as porometric or gravimetric methods. Sensors placed on or in the stem can be used to investigate water movement without disrupting leaf microclimates. Modern data-logging equipment allows sapflow to be assessed at frequent intervals and over long periods. Continuous datasets afford the capacity to significantly enhance our understanding of the dynamics of plant response to rapidly changing environmental factors (Oren *et al.*, 1999; Ewers & Oren, 2000). However, there are a number of challenges to applying sapflow gauges to co-existing diverse functional types. The majority of sapflow studies have been done on large woody species (Wullschleger *et al.*, 1998), due mostly to practical difficulties inherent in working with small stems. Ensuring proper thermal contact between sensors and xylem tissue is difficult and low flow rates (often encountered in small stemmed individuals) makes estimations of sapflow prone to inaccuracies (Marshall, 1958). Monocotyledonous stems or culms provide further and unique challenges. The presence of isolated and irregularly spaced vascular bundles may lead to variation in sap flux between sensors placed in different areas (Madurapperuma *et al.*, 2009). If sapflow sensors are placed in close proximity to large conduits, it may provide an overestimation of whole-plant sap flux. Alternatively, if sensors are placed in areas with few conduits, convective heat flux must be detected through non-conducting tissue and this may result in an underestimate of whole-plant transpiration. Despite this, several studies have shown that current sapflow methods can provide accurate estimates of whole-plant transpiration in large-stemmed monocotyledonous species, including moso bamboo (*Phyllostachys pubescens*) (Kume *et al.*, 2010), cocos palms (*Syagrus romanzoffiana*) (Madurapperuma *et al.*, 2009) and corn (*Zea mays*) (Cohen & Li, 1996). Since these are all relatively large species, needle probes could be used. However, probes are unsuitable for smaller-stemmed species. To our knowledge, external sapflow sensors have not yet been used on small-stemmed monocotyledonous species. The ability to obtain long-term field measurements of sapflow in small-stature species with highly contrasting stem morphologies would greatly advance our ability to understand the key drivers of plant response. Significant advances have recently been made in heat-pulse techniques which allow measurement of low and reverse flow rates in a range of stem sizes (Burgess *et al.*, 2001; Clearwater *et al.*, 2009). Burgess et al. (2001) developed the HRM, which measures the ratio of the increase in temperature, following the release of a discrete pulse of heat, of two equidistant points above

and below a heater. This method is able to capture velocities ranging from approximately −54 cm h^{-1} to 54 cm h^{-1} (Burgess *et al.*, 2001), but is limited to larger stems as it requires the insertion of needles into the xylem. Recently, a modification of the HRM has been developed for small sensors placed on the outside of stems/petioles which offers the potential of obtaining long-term, accurate measures of sapflow on stems/petioles as small as 2 mm (Clearwater *et al.*, 2009). Recent work has shown this to work for both leaf petioles and flower pedicles (Roddy & Dawson, 2012). However, it has yet to be shown how well these external HRM sensors work on plants of highly contrasting whole-plant structure and stem anatomies in a field context. In this study, we addressed several key practical issues that would allow reliable deployment of such sensor systems in our research. Aspects of sensor construction, calibration and function in both a controlled and field setting were investigated. We aimed to test whether these sensors would be able to accurately approximate transpiration in diverse co-existing functional types. Specifically, we hypothesised that the external HRM sensor would be in contact with a sufficiently large area of xylem conducting tissue of a Restionaceae culm to permit measurement of sapflow and that this measure would be directly related to gravimetric transpiration. In addition, we hypothesised that the external HRM sensor would be sensitive enough to capture low flow rates in small stems of Restionaceae and Ericaceae species as well as potentially high flow rates in large-stemmed proteoids. Finally, we hypothesised that diurnal sapflow would be directly related to environmental drivers of transpiration in the three functional types. We compared estimations of sapflow measured with gauges to gravimetric measures of water loss in a controlled environment. We then compared estimations of sapflow obtained from gauges to measures of gas exchange of plants of three species *in situ*.

Methods and materials

Gauge design and setup

Sapflow gauges were constructed following the design presented by Clearwater et al. (2009) with slight modifications. A rectangular block of non-conductive silicone was used instead of cork to form the backing of the gauge, as this material has similar thermal conductivity and was readily available. The heating element was connected in series with a 120 Ω resistor to a 12 V battery via the datalogger (CR1000; Campbell Scientific Inc., Logan, Utah, USA). The two thermocouples were connected to a multiplexer (AM16/32 relay; CSI, Logan, Utah, USA), which was connected to the datalogger via thermocouple extension wire (Omega

Engineering Inc., Stamford, CT, USA). The datalogger was used to fire a heat pulse of 7 s every thirty minutes. An average of the thermocouple temperatures was recorded over approximately 5 s immediately prior to the release of the heat pulse and for the period 55 to 75 s after the heat pulse. The latter period was chosen because it covered the period of greatest stability in temperature differentials (Clearwater *et al.*, 2009) and because earlier measurements are prone to overestimating heat-pulse velocity (Burgess *et al.*, 2001). The average ratio of the temperature differentials was used to calculate heat-pulse velocity.

Sapflow theory

Clearwater-type sapflow gauges make use of the HRM (Burgess *et al.*, 2001) for estimating sap velocity. This method relies upon two thermocouples evenly spaced either side of a heating element along the same axis as the flow of sap (Burgess *et al.*, 2001). Marshall (1958) showed that for low rates of flow the ratio of the downstream temperature differential to the upstream differential provides an accurate estimation of the heat-pulse velocity:

$$v_h = k/x \ln (\delta T1/ \delta T2) \text{ in cm } s^{-1} \quad \text{(Eq. 2.1)}$$

where k is the thermal diffusivity ($cm^2\ s^{-1}$) and x is the distance above or below the heating element (cm). When there is no sapflow, the logarithm of the ratio of the two temperature differentials is zero. When sapflow occurs, the ratio is less than or greater than 1 and the direction of the flow is indicated by the sign. The thermal diffusivity can be estimated by recording the temperature profile of one of the thermocouples following a heat pulse under conditions of zero flow (Clearwater *et al.*, 2009). It is proportional to the amount of time it takes for the thermocouple to reach a maximum temperature, t_m, after a heat pulse:

$$k = x^2 / 4\ t_m \text{ in } cm^2\ s^{-1} \quad \text{(Eq. 2.2)}$$

For Clearwater-type gauges, k is a property of the gauge material and the properties of the stem it is in contact with. A significant proportion of heat is propagated through the gauge block and k varies little between individuals of a species (Clearwater *et al.*, 2009). We estimated k from equation 2.2 by installing gauges on excised stems of our three study species and recording heat pulses with no imposed xylem flow (Table 2.1). Thereafter, we assumed k was constant for a species and applied it in equation 2.1 for other individuals of the same species. Vandegehuchte and Steppe (2012a) showed recently that thermal diffusivity, k, of woody stems varies throughout a growing season, which affects calculations

of v_h. An improved estimate of k and how it varies throughout a growing season is desirable and may improve the fit between v_h and gravimetric transpiration.

Measured v_h provides an underestimation of actual sap velocity, v_s, since the heat pulse is propagated by conductive flow through non-hydroactive components of the stem and gauge material as well as by convective flow in the sap. This can be corrected through the use of an empirical multiplier (Cohen & Fuchs, 1989). Traditionally, v_s has been expressed as the product of the velocity of the heat pulse, v_h, and the ratio of lumen area to total sapwood area (Edwards *et al.*, 1996). This measure is considered inappropriate for use with external sapflow gauges since the gauge and stem may not be thermally homogenous and because of difficulties in estimating the proportion of the sapwood that is hydroactive (Clearwater *et al.*, 2009). The latter is especially true for monocotyledonous culms, where the vascular bundles are irregularly spaced throughout the ground tissue (Fig. 2.1). For practical purposes, we chose to make use of the slope of the relationship between measured heat-pulse velocity, v_h, and measured sap velocity, v_s:

$$v_s = v_h \, m_{sap} \qquad \text{(Eq. 2.3)}$$

This coefficient is considered less sensitive to error in small stems than multipliers based (Clearwater *et al.*, 2009) on estimations of the effective sapwood area (Clearwater *et al.*, 2009). This method requires that instrumented stems be destructively harvested and have a xylem flow imposed through them (Clearwater *et al.*, 2009).

Study site and species

Sapflow gauges were tested on three species from three different families located at Jonaskop in the Riviersonderend mountains of the Western Cape. Species were chosen to represent the three main functional types within the CFR and to cover a range of stem morphologies and anatomies (Fig. 2.1). *Erica monsoniana* L.f. (Ericaceae) is a small- to medium-sized, fine-leaved shrub with dense stems of up to 10 mm in diameter. *Protea repens* (L.) L. (Proteaceae) is a large, thick-stemmed, broad-leaved shrub distributed widely in the CFR. *Cannomois congesta* Mast. (Restionaceae) is a perennial species with a tufted, reed-like growth form consisting of cylindrical, photosynthetic culms of up to 1 m long and between 1 and 2 mm in diameter. On November 2011, at least ten individuals from each species were instrumented with sapflow gauges and insulated using expanding polyurethane foam wrapped in reflective roof insulation. The measurement campaign ended when instrumented branches

were destructively harvested in July 2012 for zeroing purposes. Due to breakages, we were able to obtain continuous data for this period for five *P. repens*, six *E. monsoniana* and two *C. congesta* individuals. The installation success rate over the six-month survey in the field was ~40% across all species, but was considerably lower for *C. congesta* (~20%). Meteorological variables were recorded every thirty minutes with a CR1000 datalogger at the site from November 2011 until July 2012. Solar radiation was measured using a CS300 pyranometer (CSI, Logan, Utah, USA). Temperature and humidity were measured using a HMP45C temperature and relative-humidity (RH) probe (CSI, Logan, Utah, USA). Wind speed and direction were measured with a CS03001 wind speed and direction sensor (CSI, Logan, Utah, USA). Vapour pressure deficit (VPD) was calculated using temperature (T in °C) and RH values.

Table 2.1: Summary of the parameters used to calculate heat-pulse velocity, v_h, and sapflow, v_s, for the three species used in this study. The mean time between the heat pulse and the maximum temperature rise, t_m, was used to calculate the thermal diffusivity, k, for each species using equation 2.2. The slope of the relationship between v_h and gravimetrically measured sapflow, v_s, under experimentally controlled conditions was taken as m_{sap} for each species (Eq. 2.3). Numbers in brackets indicate n for each measurement.

Species	$t_m \pm$ s.d. (s)	k ($cm^2\ s^{-1}$)	$m_{sap} \pm$ s.d.
E. monsoniana	66 ± 15 (4)	0.0015 ± 0.0001 (2)	4.05 ± 0.73 (3)
P. repens	62 ± 14 (4)	0.0016 ± 0.0000 (2)	3.68 ± 1.57 (3)
C. congesta	86 ± 2 (2)	0.0010 (1)	7.81 ± 1.82 (2)

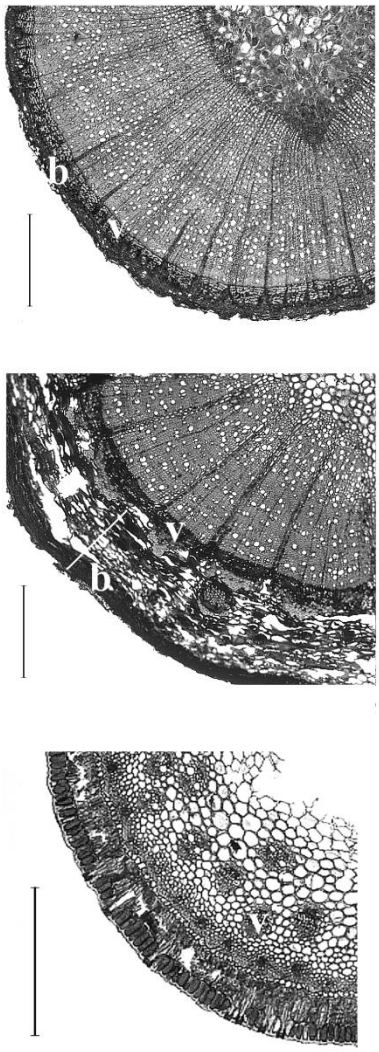

Figure 2.1: Transverse section through an *E. monsoniana* and a *P. repens* stem and a *C. congesta* culm showing the variation in morphological features between the three functional types. Letters indicate bark (b) and vascular tissue (v). Scale bar = 0.5 mm.

Comparison between sapflow measured by gauges and gravimetric method

Cut stems were collected from well-hydrated, healthy-looking field-grown individuals of the three species and transported to the laboratory in water. Stems were re-cut under water and, without being exposed to air, were then placed in a beaker and sealed to prevent evaporation. A strip of bark was removed from the *P. repens* and *E. monsoniana* individuals and the sapflow gauges were placed on the exposed area. Clearwater *et al.* (2009) showed that the presence or absence of a bark layer affected the multiplier m_{sap} and that values of m_{sap} were closer to 1 when the bark layer was removed. To prevent damage by removing the epidermal or chlorenchyma layers, *C. congesta* culms were left intact and the gauges were installed directly onto their surface. Sapflow gauges were insulated and the beakers and stems were placed in a controlled-growth chamber at the University of Cape Town for several days. Each day the lights were set to gradually switch on from 06:00, reach full intensity by 08:00 and gradually switch off between 20:00 until 21:00. The temperature was set to change between 15 °C and 25 °C during dark and light periods, respectively. The total weight of the beaker and plant material was recorded every thirty minutes for several days and from these measures sap velocity in g h^{-1}, v_s, was calculated. Gauges were set to measure velocity of the heat pulse, v_h, every thirty minutes. The slope of the relationship between v_s and v_h was taken as m_{sap} (Eq. 2.3).

Comparison between sapflow measured by gauges and gas exchange

As an independent test of the external HRM sensors, the relationship between sapflow and gas exchange of field-grown plants was investigated at Jonaskop. We reasoned that a qualitative agreement between the E and v_s curves would constitute a validation of our ability to capture fine-scale variations in environmental response with the external HRM. Sapflow gauges were installed on several individuals of the three species (see "*Study site and species*" above) and recorded v_h every thirty minutes. Heat-pulse velocities were converted to v_s using mean m_{sap} values determined for each species (Table 2.1). Full diurnal cycles of leaf-level gas exchange were measured in February 2012 using a conifer chamber (Li-Cor 6400-05 conifer chamber; Li-Cor, Lincoln, Nebraska, USA) attached to an infra-red gas analyser (IRGA) (Li-Cor 6400 IRGA; Li-Cor, Lincoln, Nebraska, USA). Leaf temperature and light intensity were not controlled and tracked ambient conditions, while RH inside the chamber was maintained slightly below ambient. Leaf-level transpiration (E) from mature, fully exposed leaves was measured every thirty minutes on a single individual of each species. These diurnal traces

were then compared to the measure of sapflow obtained from the gauges of individuals of the same species from the same day. There were two potential sources of error in this relationship. Firstly, to avoid interference with our sapflow measurements, measures of v_h and E were made on separate individuals. These individuals may have had varying responses, caused by, for example, exposure to slightly different microclimate conditions or phenotypic differences. Secondly, the measurement areas were different for the two methods. Our measure of sapflow, v_s, represented an average sap velocity per stem or culm cross-sectional area. This cross-sectional area supplied sap to a large leaf area for *P. repens* and *E. monsoniana* and an entire culm for *C. congesta* and therefore represented an average measure of flow across a relatively large leaf or culm surface area. In contrast, the gas-exchange measurements were taken from < 25 cm^2 of leaf area or 5 cm of culm length and therefore represented an average measure of water loss from a comparatively small surface area.

Data analysis

All analyses were conducted and figures made using R (R Development Core Team, 2013). Due to the relatively high amount of variation in the instantaneous v_h or meteorological measurements, we plotted smoothed lines modelled using the loess curve-smoothing function. This function builds up a smoothed modelled surface by fitting simple non-parametric models to subsets of the continuous explanatory variable (Cleveland & Devlin, 1988). We set the span to 0.2, meaning that each local fit used approximately 20% of the daily data. Total daily sapflow for all three functional groups and total daily solar radiation was calculated by integrating the area under the curves produced from modelled data using the "integrate" function in R. Daily mean VPD was calculated from half-hour values recorded during daylight hours (solar radiation > 0.01 kW m^{-2}).

Results

There were significant relationships between heat-pulse velocity, v_h, and sapflow, v_s, measured gravimetrically under experimentally controlled conditions for all three species. Although the r^2 values for *C. congesta* were the lowest recorded (0.78), they were highly significant when compared to a null model ($p < 0.0004$). The gauges were able to capture rapid, subtle variations in flow for all three functional types (Fig. 2.2). Although there was generally little noise in the traces over several days, apparent outliers were occasionally observed during periods of steep temperature gradients. Sapflow traces were most variable

during periods when the temperature in the chamber changed from 15 °C to 25 °C or vice versa (see *E. monsoniana*, Fig. 2.2b,e). We suspect that this noise was due to inadequate insulation of the gauges and recommend that special attention be paid to this in future studies. Most of the obviously erroneous datapoints could be removed with a simple algorithm designed to delete points whose absolute value was more than double that of both points immediately adjacent to them. Gravimetric water loss expressed per stem area was between 2.03 and 9.1 times greater than v_h for the three species in this study. The m_{sap} values for *P. repens* and *E. monsoniana* were similar to those reported for several other species by Clearwater et al. (2009). However, m_{sap} for *C. congesta* was approximately double the previously reported maximum value for any species, presumably caused by a dampening of the heat-pulse trace by the thick epidermal and chlorenchyma layers and central-ground tissue. The variability of m_{sap} values was relatively high for *P. repens* in comparison to the other two species (Table 2.1).

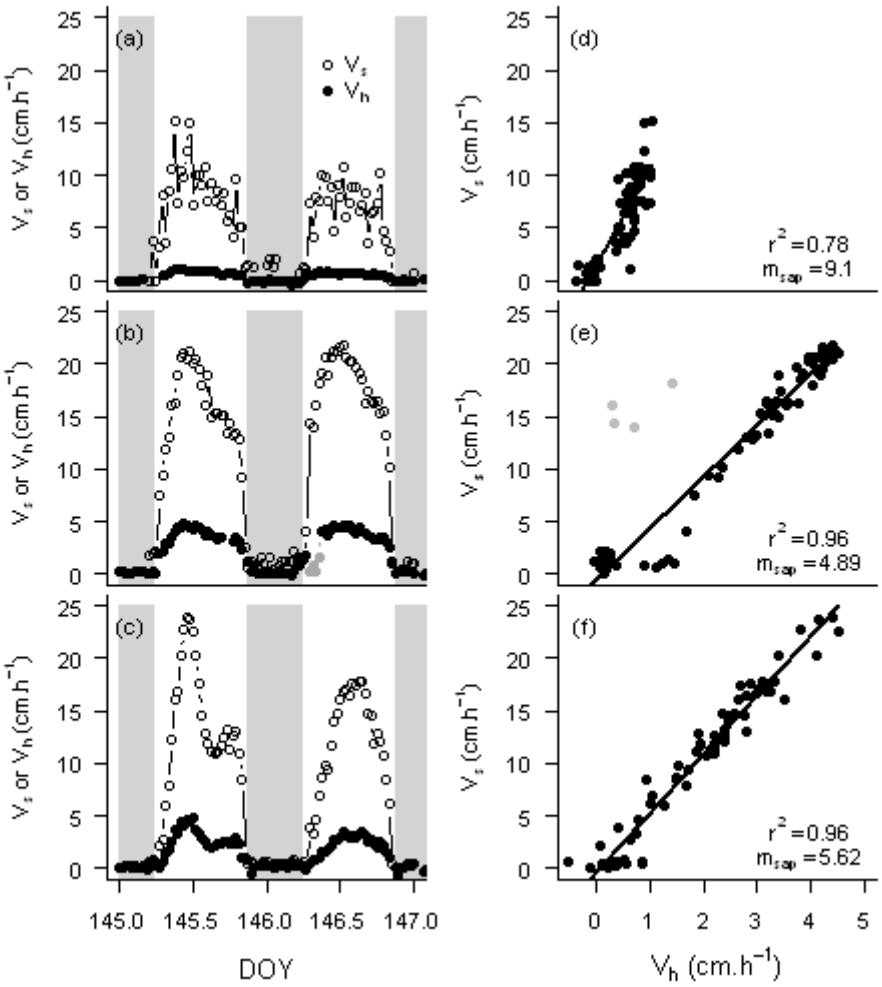

Figure 2.2: Examples of the relationship between heat velocity, v_h, and sap velocity, v_s, measured gravimetrically in a controlled environment for (a) and (d) a *C. congesta* shoot, (b) and (e) an *E. monsoniana* shoot and (c) and (f) a *P. repens* shoot. Occasional outliers were recorded by the sapflow gauges during periods of rapid temperature change, as in the *E. monsoniana* trace (grey points in (b) and (e)). These were most likely caused by insufficient thermal insulation of the gauge in that individual (see "*Discussion*" below). Shaded rectangles indicate periods of darkness.

Although sapflow gauges installed on plants in the field generated more noise compared to those installed on plants in the controlled-growth chamber, they were able to capture dynamic patterns of sapflow in the field (Fig. 2.3, 2.4 & 2.5). Traces from *C. congesta* individuals were generally slightly noisier compared to those from *E. monsoniana* and *P. repens* individuals. For all three species, sapflow responded most strongly to changes in solar radiation and VPD, exhibiting a positive linear response to both of these variables on most days (Fig. 2.3, 2.4 & 2.5). Rapid changes in wind speed caused only slight fluctuations in sapflow in all three species. Variability in total daily sapflow in all three species was caused mostly by fluctuations in total daily solar radiation and mean daily VPD (Fig. 2.6). All three species exhibited an asymptotic relationship between total daily sapflow and mean daily VPD (Fig. 2.6a,d,g). Although *P. repens* displayed the steepest response in the linear portion of the curve (at VPD = 1, m = 66.7), this was similar to that of *C. congesta* (at VPD = 1, m = 61.9). *E. monsoniana* displayed the shallowest response to increasing daily mean VPD (at VPD = 1, m = 49.9) and an earlier levelling of sapflow values compared to the other two species. Daily sapflow reached an asymptote in this species from mean daily VPD values below 2 kPa, compared to above 3 kPa for *P. repens* and *C. congesta*. None of the species exhibited a clear response to mean daily wind speed (Fig. 2.6b,e). Daily sapflow in *C. congesta* was linearly related to solar radiation, while that in *E. monsoniana* and *P. repens* was asymptotic (Fig. 2.6c,f,i).

The relationship between v_s and transpiration measured in the field was linear for all three species (Fig. 2.7), yet not as strong as that between v_h and v_s measured gravimetrically in the controlled setting. The strongest relationship between these two measures was for *P. repens* ($r^2 = 0.74$, $p < 0.004$), while the weakest was for *C. congesta* ($r^2 = 0.59$, $p < 0.004$). We considered reasonably strong linear relationships, together with the qualitative agreements in the shapes of the diurnal curves (Fig. 2.7), as support for the efficacy of our sapflow gauges at detecting rapid variations in transpiration in response to environmental drivers.

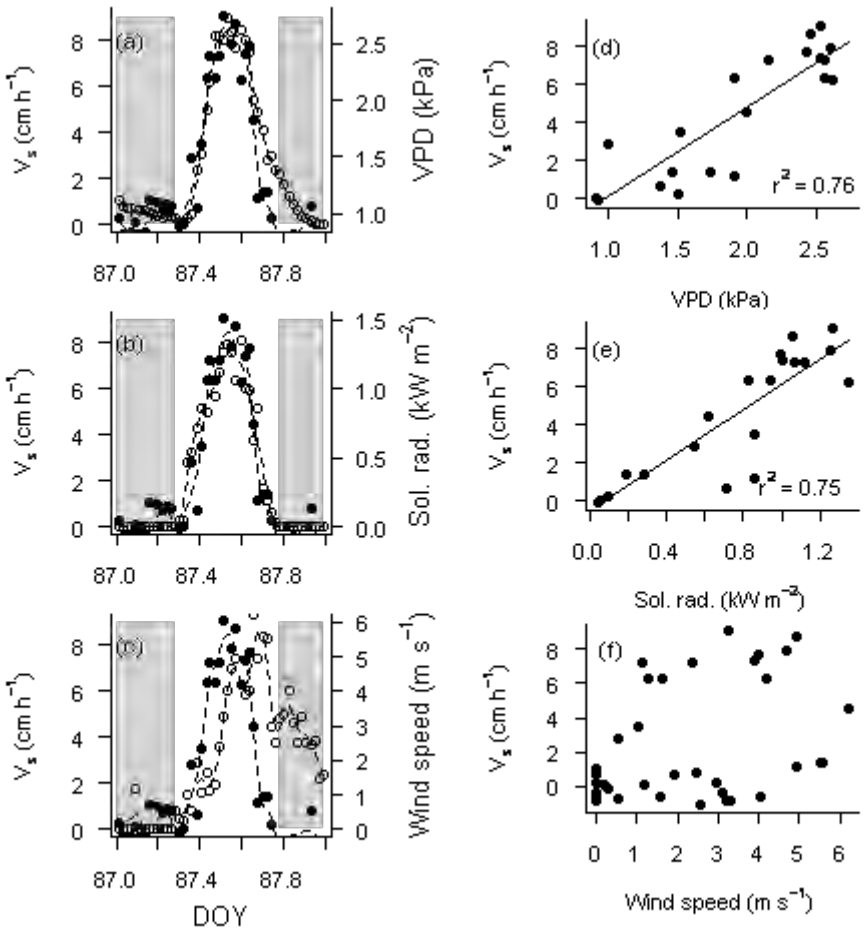

Figure 2.3: Examples of contrasting diurnal responses of sapflow measured *in situ* to changes in ((b) and (f)) VPD, ((c) and (g)) solar radiation and ((d) and (h)) wind for a *P. repens* individual on two separate days. Smoothed curves of sapflow and meteorological variables were modelled using the loess function. Shaded areas indicate periods of darkness (solar radiation < 0.01 kW m^{-2}).

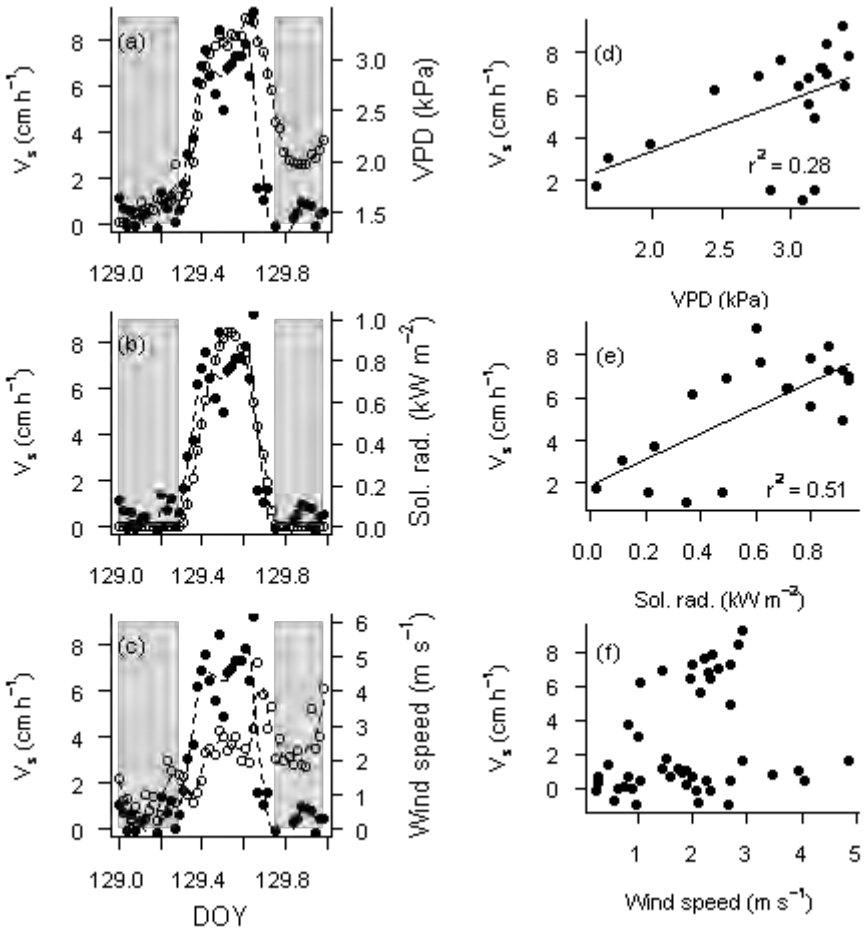

Figure 2.4: Example of *in situ* diurnal response of sapflow (closed circles) of an *E. monsoniana* individual to changes in ((a) and (d)) VPD, ((b) and (e)) solar radiation and ((c) and (f)) wind speed (open circles). Smoothed curves of sapflow and meteorological variables were modelled using the loess function. Shaded areas indicate periods of darkness (solar radiation < 0.01 kW m^{-2}).

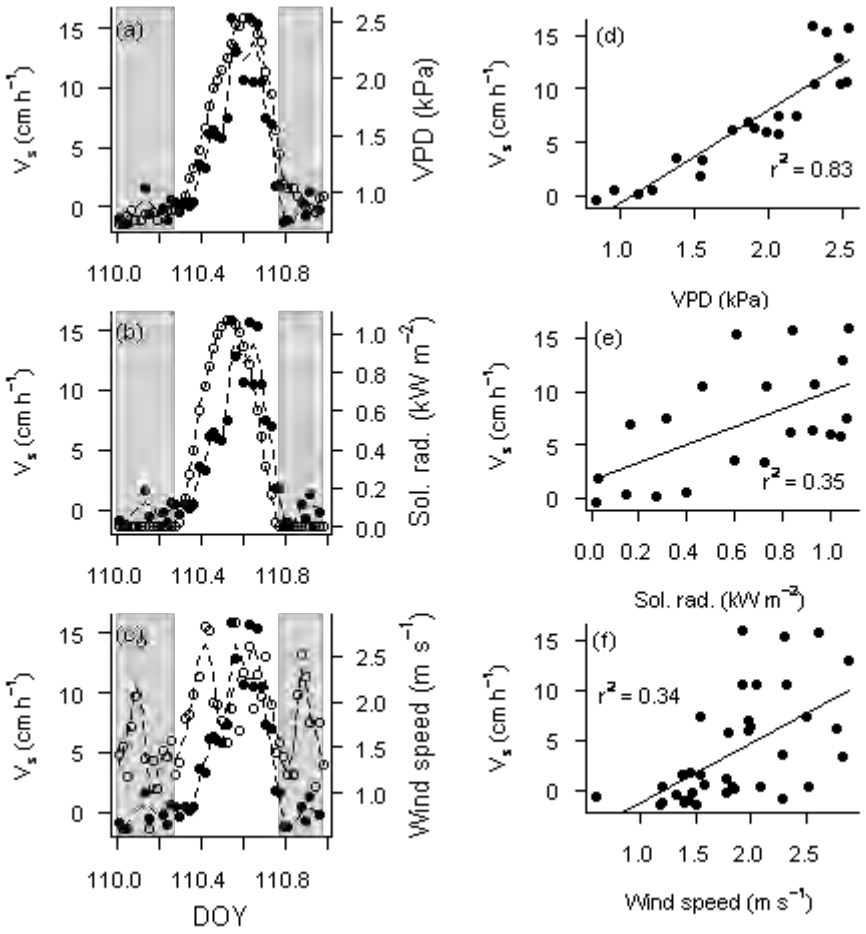

Figure 2.5: Example of *in situ* diurnal response of sapflow (closed circles) of a *C. congesta* individual to changes in ((a) and (d)) VPD, ((b) and (e)) solar radiation and ((c) and (f)) wind speed (open circles). Smoothed curves of sapflow and meteorological variables were modelled using the loess function. Shaded areas indicate periods of darkness (solar radiation < 0.01 kW m^{-2}).

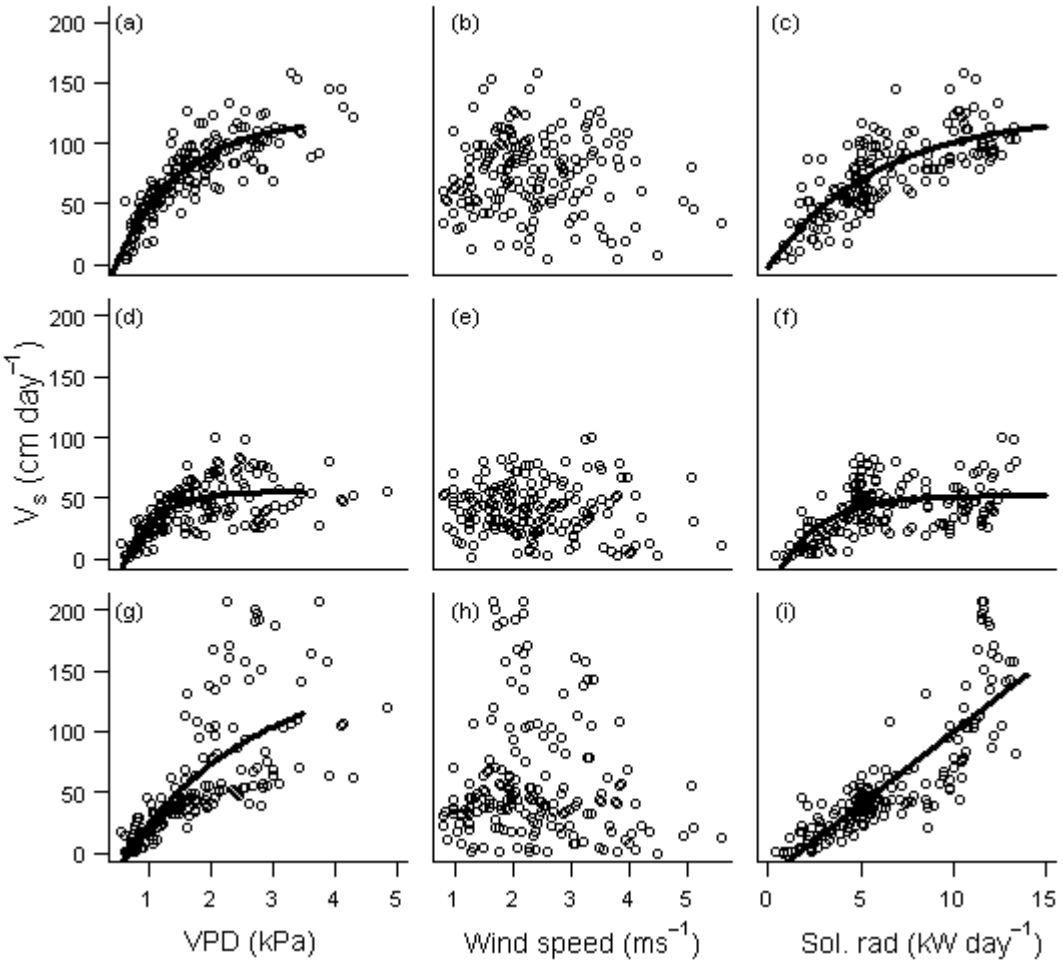

Figure 2.6: Relationship between total daily sapflow, v_s, and mean VPD and wind speed and total daily solar radiation for ((a), (b) and (c)) *P. repens* (n = 5), ((d), (e) and (f)) *E. monsoniana* (n = 6) and ((g), (h) and (i)) *C. congesta* (n = 2), respectively. The solid lines were modelled using either linear or quadratic functions.

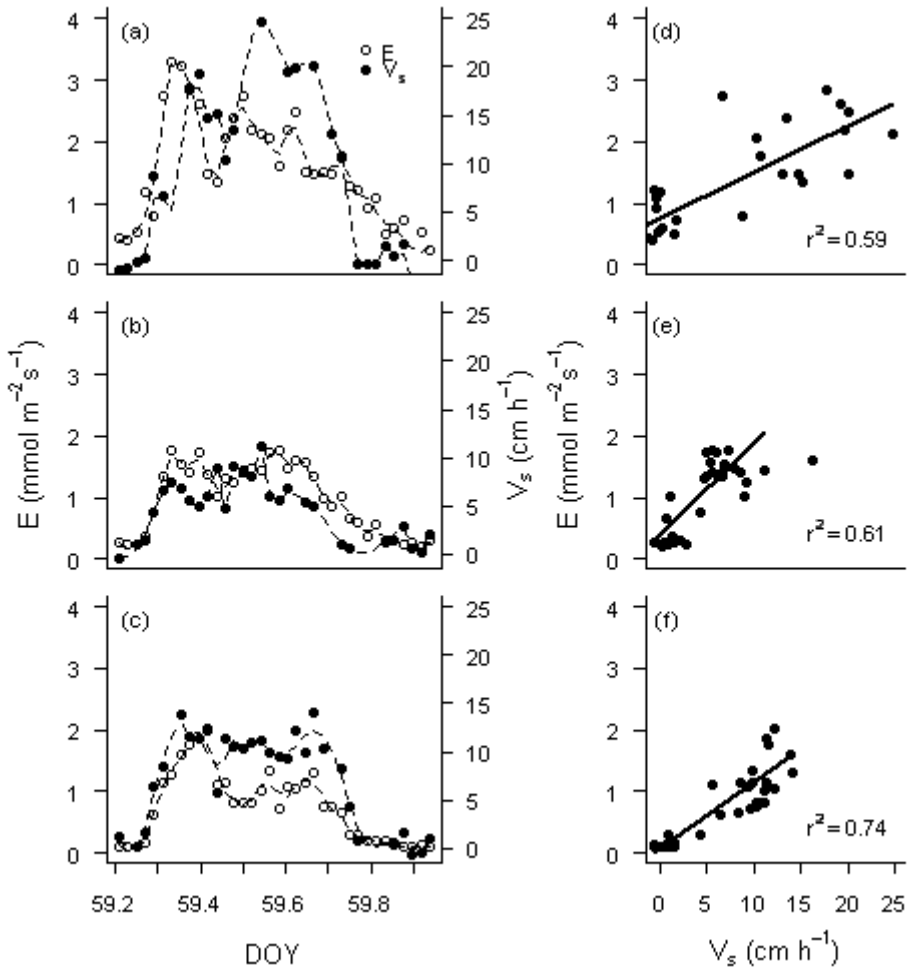

Figure 2.7: Diurnal patterns of *in situ* sapflow, v_s, and transpiration, E, and the relationship between these variables for ((a) and (d)) *C. congesta*, ((b) and (e)) *E. monsoniana* and ((c) and (f)) *P. repens* individuals. Smoothed curves for E or v_s were modelled using the loess function.

Discussion

External HRM-type sapflow sensors were able to capture the dynamics of water movement in diverse, co-existing functional types with contrasting stem morphologies in both controlled environments and in a field setting. To the best of our knowledge, this study is the first attempt at applying external HRM sapflow gauges to diverse functional types, including monocotyledonous individuals with culms of diameter less than 5 mm. Our data confirmed our first hypothesis that external HRM sensors would be able to contact a sufficiently large area of xylem conducting tissue of a restioid culm to permit measurement of v_h. We observed highly significant r^2 values for the relationship between v_h and v_s in a controlled setting for *C. congesta.* This indicates that, once contact is established in *C. congesta*, it provides a signal comparable to those obtained for *P. repens* and *E. monsoniana*. Although m_{sap} values were highest for *C. congesta*, the standard error was comparable to that in *E. monsoniana* and lower than that observed in *P. repens*. This suggests that, although the heat pulse was dissipated in the non-hydroactive tissues to a greater extent, the sensors were in contact with a sufficiently large surface area to integrate across several vascular bundles and provide reasonably consistent multiplier values. Our success rate in capturing *in situ* sapflow in *C. congesta* over a six-month period was lower compared than that for *P. repens* and *E. monsoniana*. Small-stemmed restioids (and other non-woody monocotyledonous species) present two major challenges in a field setting which reduce the likelihood of successful gauge installation. Firstly, the small diameters of restioid culms increase the difficulty of ensuring contact between the gauges and an adequate amount of vascular tissue. Obtaining commensurate sample sizes for different functional types will require installation of additional gauges in restioids. Secondly, since the culm is photosynthetic in restioids, any surface area that is covered by insulation material (necessary to reduce thermal noise in the measurement) reduces the surface area for gaseous exchange and thus transpiration from that culm. Therefore, for restioids, a trade-off exists between the quantities of noise the gauges capture and the magnitude of v_h. Consequently, in our study, the degree of gauge insulation was generally lower for *C. congesta* compared to the woody-stemmed *P. repens* and *E. monsoniana*, which explains why the traces for this species were slightly noisier. Future studies with small-stemmed monocotyledonous species will need to incorporate these issues into their sampling design. A final measure of the suitability of the external HRM gauges to capture v_h in restioids was the linear relationship between v_s and E, measured by gas exchange, for *C. congesta*. Considering the potential sources of error for the sapflow-gas

exchange comparison, the two measures approximated each other remarkably well. However, there was more noise in the relationship between v_s and E in *C. congesta* compared to the other two species. Although this could be related to slightly noisier sapflow traces observed in this species, an equally likely explanation is that it was due to greater error in the measurement of E. E may have been more variable in *C. congesta* compared to *P. repens* and *E. monsoniana* due to the smaller culm surface areas (± 3 cm^2 for *C. congesta*, ± 25 cm^2 for *P. repens* and ± 14 cm^2 for *E. monsoniana*) from which E was measured. Measuring gas exchange at low rates (i.e. on small leaf areas) has the potential to magnify small inherent variations between sample and reference IRGA cells, resulting in increased noise and possible offsets from zero (Wang *et al.*, 2012). This may also partly explain the slight positive intercept observed in the relationship between v_s and E (Fig. 2.7d).

Our second hypothesis, that external HRM sensors were sensitive enough to capture low flow rates in small-stemmed restioids and ericoids as well as high flow rates in proteoids, was well supported by our data. For all functional types, the sensors generally performed well in a controlled setting, with neither large amounts of noise nor any obviously aberrant data points. Furthermore, the relationship between v_s and v_h was approximately linear for all values of v_h for all three functional types. Exceptions occurred in certain individuals during periods with rapid and steep changes in temperature (e.g. Fig. 2.2b) and were most likely caused by insufficient thermal insulation of the gauges and resultant variability in raw temperature readings. Alternative explanations for these data are that they were produced by lower ranges of observed heat-ratio values caused by low flow rates or the decoupling of sapflow and transpiration caused by stem capacitance. Theoretically, heat-ratio values could be more sensitive to slight deviations in the signal caused by external thermal gradients at low velocity ranges. Also, if stem capacitance is high, there will be a lag in the response time of v_s compared to E. We feel these are unlikely explanations for our aberrant data since these trends were absent in other individuals of the same species. Variation in m_{sap} values between individuals of the same species was highest in *P. repens*. Since heat-pulse measurements rely on thermal equilibrium being established between stationary sapwood and moving sap, under conditions of high flow rates the relationship between v_h and v_s may be skewed. However, we found no evidence of this in *P. repens* nor any of the other species in our investigation as the relationship between v_s and v_h remained linear for the entire range of observed values. Although considerable care was taken to minimise variation in contact between the stem and the conductive tissue, theoretically, this could have influenced m_{sap} between individuals. Our

findings highlight that it will be important for future studies to describe intra- and inter-specific variation in m_{sap}, particularly if accurate quantitative measures of v_s are desired. The potential of the gauges to provide near-continuous quantitative data from a field setting was further validated by the linear relationship for all three species between sapflow and transpiration measured by gas exchange (Fig. 2.7).

Finally, external HRM gauges captured the response of sapflow to environmental drivers of transpiration in all three functional types, providing strong support for our third hypothesis. The gauges showed that variation in diurnal sapflow is determined mainly by changes in VPD and solar radiation in these three functional types (Fig. 2.3, 2.4 & 2.5). Such data will permit the comparative evaluation of environmental drivers of transpiration for co-existing functional types at a previously unattained temporal resolution in the CFR (see West *et al*., 2012) Over longer periods, the relationship between total daily sapflow and environmental variables will permit the evaluation of major seasonal drivers of plant response. For example, *E. monsoniana* individuals showed greater limitation of v_s at high VPD and solar radiation compared to *P. repens* and *C. congesta* (Fig. 2.6), suggestive of greater drought-induced reductions in transpiration in this species. The ability to provide near-continuous, concurrent measurements of water movement for numerous species in response to environmental variability in the field without disturbing the leaf microenvironment presents a considerable advancement over traditional gas-exchange measurements.

Detailed physiological datasets, such as those shown in this study, are important for understanding the drivers of plant response in a complex flora and for answering fundamental questions in community ecology. Continuous datasets will enable the detection of the dependence of species on varying or transient water sources (e.g. deep versus shallow soil moisture, summer versus winter rainfall or cloud moisture). This is particularly relevant in highly pulsed environments, such as the CFR, where periodic campaign measurements might inadequately capture response to potentially important ephemeral events, such as small summer rain events, cloud events (Marloth, 1903, 1905; Nagel, 1956) or hot, dry winds. Importantly, higher temporal resolution of the dynamics of plant-water relations will allow further separation of co-existing species into hydraulic niche space (Araya *et al.*, 2011). This knowledge combined with other physiological measures and experimental manipulations would greatly assist predictions for how complex communities are likely to respond to future climate change. For instance, continuous sapflow data coupled with plant-water potential

may prove invaluable in evaluating the hydraulic strategy of a species (McDowell *et al.*, 2008; West *et al.*, 2012). This information about the response to temporally variable atmospheric or soil drought, coupled with simulated drought or irrigation experiments exposing plants to conditions outside their current niches, would greatly inform predictions about a community's response to future climate change.

Acknowledgements

The authors would like to thank the South African Environmental Observation Network (SAEON) for the funding granted to RPS and the Andrew W. Mellon foundation for that granted to AGW. The authors also wish to thank two anonymous reviewers for insightful comments on the manuscript and Adam Roddy for technical discussion. We also thank Cape Nature for providing access permits to the study site.

Chapter Three: Continuous sapflow measurements reveal contrasting water regulation strategies of fynbos functional types

Abstract

Background/Questions/Methods

Global-change-type drought events pose a severe threat to the diversity of floras around the world. Recent studies have highlighted the importance of a hydraulic-based framework for understanding and predicting the response of vegetation to drought. However, currently the importance of the hydraulic framework in diverse communities is poorly understood. Drought-related plant mortality is of particular concern in South Africa's fynbos biome, a global biodiversity hotspot. This Mediterranean-type region is predicted to experience an increase in drought, with unknown consequences for the endemic flora. We asked whether drought affected this diverse ecosystem in a predictable manner and if these effect patterns fit existing frameworks of plant drought-mortality mechanisms. To answer these questions, we conducted a long-term field study aimed at quantifying environmental variability and the physiological response of three co-occurring species representing three diverse functional types. The species were *Protea repens* (L.) L. (Proteaceae), a large, deep-rooted overstory shrub, *Erica monsoniana* L.f. (Ericaceae), a small, shallow-rooted shrub and *Cannomois congesta* Mast. (Restionaceae), a reed-like graminoid. We measured key functional traits, including water potential, vulnerability to cavitation, gas exchange and sapflow to examine the response of these species to naturally occurring seasonal drought.

Results/Conclusions

P. repens displayed consistently high water potentials, despite seasonal declines in sapflow in response to summer drought periods. The combination of deep-rooting and stomatal regulation of water potential resulted in both < 25% loss of conductivity and few periods of carbon deficit during the summer drought. The shallow-rooted *E. monsoniana* experienced seasonal declines in both water potential and sapflow, with up to 80% loss of conductivity. A model of leaf-level carbon gain indicated extended periods of carbon deficit during drought. Thus, *E. monsoniana* experienced both high levels of hydraulic failure and carbon limitation during drought. Surprisingly, the shallow-rooted *C. congesta* was also able to maintain water potentials above −2 MPa, as well as positive gas exchange. High vulnerability to cavitation of

the culms resulted in up to 90% loss of conductivity over the drought, yet, surprisingly, with few periods of carbon deficit. This study provides increasing support for the use of functional types to characterise drought responses in fynbos communities and further emphasises the important role of the hydraulic framework for predicting drought-related mortality under future climate.

Introduction

Global-change-type drought events pose a severe threat to the diversity of floras around the world (Allen *et al.*, 2010). Reports of widespread regional plant die-off are becoming more frequent (Breshears *et al.*, 2009; Allen *et al.*, 2010). Recent studies have highlighted the importance of a hydraulic-based framework for understanding and predicting the response of vegetation to drought (McDowell *et al.*, 2008; Sevanto *et al.*, 2013). This framework distinguishes between isohydric species, which rapidly reduce stomatal conductance under drought conditions to maintain constant water potential, from anisohydric species, which maintain relatively high g_s, thereby maintaining carbon assimilation, albeit at the cost of declining water potential (McDowell *et al.*, 2008). These two different water regulation strategies result in different potential mechanisms of mortality under drought. Isohydric species avoid cavitation-induced loss of conductivity but are vulnerable to carbon starvation, while anisohydric species maintain carbon assimilation but are susceptible to hydraulic failure (Tyree & Sperry, 1988; Sperry *et al.*, 2003; McDowell *et al.*, 2008). Strong interactions between hydraulic strategy and prevailing drought conditions influence which mechanism is more likely to occur under any particular drought scenario (Mitchell *et al.*, 2008, 2014; Breshears *et al.*, 2009; Anderegg *et al.*, 2013). This complexity and our limited knowledge of the physiological strategies of different species in diverse communities hinder our ability to predict the response of complex communities to future drought. There exists a great need to examine in detail the physiological response of diverse species in highly heterogeneous environments if we are to improve this ability (West *et al.*, 2012; Poot & Veneklaas, 2012; Zeppel *et al.*, 2013).

Mediterranean-type ecosystems (MTEs) contain exceptional species richness, supporting *c*. 20% of the world's species on 5% of its surface area (Cowling *et al.*, 1996). MTEs are also highly seasonal environments, experiencing cold, wet winters and hot, dry summers. The predominantly winter rainfall regime in these areas ensures that water availability in summer is frequently one of the most limiting abiotic factors for plant productivity and strongly influences the predominant native vegetation types (Ackerly, 2004). Functional trait evolution has been driven by the amount and seasonality of precipitation, often resulting in convergence between distantly related species in different MTEs (Ackerly, 2004; Bhaskar *et al.*, 2007; Jacobsen *et al.*, 2009). High functional diversity and the importance of water

availability suggest that MTEs provide excellent environments in which to test the hydraulic framework and the relevance of hydraulic strategies in determining species' responses to drought. Despite this, there remains a paucity of research investigating the relevance of the hydraulic framework in these floras (e.g. West *et al.*, 2012).

The Cape Floristic Region (CFR) of South Africa is both one of the most diverse MTEs and particularly threatened by future climate change (Thuiller *et al.*, 2006; Midgley & Thuiller, 2010). Recent climate models have predicted drier and warmer climates and a reduction in summer rainfall for parts of the CFR (Hewitson & Crane, 2006; Lumsden *et al.*, 2009). Changes in the structure of moisture resource availability could have significant implications for the ecology of the region (Foden *et al.*, 2007; Hoffman *et al.*, 2009). Previous studies have revealed that there are three major functional types that display considerable variation in functional traits and hydraulic strategies and, as a result, may utilise different moisture resources (van der Heyden & Lewis, 1990; West *et al.*, 2012). To avoid desiccation in dry periods, large overstory proteoid shrubs rely on a combination of access to permanently moist soil layers, achieved through being deep-rooted, and isohydric stomatal regulation (West *et al.*, 2012). Reed-like restioid species also tend to maintain high water potentials despite being shallow-rooted, although it is unclear whether this is as a consequence of isohydric regulation or an ability to capture cloud or fog moisture (West *et al.*, 2012). Small-leaved ericoid shrubs, on the other hand, tend to be relatively shallow-rooted and exhibit anisohydric regulation and, consequently, suffer large declines in water potential during drought events (West *et al.*, 2012).

A major drawback of previous plant hydraulic studies was an inability to adequately capture the highly temporally resolved datasets needed to examine the response to short-term changes in environmental conditions. Recent advances in sapflow technology allow us to do this and may provide valuable insight into plant response (Skelton *et al.*, 2013). For example, few studies have addressed whether any species of mountain fynbos— the predominant vegetation type in the CFR—utilise moisture derived from summer rainfall events. In the south-western corner of the CFR, it is extremely rare to go longer than fourteen days without a rainfall event, the majority of which are < 5 mm (Agenbag *et al.*, 2008). Although it comprises a small proportion of total annual rainfall, summer rainfall may be crucial for relieving periods of protracted drought.

The objectives of this study were to (a) identify the environmental variables that determine plant-water relations of major functional types and (b) identify potential mechanisms of mortality in functionally diverse communities. To achieve these objectives, we conducted a long-term field study aimed at quantifying environmental variability and the physiological response of three co-occurring functional types. We monitored plant-water relations and sapflow both over multiple years with contrasting environmental patterns and in response to pulsed summer rainfall events. We also quantified the degree of hydraulic failure and carbon limitation for each species using a combination of field data and laboratory-based measures of vulnerability and stomatal response. We reasoned that functional differences would be most obvious during times of stress and that these conditions would be sufficient to indicate pathways of mortality. We also reasoned that there would be predictable interactions between hydraulic strategy, functional traits and potential mechanisms of mortality, allowing us to develop the following specific hypotheses: first, shallower-rooted, anisohydric species would be more sensitive to changes in soil moisture and more reliant on summer precipitation events compared to deeper-rooted isohydric species; and second, to avoid hydraulic failure, deeper-rooted isohydric species would be more sensitive to changes in atmospheric vapour pressure deficit (VPD) compared to shallower-rooted anisohydric species. Highly detailed physiological investigations such as these are crucial to ongoing efforts to understand and predict future response of complex communities to drought.

Methods and materials

Study site and species

The field site was situated at Jonaskop in the Riviersonderend Mountains, which forms part of the Cape Fold Belt in the Western Cape of South Africa. The geology of the area consists mostly of quartzitic sandstone of the Table Mountain group. The study site and micrometeorological station was located on a relatively level, slightly north-facing plateau at an elevation of 980 m a.s.l. (33° 56′ 30.45″ S and 19° 31′ 34.18″ E) and all measured plant individuals were located within a zone of approximately 100 m radius from the station. Soils at the site were shallow and rocky, consisting mostly of quartzitic sandstone-derived sand. The dominant vegetation type was mountain fynbos, with a 2–3 m tall overstorey dominated by *Protea repens* (L.) L. (Proteaceae). Species chosen for detailed physiological monitoring were: *Erica monsoniana* L.f. (Ericaceae), a small- to medium-sized, small-leaved woody shrub; *P. repens*, a dominant, broad-leaved overstorey shrub; and *Cannomois congesta* Mast.

(Restionaceae), a reed-like monocotyledonous graminoid. These three species are representative of the three major functional types found within mountain fynbos: the restioid, proteoid and ericoid functional types.

Monitoring of micrometeorological variables

A micrometeorological station was erected at the study site in November 2011 and monitored environmental variables continuously until May 2014. All meteorological variables were logged at half-hour intervals with a CR1000 data logger (Campbell Scientific Inc., Logan, Utah, USA). The micrometeorological station consisted of a CM106 tripod (Campbell Scientific Inc.) and various sensors, including a CS300 pyranometer (Campbell Scientific Inc.), a HMP45C temperature and relative-humidity probe (Campbell Scientific Inc.), a 237 leaf-wetness sensor (Campbell Scientific Inc.) and a 03002 wind-sentry set. A tipping-bucket rain gauge (Campbell Scientific Inc.), EnviroSMART soil water content profile probe (Campbell Scientific Inc.) and two CS615 water content reflectometers (Campbell Scientific Inc.) were placed approximately 5 m from the tripod. Soil moisture was measured at four depths along the soil profile and at three locations within the site. At periodic intervals throughout the study, soil water content was assessed gravimetrically from samples collected at 20 cm, 40 cm and 50 cm depths at the site and within approximately 1 m of the EnviroSMART probe. This allowed us to calibrate the probe and to express soil moisture content in grams of H_2O per gram of soil. VPD was calculated from temperature, T in °C, and relative humidity, RH, using (Campbell & Norman, 1998):

$$VPD = ((100 - RH)/100) \cdot 610.7^{107.5\,T/(237.3 + T)} \quad \text{(Eq. 3.1)}$$

Sapflow

Sapflow velocity was monitored almost continuously in at least five individuals of each of the three study species. Sapflow was measured using the external heat-ratio method (HRM) and miniature gauges described in Clearwater et al. (2009) and Skelton et al. (2013). The details of our methodological development of these sensors are presented in Chapter Two. Heat-ratio values were logged every half-hour using a CR1000 Campbell data logger (Campbell Scientific). The heat ratio was converted to sap velocity (v_h in cm s^{-1}) using equations from Chapter Two. This was then converted to sapflow (v_s in g s^{-1}) using m_{sap}, the mean slope of the relationship between sap velocity and sapflow measured gravimetrically for each species which is provided in Chapter Two (Skelton *et al*., 2013). Sap flux density (J_s in g m^{-2} A_s s^{-1})

was found by dividing v_s by the cross-sectional area of the conducting tissue (A_s) for each individual. We were able to convert sap flux density to leaf-specific transpiration (g cm^{-2} A_l s^{-1}) by multiplying J_s by the ratio of total stem area to total leaf area (A_s : A_l). We obtained A_s : A_l for ten individuals of each species and calculated a species mean. The leaves of *P. repens* were large enough to enable us to use a leaf-area meter (Li-Cor BioSciences, Lincoln, Nebraska) to quantify total leaf area. For *E. monsoniana*, we removed and scanned each individual leaf and used ImageJ to quantify total leaf area. For *C. congesta*, we measured the diameter and length of each culm segment and then quantified the surface area of a cylinder with these parameters. We estimated the total leaf area of those individuals that had sapflow monitored using the mean ratio for each species and the stem area of each individual.

Periodic gas exchange and water potential

Midday gas exchange and predawn and midday shoot water potential (P_{pd} and $P_{md,}$ respectively) were measured approximately every month at the study site from February 2012 until May 2014. Measurements were made more frequently during periods of drought stress, when plants exhibited relatively rapid changes in water potential. Midday measurements were made between 12:00 and 14:00 and predawn measurements were made approximately one and a half hours before sunrise. Stomatal conductance, carbon assimilation and transpiration were measured using a Li-Cor 6400 infra-red gas analyser (Li-Cor BioSciences, Lincoln). Light intensity in the cuvette was set at 1500 μmol m^{-2} s^{-1}, humidity was maintained slightly below ambient and reference CO_2 concentration was held at 400 mmol m^{-2} s^{-1}. Leaf temperature was maintained between 25 °C and 33 °C as calculated using energy balance equations in an attempt to track ambient conditions. Stomatal conductance, transpiration and carbon assimilation were expressed per leaf area. P_{pd} and P_{md} were measured using a Scholander pressure chamber (PMS instruments). We modelled the relationship between g_s (converted to a percentage of g_{max}) and P_{md} for each species using either a linear model or a logistic function (Eq. 3.2) (Damour *et al.*, 2010; Guyot *et al.*, 2012) (Domec & Gartner, 2001):

$$g_s = 100 - 100 / (1 + e^{a\,(P - b)}) \qquad \text{(Eq. 3.2)}$$

where a is proportional to the slope of the response and b is the water potential inducing 50% stomatal closure (Domec & Gartner, 2001). The slope of the response at any given water potential is given by the derivative of equation 3.2:

$$dg_s / dP = -a \cdot (e^{a(P - b)}) \cdot 100 / (1 + e^{a(P - b)})^2 \quad \text{(Eq. 3.3)}$$

At the water potential inducing 50% stomatal closure both $e^{a\,(P - b)}$ terms are equal to one, which then makes the slope at this point simple to calculate:

$$\text{slope} = a \cdot 100 / 4 \quad \text{(Eq. 3.4)}$$

The straight line defined by this slope can then be used to find the point at which g_s is 12% of g_{max}, which is a useful parameter for defining the point of stomatal closure (Domec & Gartner, 2001). Since the line passes through the point (b, g_{s50}), the point at which it intersects the water potential axis is:

$$c = 50 / \text{slope} + b \quad \text{(Eq. 3.5)}$$

We define c as the point of stomatal closure, P_{g12}, and use this as a point of comparison between the three species. This analysis is used more extensively in Chapter Four.

Vulnerability curves

Vulnerability curves were constructed using the benchtop dehydration method (Tyree & Sperry, 1989; Sperry & Saliendra, 1994). Prior to collecting stems from the field, an analysis was done to determine the maximum vessel length for each species (Cochard *et al.*, 2013). Stems from five individuals of each species were cut under water and transported back to the laboratory. These stems were connected to a pressurised air cylinder at one end and placed under water. Segments of 1 cm were cut from the open end until bubbles appeared. The length of stem at that point was recorded as the maximum vessel length for each individual. Stems from at least forty individuals were cut under water in the field and transported back to the laboratory, where they were placed in a 4 °C room overnight to rehydrate. Stems were subsequently dehydrated to various water potential values by placing them on a workbench. Once they had reached the desired water potential, they were placed in a sealed bag in darkness for at least an hour to ensure equilibration. Water potential of a terminal shoot was assessed using a Scholander pressure chamber (PMS Instruments). The remaining branch was placed under water and several cuts were made from each end with brief intervals to ensure that the xylem had relaxed and that we did not introduce artefact embolism (Wheeler *et al.*, 2013; Rockwell *et al.*, 2014; Wheeler, 2014). Sections were at least the length of the maximum vessel length for each species. Flow rate through the stem was assessed by

connecting one end of the stem to a pressure head of < 12 kPa and collecting and weighing the water that emerged from the other end (Tyree & Sperry, 1989; Sperry & Saliendra, 1994). Flow rate was converted to native stem conductance (k_{native}) after controlling for temperature and pressure and the diameter of the stem. Stems were subsequently flushed with degassed, filtered 0.2 mM KCl solution at 150 kPa for at least an hour. Immediately following this, stems were reconnected to the pressure head and flow rates through them were re-measured. This measure was converted to maximum stem conductance (k_{max}). Percentage loss of conductivity (PLC) was calculated as:

$$PLC = (k_{max} - k_{native}) / k_{max} \cdot 100 \quad \text{(Eq. 3.6)}$$

A Weibull function was fitted to these data using the following formula (Pammenter & Vander Willigen, 1998):

$$PLC = 100 / (1 + e^{(a\,(P - b))}) \quad \text{(Eq. 3.7)}$$

where a is proportional to the slope at 50% loss of conductivity and b is the water potential at 50% loss of conductivity and both are obtained from the data using least-squares regression.

Modelling carbon gain and seasonal PLC

Leaf-level net photosynthetic carbon gain over the study period was modelled for each species using a combination of field- and laboratory-based measures of assimilation rates and water potential. Midday assimilation rates and midday water potential were quantified *in situ* as stated under "*Periodic gas exchange and water potential*" above. Laboratory-based measurements of assimilation and water potential were taken on branches that were collected under water from the field and subsequently dried on a laboratory workbench. Assimilation was quantified using an Infra-red Gas Analyser (Li-Cor BioSciences, Lincoln, Nebraska). Conditions in the cuvette were maintained at constant values for all measurements. Light was set to 1500 μmol m^{-2} s^{-1}, CO_2 was held constant at 400 ppm and humidity was maintained just below ambient. Immediately after the assimilation rate was taken, the shoot was cut and water potential was measured using a Scholander pressure chamber (PMS Instruments). These laboratory data allowed us to extend the relationship of assimilation and water potential to beyond the range of values observed in the field. We fitted a logistic function to these data:

$$A_{pred} = A_{max} / (1 + e^{(b - P) / c}) \quad \text{(Eq. 3.8)}$$

where A_{max} is the maximum assimilation rate, b is the water potential at 50% of A_{max} and c is an empirical scalar established using least-squares regression (Quinn & Keough, 2002). To estimate net leaf-level assimilation rates, we subtracted a respiration value, which we assumed to be 55% of maximum assimilation based on values from the literature (Van der Werf *et al.*, 1994; Lambers *et al.*, 2008; McDowell *et al.*, 2008). Finally, we used field-based midday water potentials in combination with this modelled function to predict net leaf-level carbon gain during the study period.

We estimated in situ PLC for each species based on laboratory-based vulnerability curves (see "*Vulnerability curves*" above) and predawn and midday shoot water potentials (see "*Periodic gas exchange and water potential*" above) measured throughout the course of the study. We used these measurements to describe an envelope of the likely PLC of stem xylem experienced in situ by each species throughout the course of the study. Specifically, the PLC at water potentials equivalent to midday shoot water potentials was taken to represent an upper bound on PLC experienced in the stem. Hydraulic resistance of leaves is frequently much greater than for stems, indicating that shoot water potential might overestimate stem water potential and thus exaggerate PLC (Melcher *et al.*, 2001). We used predawn shoot water potentials as an estimate for the lower bound of PLC experienced in the stem in situ. Predawn shoot water potential might also overestimate stem water potential when night time transpiration is high (Donovan *et al.*, 2003). Support for this envelope approach can be found by comparing different measures of water potential. In particular, the approach is justifiable if predawn shoot water potential is consistently less negative than stem water potential and midday shoot water potential is consistently more negative than stem water potential. To investigate this, we obtained measures of stem water potential for *P. repens* from a separate study conducted at Jonaskop concurrently with the current study. Stem water potential of *P. repens* was found by bagging leaves from five different individuals during the night and measuring their water potential at midday. An alternative option would have been to have brought stems into the laboratory and measure native PLC from measurements of conductivity before and after flushing. However, we opted against this approach since it is both destructive, time-consuming and might promote overconfidence in a single value rather than a likely range within an individual.

Plant-water isotopes

We measured the ratio of stable hydrogen (δ^2H) and oxygen ($\delta^{18}O$) isotopes in water extracted from plant stems from each of the three study species as a proxy for rooting depth. Suberised stems of *P. repens* and *E. monsoniana* and rhizomes of *C. congesta*, as well as soil samples from the top 50 cm, were collected from the field site and immediately placed in screw-capped glass vials and sealed with Parafilm (Pechiney Plastic Packaging, Chicago, IL, USA). Samples were kept at −20 °C until extraction. Water was cryogenically extracted at the University of Cape Town using the methodology from West *et al.* (2006). Hydrogen isotope ratios were measured by injecting microliter quantities of water into an H/Device coupled to a Delta Plus mass spectrometer (ThermoFinnigan, Bremen, Germany). The injected H_2O was reduced to H_2 gas in a hot chromium reactor and the ^2H / H ratio of this gas was analysed by mass spectrometry (Brand, 1996). Oxygen isotope ratios were measured by CO_2 equilibration. Water samples were left to equilibrate with a 0.2% CO_2 headspace for forty-eight hours at 21–23 °C. Following this, the vials were inserted into a GasBench II connected to a Delta Plus XL mass spectrometer (ThermoFinnigan, Bremen, Germany). The GasBench II was slightly modified with a ten-port injection valve, allowing a 0.2% CO_2 reference injection to follow each sample CO_2 injection. All isotope analyses were conducted at the University of Cape Town. Ratios are expressed in per mil notation (‰) relative to the standard V-SMOW following the equation:

$$\delta^n E = (R_{sample} / R_{standard}) - 1 \quad \text{(Eq. 3.9)}$$

where n is the heavy isotope of element E and R is the ratio of the heavy to the light isotope.

Sensitivity of stomatal response to VPD

By comparing the slope of the relationship between stomatal conductance and VPD to a reference stomatal conductance (g_s at 1 kPa) we were able to quantify stomatal sensitivity to VPD for the three study species (Oren *et al.*, 1999). We calculated stomatal conductance as the quotient of E obtained from midday J_s, and A_s : A_l and VPD according to the following equation (Monteith, 1995; Oren *et al.*, 1999; McDowell *et al.*, 2008):

$$g_s = E / VPD \quad \text{(Eq. 3.10)}$$

Here, we have made the assumption that $T_{leaf} = T_{air}$ for the estimate of leaf to air VPD. If this assumption is violated it may lead to substantial errors in estimating VPD (Oren *et al.*, 1999). This is unlikely to be a major cause of error in the current study for two reasons. Firstly, all the species in the study have relatively small leaf or culm surface areas, which may serve to reduce the difference between T_{air} and T_{leaf}. *Erica* and *Protea* species have small leaves and are likely to be well-coupled to the air temperature (Yates *et al.*, 2010b). *Cannomois* has a cylindrical culm of a diameter of < 2mm. Secondly the canopy in Fynbos communities is relatively open or sparse allowing substantial air movement between the canopy and the air above the canopy. In vegetation where the air in the canopy volume is well mixed with the air above the canopy a single point of measurement of T_{air} is often sufficient (Oren *et al.*, 1999; Ewers & Oren, 2000).

After discarding values for which VPD was lower than 1 kPa (Monteith, 1995; Oren *et al.*, 1999), we obtained the slope and intercept of the linear portion of the relationship between g_s and lnVPD (Oren *et al.*, 1999). The slope of the linear part of this relationship is taken to be equivalent to dGs / dlnVPD, while the intercept is the reference stomatal conductance at VPD = 1, since ln1 = 0 (Oren *et al.*, 1999). The reference g_s provided a standardised measure of the differences in stomatal conductance under optimal conditions between each species.

Data analysis

Statistical analyses were conducted to assess whether we could detect differences between the sapflow-VPD response curves for early and late season for each year within each species. Early season is defined as the period between 1 October and 31 December and late season as that between 1 January and 31 March. To assess the mean response of sapflow to VPD for each species within each year, a mixed linear model was fitted to the data using the following formula (Dobson & Barnett, 2008):

$$J_s = \beta_{0early} + \beta_{0late} + \beta_{1early} \cdot vpd + \beta_{1late} \cdot vpd + \varepsilon \qquad \text{(Eq. 3.13)}$$

where β_0 is intercept for early and late season, β_1 is the slope of the responses for early and late season and ε is the error. Individuals of each species were treated as random effects and VPD, species and season as fixed effects. The mixed linear model was implemented in R (R Development Core Team, 2013) using the "lme4" package. Confidence intervals for each parameter were obtained using the bootstrap method and were used to infer whether mean response for each season differed significantly (Dobson & Barnett, 2008). We considered the

mean response of early and late season to be significantly different if the mean response of the late season fell outside of the 95% confidence region of the early season.

We also conducted statistical analyses to assess changes in hydraulic conductivity before and after a summer rainfall event for each species. We used a t-test to infer whether leaf- and stem-level hydraulic conductivity was significantly higher after the rainfall event than before. All analyses were conducted in R (R Development Core Team, 2013).

Results

Environmental conditions

There were several significant differences in environmental conditions between the summer periods of 2012/13 and 2013/14. The total amount of rain falling over the period from 1 November to 30 April rose from 66 mm in 2012/13 to 251 mm in 2013/14 (Table 3.1), due mostly to two large storm events in November 2013 and January 2014 (Fig. 3.1). Mean daily VPD was similar in both years, although mean daily wind speed declined in 2013/14 (Table 3.1). Increased rainfall in the summer of 2013/14 resulted in significantly higher soil moisture content compared to 2012/13 (Table 3.1, Fig. 3.1).

Table 3.1: Mean annual and seasonal values for a range of environmental variables at Jonaskop for 2012, 2013 and 2014. Summer is defined as the months between 1 November and 31 January, autumn as those between 1 February and 30 April and spring as those between 1 August and 31 October.

Time period and year of measurements		**Soil moisture at 50 cm (g g^{-1})**	**VPD (kPa)**	**Rainfall (mm)**	**Wind speed (m s^{-1})**
Annual	2012	0.083 ± 0.001	1.90 ± 0.08	-	2.74 ± 0.11
Annual	2013	0.084 ± 0.001	1.83 ± 0.05	389	2.56 ± 0.06
Spring	2012	0.103 ± 0.001	1.35 ± 0.12	-	2.83 ± 0.20
Summer	2012/13	0.076 ± 0.002	2.18 ± 0.07	12	2.72 ± 0.10
Autumn	2013	0.054 ± 0.001	2.29 ± 0.10	44	2.44 ± 0.10
Spring	2013	0.101 ± 0.001	1.43 ± 0.08	141	2.66 ± 0.13
Summer	2013/14	0.133 ± 0.003	2.37 ± 0.10	179	2.55 ± 0.08
Autumn	2014	0.115 ± 0.003	2.35 ± 0.11	72	2.11 ± 0.09

Table 3.2: Critical values for gas exchange, water potential and vulnerability curves for each species at Jonaskop.

Species	**P_{min} (MPa)**	**P_{50} (MPa)**	**P_{g12} (MPa)**
P. repens	−1.67	−3.00	−1,52
C. congesta	−1.88	−0.90	−2.70
E. monsoniana	−5.01	−1.60	−2.17

Sapflow

We captured continuous daily sapflow for all three species over two contrasting summer periods in 2012/13 and 2013/14 (Fig. 3.1). For all three species, total daily sapflow was highest during late spring/early summer and declined over the course of the summer period alongside declining soil moisture (Fig. 3.1). Total daily sapflow values were lowest in late autumn in both years for all three species (Fig. 3.1). Following the first heavy rain event in late autumn/early winter, sapflow recovered slightly (Fig. 3.1). *E. monsoniana* was the only species to show marked recovery of sapflow during the summer period (Fig. 3.1, 3.14 & 3.15). Annual comparisons of sapflow showed highly contrasting patterns for each of the three species (Fig. 3.2). *C. congesta* displayed remarkably similar trends in sapflow for both years (Fig. 3.2), despite 2012/13 being much drier compared to 2013/14. *E. monsoniana* was strongly affected by the summer rain in 2013/14, displaying much greater total daily sapflow in that year compared to 2012/13 (Fig. 3.2). The opposite was observed for *P. repens*: total daily sapflow in 2013/14 was at lower levels than in 2012/13 (Fig. 3.2). This may have been a result of leaf damage caused by waterlogging from the heavy rainfall events in November 2013 and January 2014 (Plate 3.1).

Water potential regulation strategies

We observed contrasting patterns of water potential regulation for the three species in response to declining soil moisture (Fig. 3.3). Predawn water potentials for *E. monsoniana* declined to around −4 MPa in the relatively dry summers of 2011/12 and 2012/13. These values were the lowest of all three species during summer drought periods. By contrast, predawn water potentials of *P. repens* and *C. congesta* were maintained at higher values, even during summer drought periods. Predawn water potential declined to a minimum of −0.84 MPa for *P. repens* and −1.02 MPa for *C. congesta* during the summer drought period of 2012/13 (Fig. 3.3a). Midday water potential displayed a very similar trend for the three species. Midday values were lowest during periods of protracted drought for *E. monsoniana*, declining to below −5 MPa during the summer drought period of 2011/12 (Fig. 3.3b). In contrast the minimum water potentials for *P. repens* and *C. congesta* did not fall to below −2 MPa during the entire study period. Minimum P_{md} values were −1.67 MPa for *P. repens* and −1.88 MPa for *C. congesta*. P_{md} values during the relatively wet summer of 2013/14 reached a minimum of −2.13 MPa for *E. monsoniana*, −1.43 MPa for *P. repens* and −1.18 MPa for *C. congesta*. A comparison of the P_{pd} between spring and summer for each species showed that

summer values declined much more in *E. monsoniana*, but not in the remaining two species (Fig. 3.4).

Plate 3.1: *P. repens* individuals with dead leaves, possibly caused by waterlogged soils at Jonaskop during autumn 2014. Photograph by Adam West.

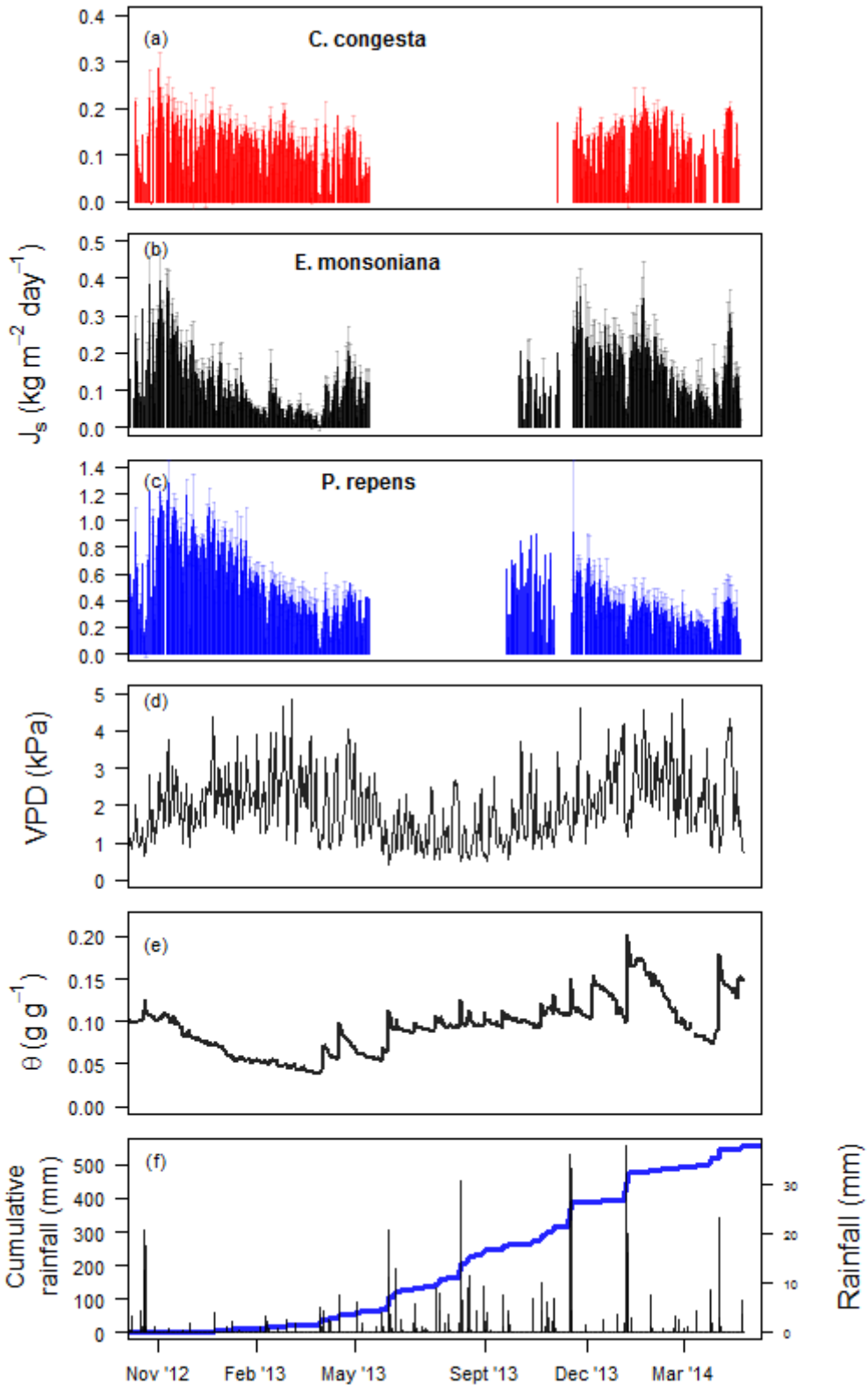

Figure 3.1: Timeline of mean total daily sapflow for three species ((a)–(c)) in response to key meteorological variables ((d)–(f)) for the entire study period starting in November 2012 and ending in May 2014. Soil moisture (θ) at 50 cm and VPD are expressed as daily averages and rainfall as a daily total.

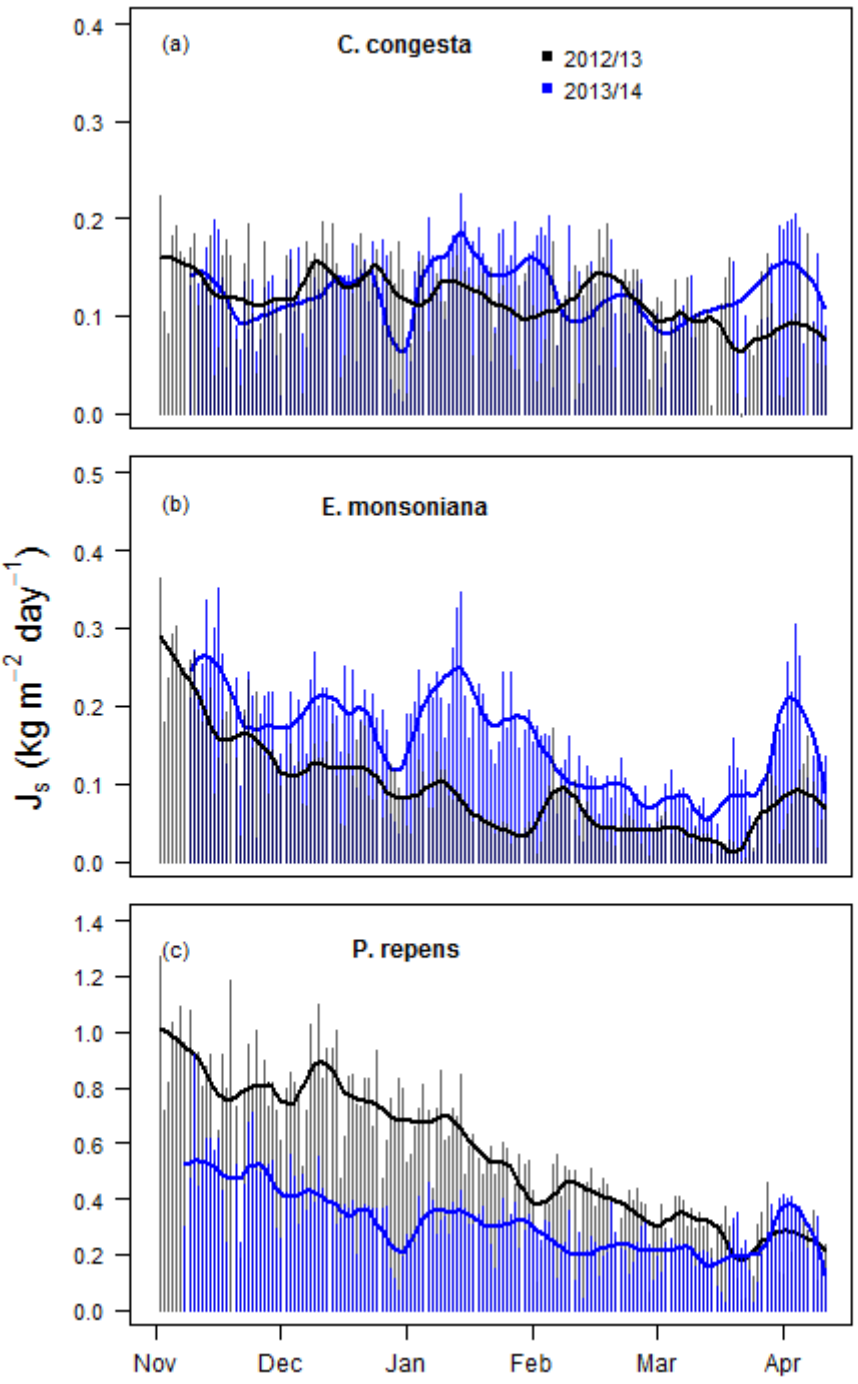

Figure 3.2: Mean total daily sapflow of three species for the summers of 2012/13 and 2013/14 showing differences between years.

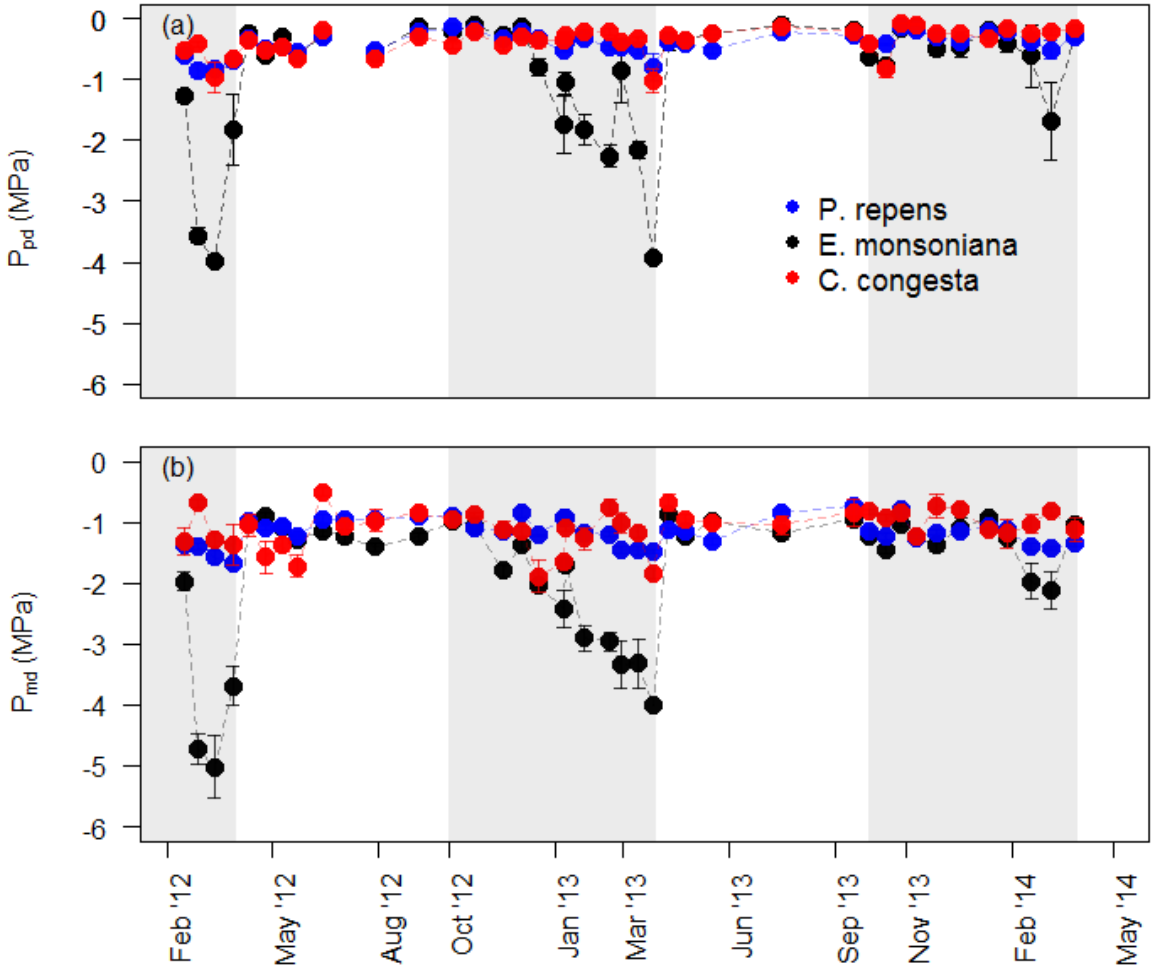

Figure 3.3: Timeline of mean (a) predawn and (b) midday shoot water potential for the three study species for the entire study period. The grey bars indicate summer, when moisture is limiting.

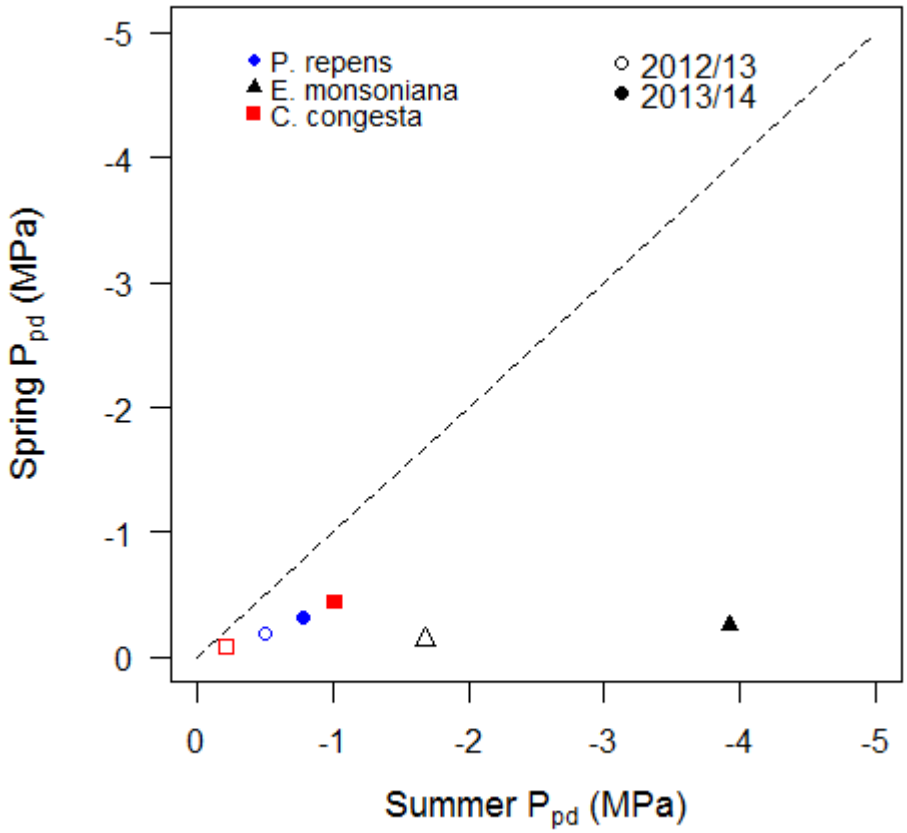

Figure 3.4: Relationship between mean midday water potential during spring (November) and summer (March) for the three study species highlighting the degree of regulation of water potential over the summer period.

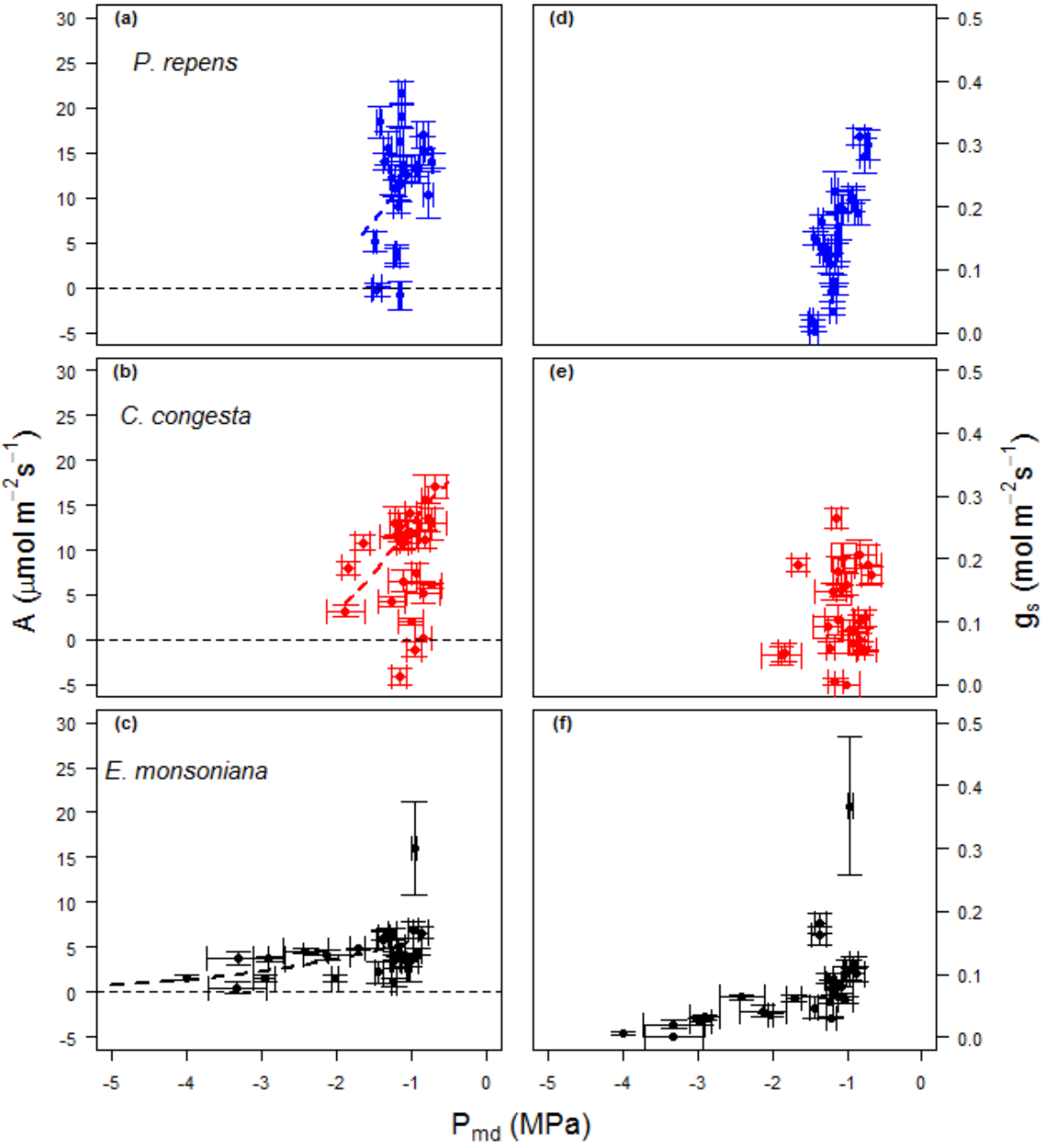

Figure 3.5: Relationships between midday water potential and assimilation ((a)–(c)) and stomatal conductance ((d)–(f)) for the three study species measured at the study site on Jonaskop over the course of the study period. The dotted lines ((a)–(c)) are the modelled functions used in the seasonal carbon gain analysis.

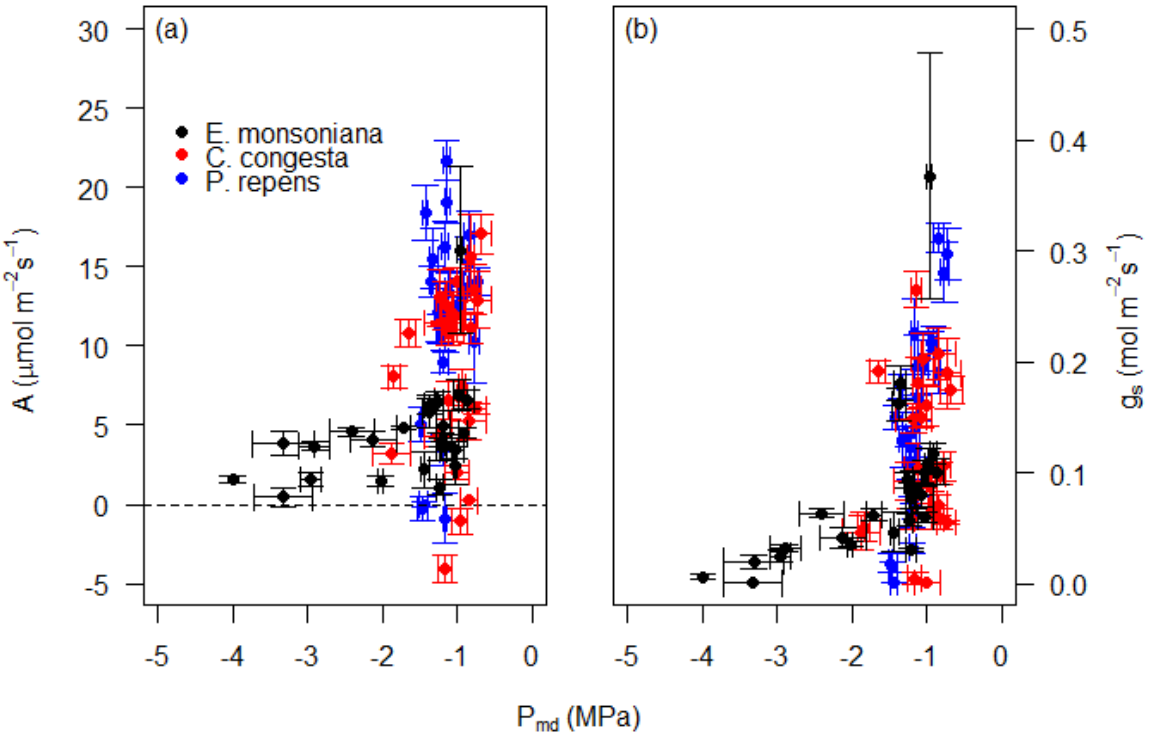

Figure 3.6: Distributions of stomatal conductance and midday water potential for three species showing the hydraulic envelope in which each operates.

Gas-exchange response

All three species displayed decreasing gas exchange rates with declining water potential (Fig. 3.5). Stomatal conductance and assimilation declined most rapidly in *P. repens* in response to declining water potential (Fig. 3.5 & 3.6). The water potential inducing stomatal closure in *P. repens* was −1.52 MPa (Fig. 3.5, Table 3.2), which was similar to the P_{min} value of −1.67 MPa and is consistent with isohydric regulation of water potential. P_{g12} in *E. monsoniana* was −2.17 MPa (Fig. 3.5f, Table 3.2), well above the P_{min} value for this species (−5.02 MPa) and indicative of a lack of tight stomatal regulation of water potential. *E. monsoniana* maintained A and g_s at higher values for much lower water potentials than *P. repens* and *C. congesta* (Fig. 3.5 & 3.6). The gas-exchange envelopes for *E. monsoniana* are indicative of anisohydric regulation of water potential (Fig. 3.6). The low and variable seasonal P_{min} (Fig. 3.3), together with the extended gas-exchange envelopes for this species (Fig. 3.6), are indicative of anisohydric regulation of water potential. The hydraulic response of *C. congesta* is difficult to interpret as being either isohydric or anisohydric. It displayed a very similar stomatal-conductance water-potential envelope compared to *P. repens,* consistent with isohydric water potential regulation (Fig. 3.6). It also maintained a relatively high P_{min} value of −1.88 MPa, despite being relatively shallow-rooted (see "*Stable isotopes and rooting depth*" below). Nevertheless, the P_{g12} of *C. congesta* (−2.70 MPa) was the lowest for all three species, more consistent with anisohydric regulation. Since the consistently high water potential was not due to stomatal regulation of water potential, we refrain from classifying *C. congesta* as isohydric (or anisohydric).

Stable isotopes and rooting depth

Previous work in fynbos has indicated that proteoids are deep rooted and ericoids and restioids are shallow-rooted (Higgins *et al.*, 1987; West *et al.*, 2012) We sought to test this with a combination of analysis of δ^2H and $\delta^{18}O$ of soil water and on-site excavations. Unfortunately, due to technical limitations (dry sandy soils), we were unable to recover reliable isotope values from the soil samples. This limited our analysis of rooting depth to inferring relative rooting position of the three study species based on the δ^2H and $\delta^{18}O$ of stem water alone (as per West *et al.*, 2012). Our isotope data supported the hypothesis that *P. repens* was deeper-rooted than *E. monsoniana*. *P. repens* occurred closest to the global meteoric water line (GMWL) (Fig. 3.7). Xylem water from *E. monsoniana* was positioned along an evaporation line away from the GMWL relative to *P. repens*, indicating that it was

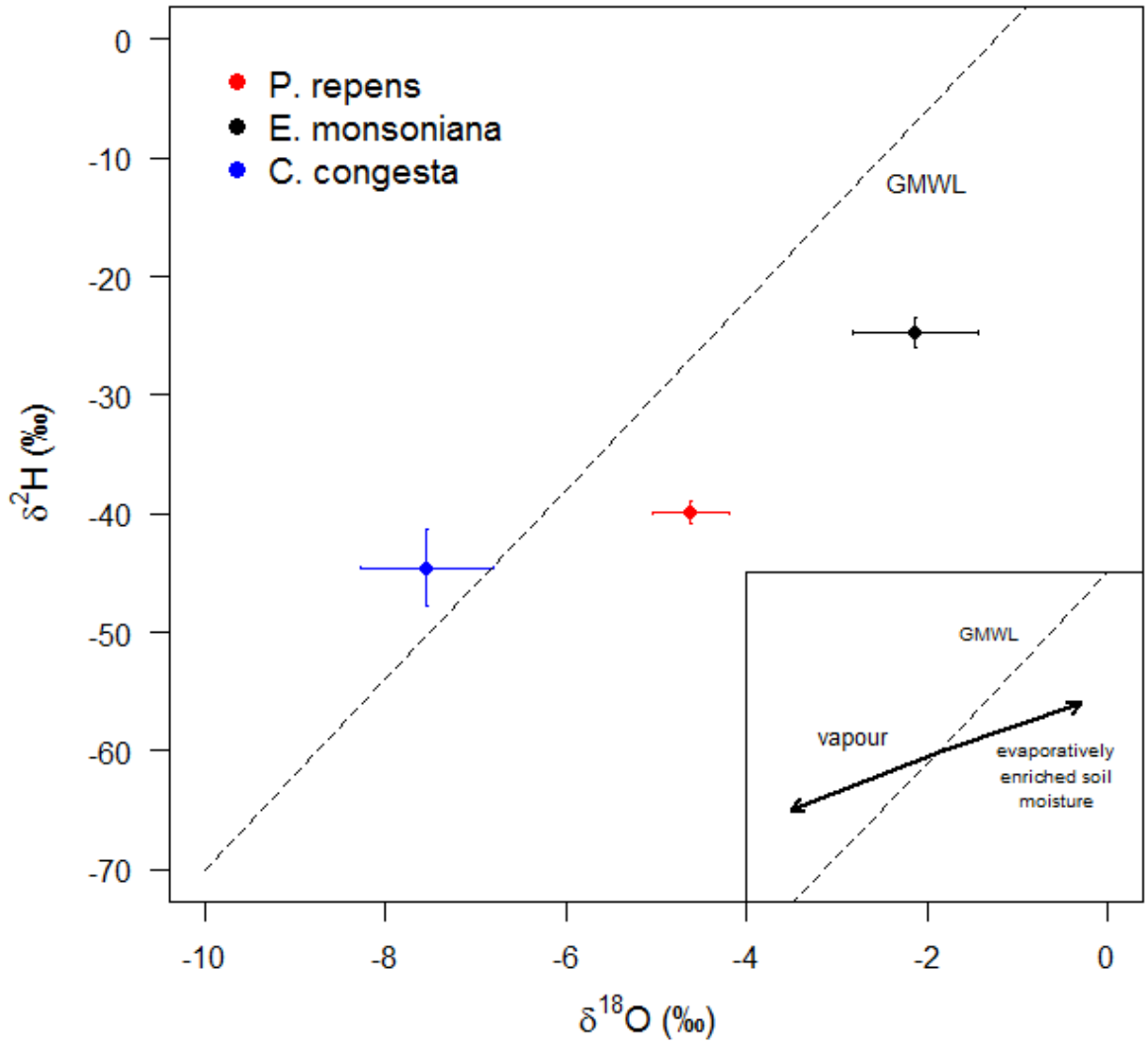

Figure 3.7: Dual stable isotopic composition of the three study species during a summer drought period in 2013. The relative position of each species is significant for determining relative rooting depth and sources of moisture (see "*Results—Stable isotopes and rooting depth*" above for details)

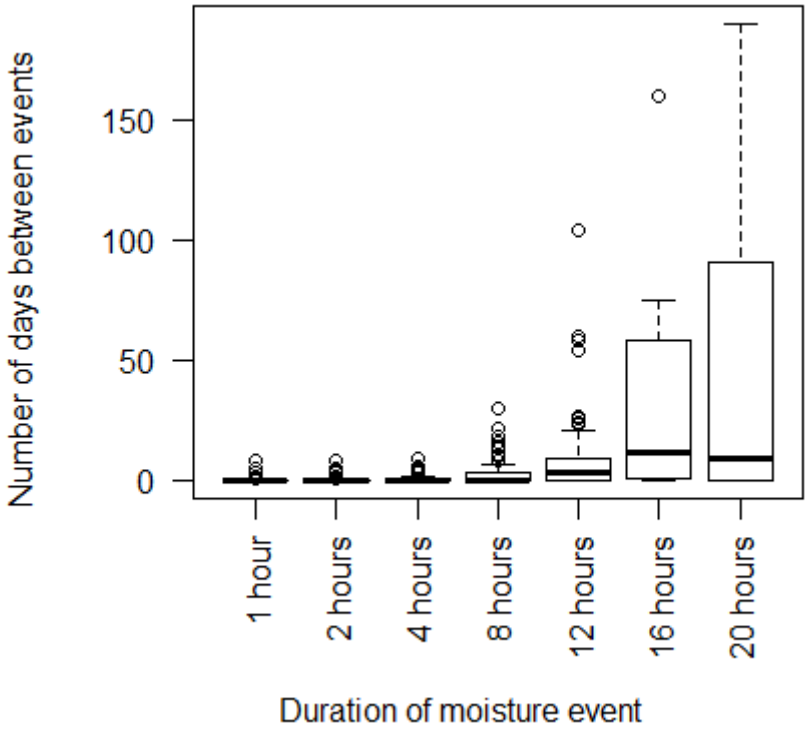

Figure 3.8: The relationship between the duration of time per day that a moisture event occurred at Jonaskop and the frequency at which these events occurred. Moisture events were inferred from a leaf-wetness sensor, which provides an indication of the amount of either rainfall or dew.

more evaporatively enriched (Fig. 3.7) and thus more likely to be taking up shallow, evaporatively enriched soil water. We used this to infer that *E. monsoniana* is relatively shallow-rooted compared to *P. repens*. Moisture extracted from *C. congesta* rhizomes was the most depleted in both $\delta^{18}O$ and $\delta^{2}H$, falling above the GMWL with a deuterium excess of approximately 5.8. This suggests that *C. congesta* either has access to deeper levels of groundwater than *P. repens* or is able to take up relatively depleted vapour. Qualitative excavations showed that *C. congesta* did not have roots deeper than approximately 20 cm and, consequently, we speculate that *C. congesta* is able to take up depleted atmospheric water sources (Clark & Fritz, 1997). Consistent with previous work in fynbos (Marloth, 1903, 1905), the local moisture source could have been cloud, fog or dew. Dew events are frequent at Jonaskop. For the duration of the study period, it was rare to go longer than a day without experiencing up to four hours of some kind of moisture event, as captured by the leaf-wetness sensor (Fig. 3.8). Although this sensor is unable to distinguish between rainfall and dew or cloud moisture, it indicates that atmospheric moisture inputs might be considerable at Jonaskop.

Species response to VPD and soil moisture

For all three species, sapflow was greatest when VPD and soil moisture were relatively high (Fig. 3.2, 3.9, 3.10 & 3.11). For all species, sapflow increased rapidly with an increase in VPD up to approximately 3 kPa. Above VPD of 3 kPa, the rate of increase in sapflow started to decline, although this response differed between years and species. Intra-species seasonal differences were most evident during the drier summer of 2012/13. During this drought period, *P. repens* and *E. monsoniana* were most strongly affected. Most noticeably, the mean late-season response to VPD fell below the 95% confidence interval of the early season response for both species, indicating that sapflow was significantly lower (Fig. 3.9). This response appeared to be caused by declining soil moisture since both species displayed steady declines in sapflow with declining soil moisture (Fig. 3.11). *C. congesta* remained relatively unaffected by the drought conditions and displayed no significant difference between early and late-season response to VPD (Fig. 3.9 & 3.10). A striking illustration of these results is shown using diurnal sapflow traces for days with similar mean VPD for early and late season in each year (Fig. 3.12). Diurnal sapflow declined to remarkably low levels in *E. monsoniana* in March 2013 compared to November 2012 (Fig. 3.12). A similar decline, yet not as extreme, was observed in *P. repens*. The diurnal sapflow traces for *C. congesta* were

consistent between early and late season (Fig. 3.12). There was also reverse sapflow in *C. congesta* individuals during periods when the dewpoint temperature was reached (e.g. Fig. 3.12), providing further evidence that they are able to take up moisture from dew events.

Seasonal differences in all species were less apparent in the wetter summer of 2013/14. Although the response of sapflow to increasing VPD was generally greater during the early season of 2013/14 for *E. monsoniana* and *P. repens* (Fig. 3.9, 3.10 & 3.12), these differences were less pronounced than the previous year (Fig. 3.10). There was no difference between the sapflow response over the early and late summer periods in *C. congesta* (Fig. 3.9, 3.10 & 3.12). These contrasting patterns can largely be explained by the higher soil moisture available in 2013/14 (Fig. 3.11 & 3.12). Although *E. monsoniana* displayed linear declines in sapflow with declining soil moisture in both years (Fig. 3.11), soil moisture did not drop as low in 2013/14. There was no obvious relationship between soil moisture and sapflow for *P. repens* and *C. congesta* in that year (Fig. 3.11). Again, the contrasting patterns of sapflow can be illustrated with diurnal traces on days with similar VPD. Diurnal sapflow for *E. monsoniana* and *P. repens* was slightly lower during the late season, but not as low as in the previous summer (Fig. 3.12). There was no difference in the diurnal sapflow traces for *C. congesta* (Fig. 3.12).

For all three species, stomatal sensitivity to changes in VPD was positively related to the reference stomatal conductance (Fig. 3.13), supporting the notion that plants with higher stomatal conductance are more sensitive to VPD (Oren *et al.*, 1999). By this measure, sensitivity to VPD was greatest in *C. congesta*, followed by *P. repens*, although there was a large amount of overlap in their responses (Fig. 3.13). *E. monsoniana* was the least sensitive to VPD in comparison with the other two species (Fig. 3.13).

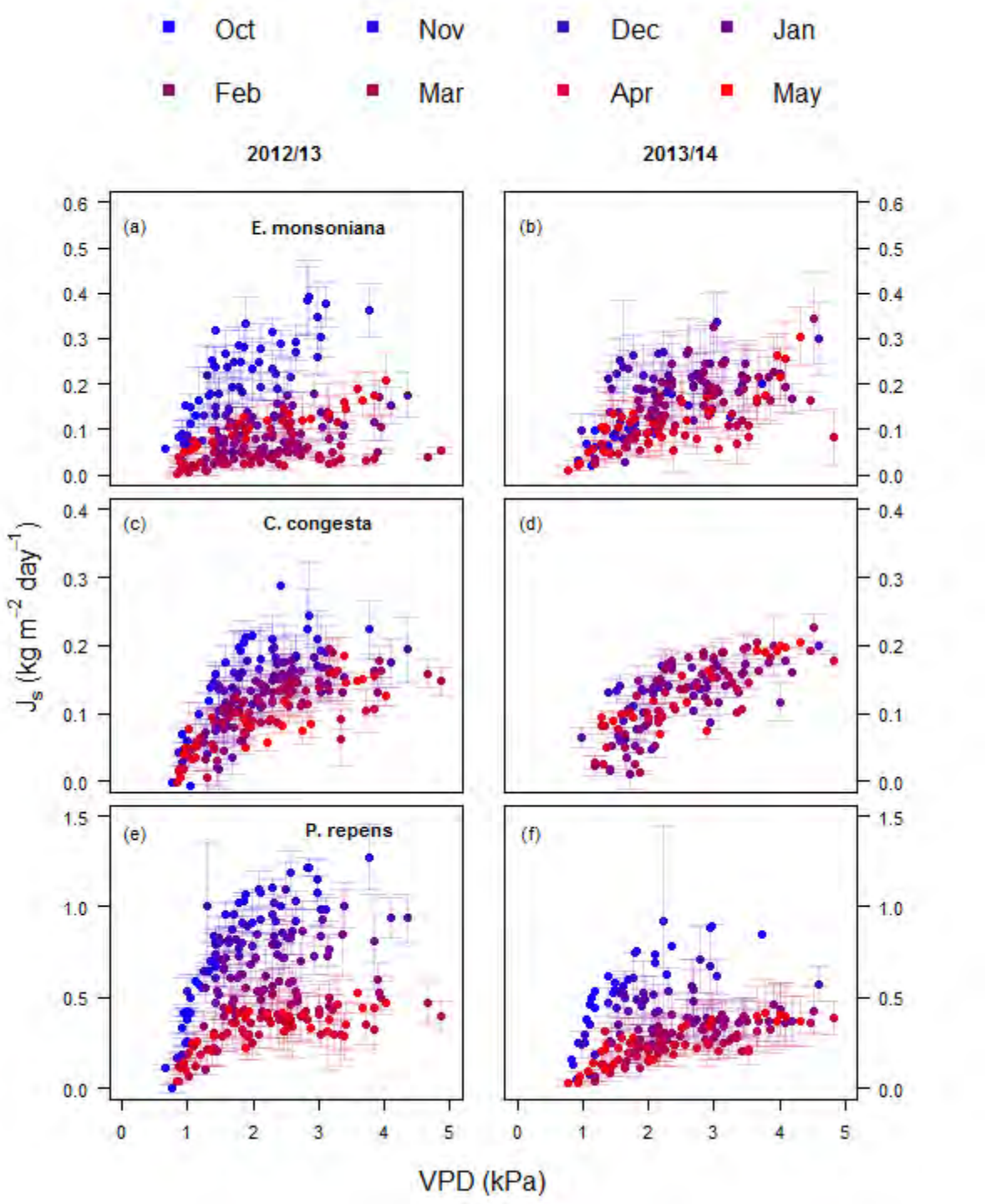

Figure 3.9: Mean total daily sapflow in response to mean daily VPD for 2012/13 ((a), (c) and (e)) and 2013/14 ((b), (d) and (e)) for *E. monsoniana* ((a) and (b)), *C. congesta* ((c) and (d)) and *P. repens* ((e) and (f)). Points are coloured by time and season to illustrate the within-season differences between years and species.

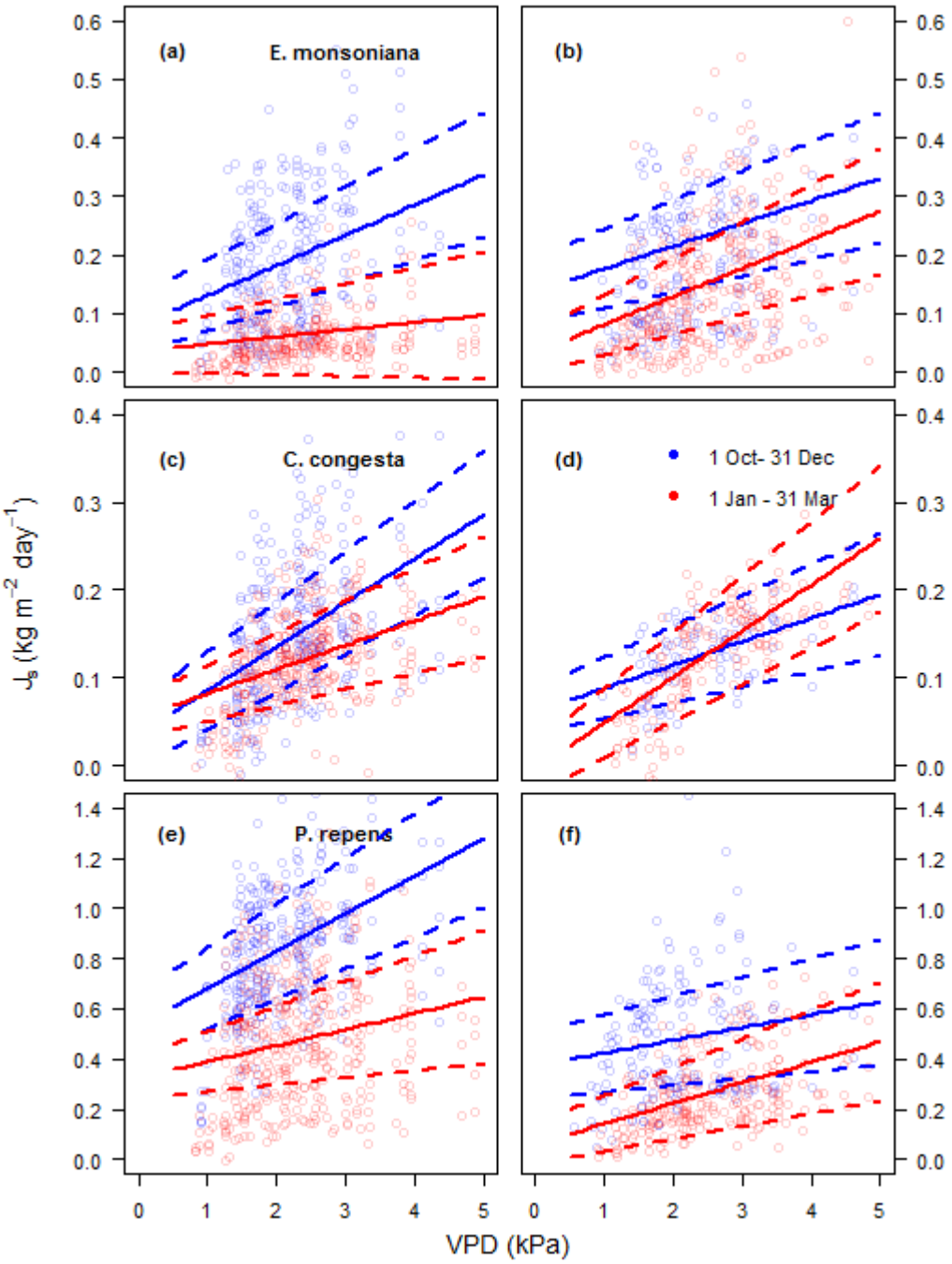

Figure 3.10: Linear model and 95% confidence intervals of sapflow response to VPD for early (1 October–31 December) and late (1 January–31 March) season for 2012/13 and 2013/14 for each of the three species. Responses were considered significantly different if the mean response of the late season fell outside of the 95% confidence region of the early season.

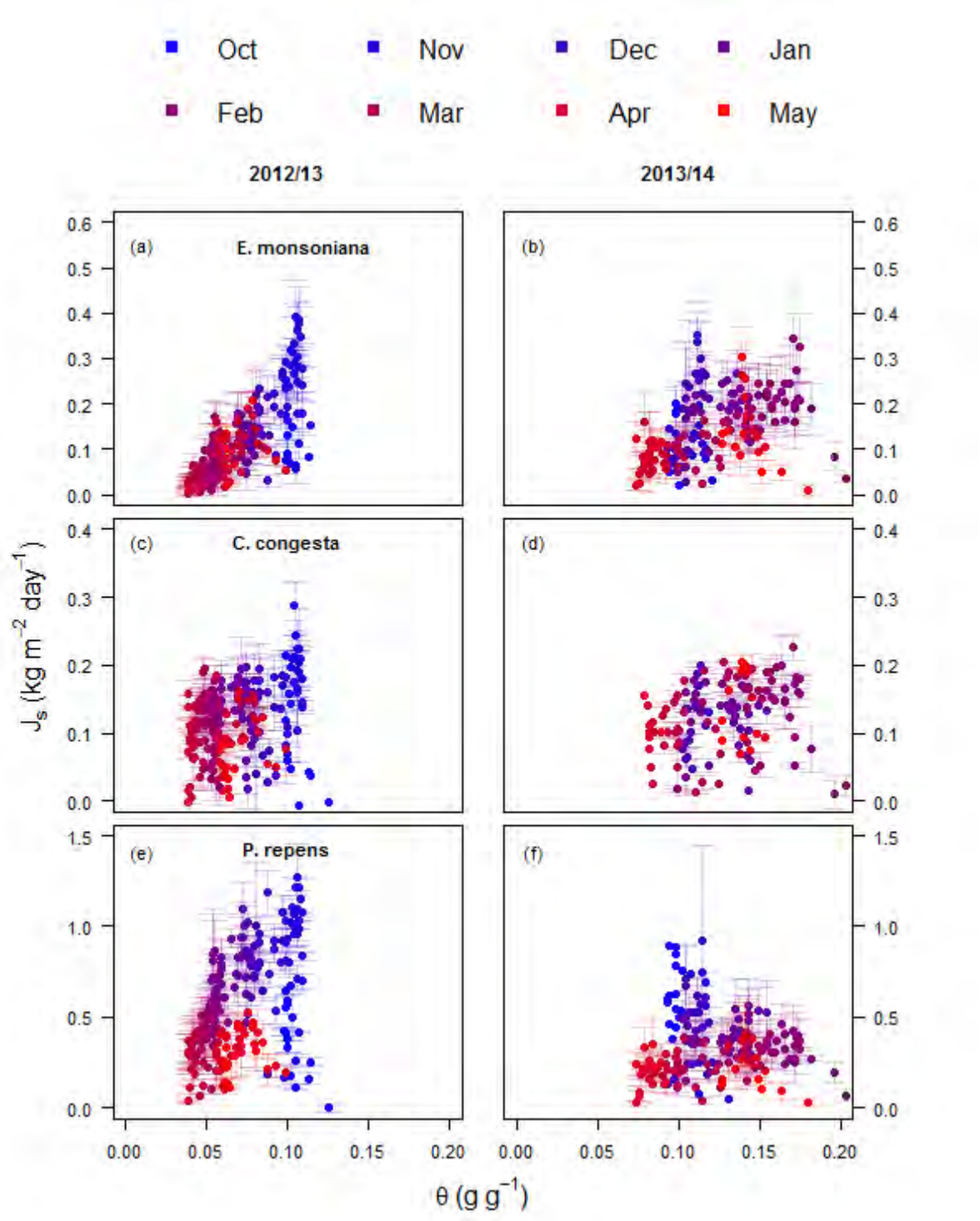

Figure 3.11: Mean total daily sapflow in response to mean daily soil moisture content (θ) for 2012/13 ((a), (c) and e) and 2013/14 ((b), (d) and (c)) for *E. monsoniana* ((a) and (b)), *C. congesta* ((c) and (d)) and *P. repens* ((e) and (f)). Points are coloured by time and season to illustrate the within-season differences between years and species.

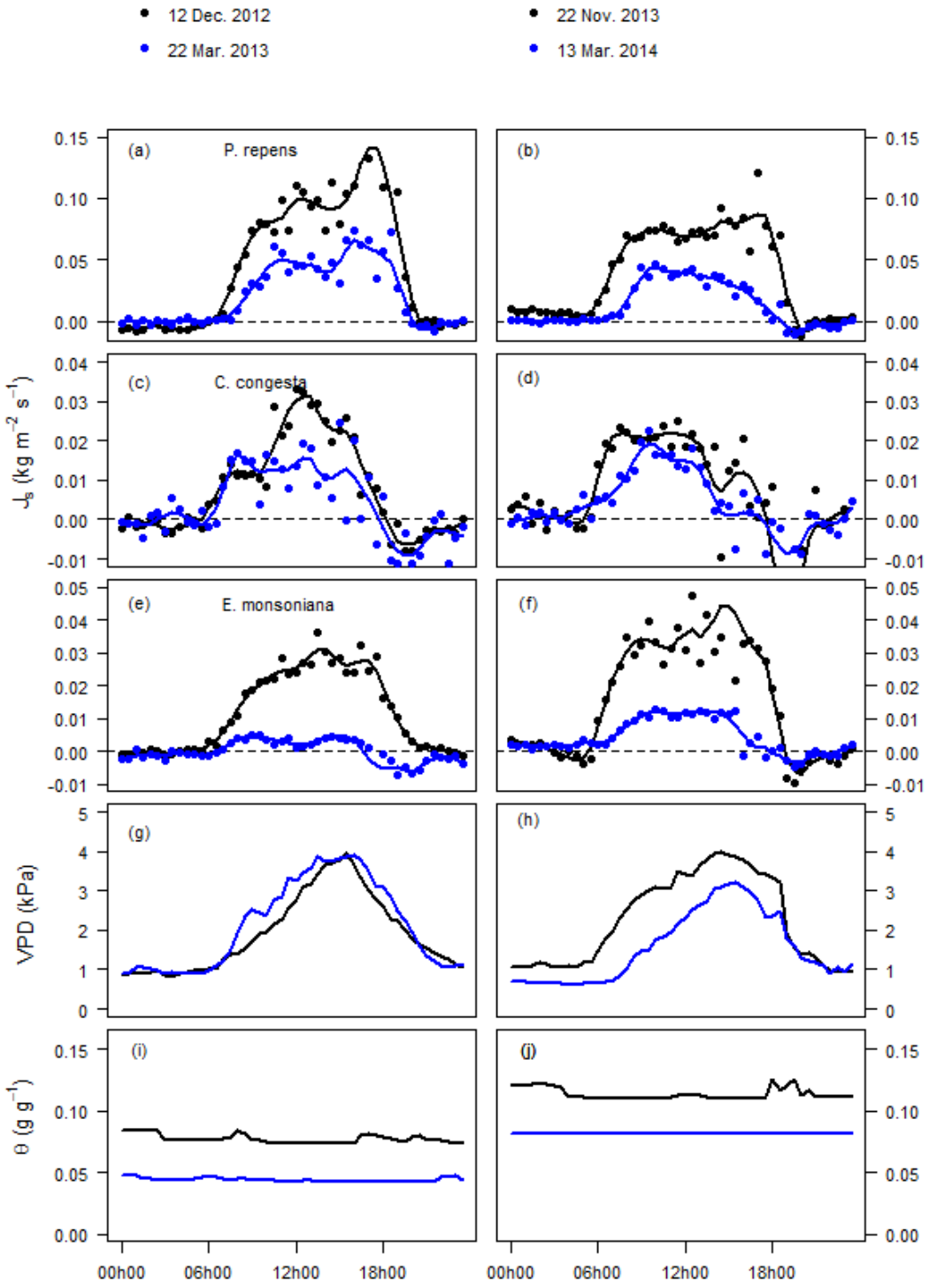

Figure 3.12: Early (black) and late (blue) season diurnal sapflow traces from two successive years for three species ((a)–(f)) showing differences caused by variation in environmental conditions. VPD ((g) and (h)) was similar on all four days, but the summer of 2012/13 was relatively dry compared to the summer of 2013/14, as shown by the soil moisture plots ((i) and (j)). See "*Results—Species response to VPD and soil moisture*" for an explanation.

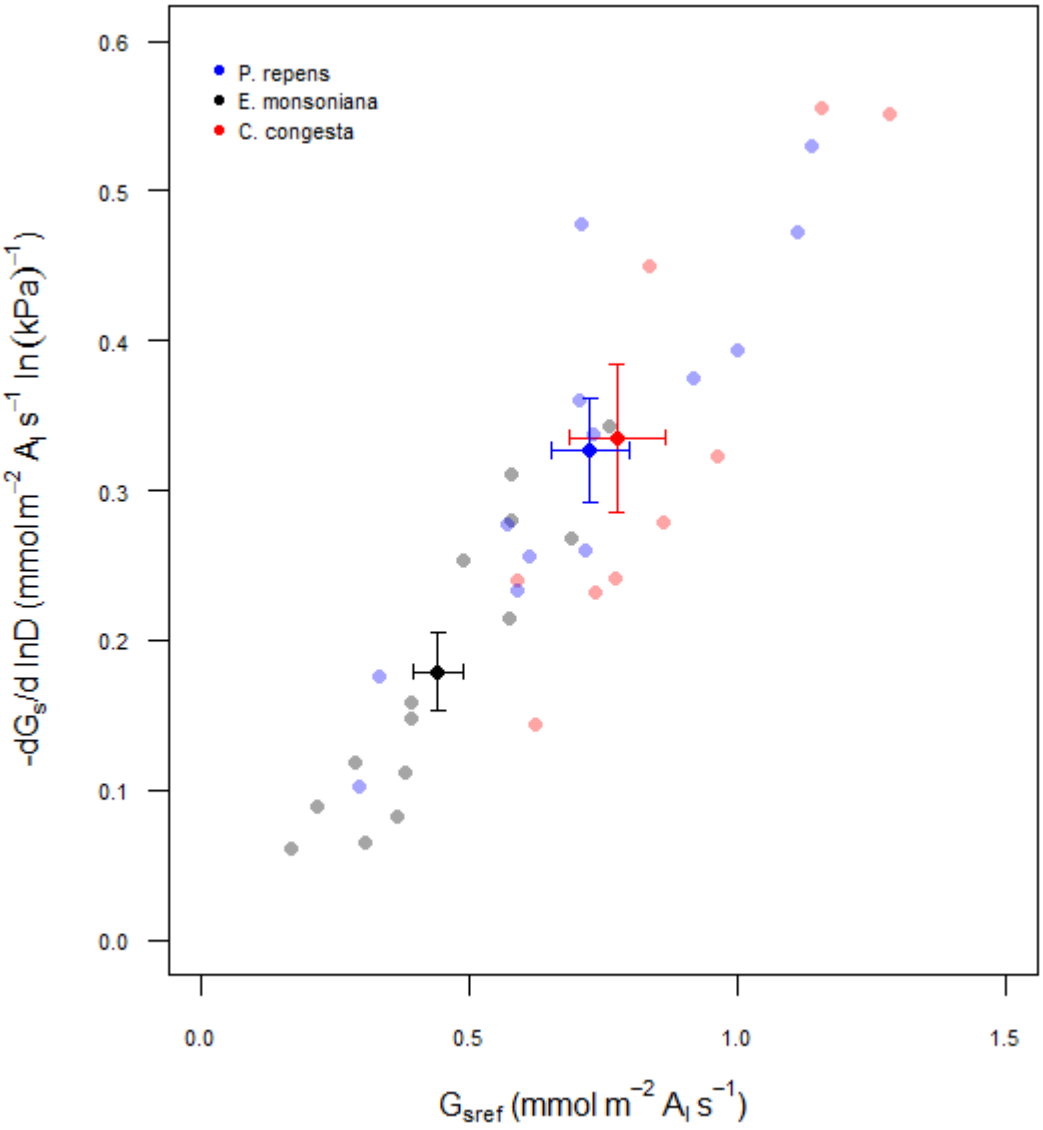

Figure 3.13: The relationship between the slope of the relationship between stomatal conductance and VPD and stomatal conductance at a VPD of 1 kPa for the three study species. Here, stomatal conductance was calculated from daily midday sapflow traces. Closed symbols with error bars represent species means with standard error, while transparent symbols represent values for individuals

Stem vulnerability to cavitation

The three study species varied in their vulnerability to cavitation, as established by the benchtop dehydration method (Fig. 3.14). *C. congesta* was the least resistant to cavitation, displaying an r-shaped vulnerability curve. Culms of this species were highly vulnerable, experiencing 50% loss of conductivity at a water potential of −0.9 MPa. There were no significant differences between males and females for this species (Fig. 3.14). *P. repens* displayed a sigmoidal vulnerability curve, experiencing 50% loss of conductivity at −3.00 MPa (Fig. 3.14). Although this value was slightly less negative than that of a previous study (−3.81 MPa) (Jacobsen *et al.*, 2009), there was a large degree of overlap between the two measures (Fig. 3.14). *E. monsoniana* also displayed an r-shaped vulnerability curve, with steep initial declines in hydraulic conductivity above −4 MPa and thereafter more gradual losses (Fig. 3.14). Although the water potential at 50% loss of conductivity was −1.6 MPa for this species, the 95% confidence interval for this measure ranged from −0.01 MPa to −3.05 MPa. Although some r-shaped vulnerability curves have been found to suffer from an "open-vessel" artefact, overestimating vulnerability of stems long vessels (Choat *et al.*, 2010), we consider this unlikely because of the method we used. The dehydration method remains the gold-standard method for determining vulnerability curves (Sperry *et al.*, 2012). Importantly, not all r-shaped curves are invalid (Sperry *et al.*, 2012). Instead, we suggest that our data for *E. monsoniana* are unlikely to be an artefact of long vessels and that they may result from a combination of large- and small-diameter vessels in the stem. Large-diameter vessels might be more vulnerable to cavitation, but would be important for efficient hydraulic conductance during wet periods (Hacke & Sperry, 2001; Hacke *et al.*, 2001).

Seasonal loss of hydraulic conductance

A comparison of P_{pd}, P_{md}, P_{stem} and P_{leaf} for *P. repens* at Jonaskop showed that the P_{pd} and P_{md} consistently provided lower and upper bounds of P_{stem} (Fig. 3.15). P_{md} was also consistently less negative than P_{leaf} (Fig. 3.15). These measurements were taken during the height of summer (October to January) in a relatively dry year (2012/13), when night time transpiration is expected to be greatest. As a consequence we feel that it is valid to assume that P_{pd} and P_{md} may provide reliable estimates of the lower and upper bound respectively of PLC experienced in the stem throughout the course of the study. This provides strong justification for the envelope approach to estimating PLC in situ that we present in this study.

This analysis allowed us to examine differences between PLC experienced by species occurring at Jonaskop.

E. monsoniana displayed large fluctuations in PLC throughout the year, with large losses of conductance during periods of drought (Fig. 3.16). Using the conservative envelope approach, our results showed that this species experienced a reduction from 35 – 40% in early summer up to approximately 70 – 80% in the late summer of 2011/12 and 70% in 2012/13 (Fig. 3.16). *E. monsoniana* therefore experienced a reduction of hydraulic conductance of approximately 40% throughout the summer season. By comparison, *P. repens* maintained PLC below 30% throughout the entire period that we measured (Fig. 3.16). Culms of *C. congesta* experienced a relatively constant PLC of between 50 and 80% throughout both years, although, during times of severe soil moisture deficit in 2011/12 and 2012/13, this value reached up to 90% loss of conductance.

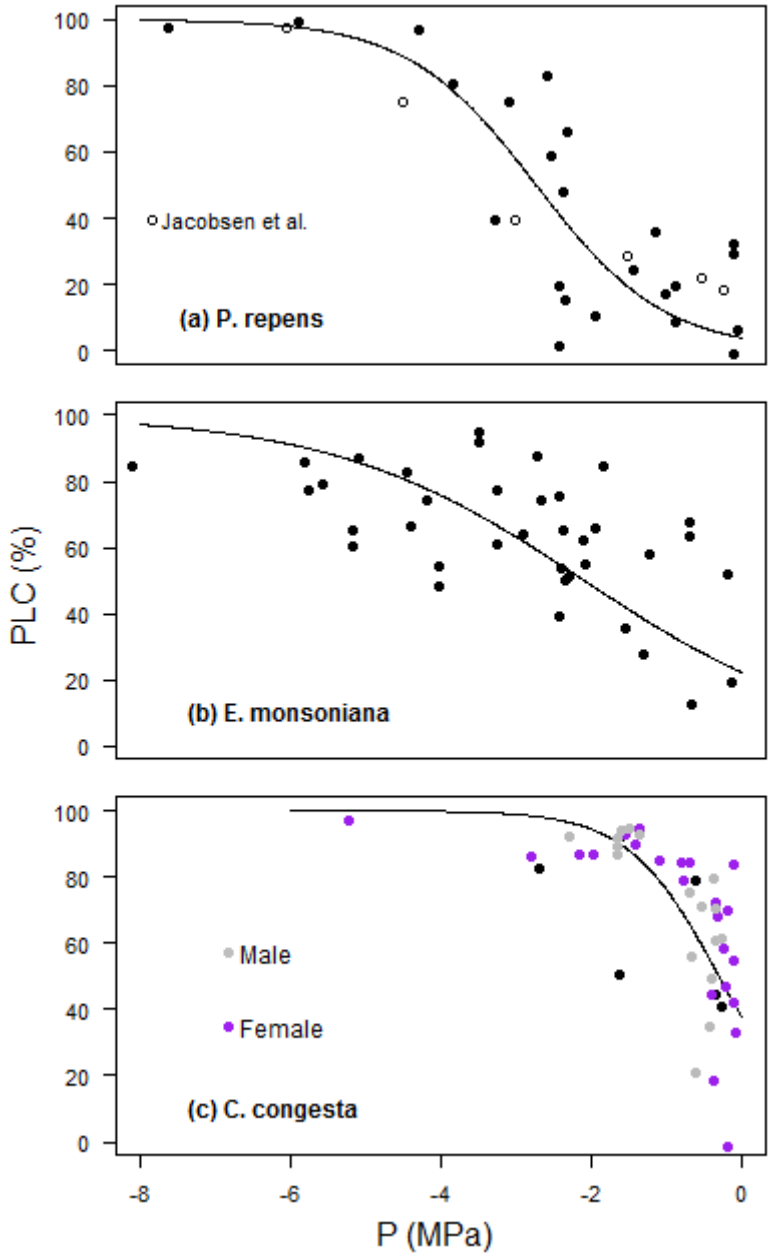

Figure 3.14: Vulnerability curves for the three study species produced using the benchtop dehydration technique. Prior measurements of vulnerability for *P. repens* from a separate study are shown in (a) (Jacobsen *et al.*, 2009). For the dioecious *C. congesta* (c), measurements were taken on males (grey) and females (purple).

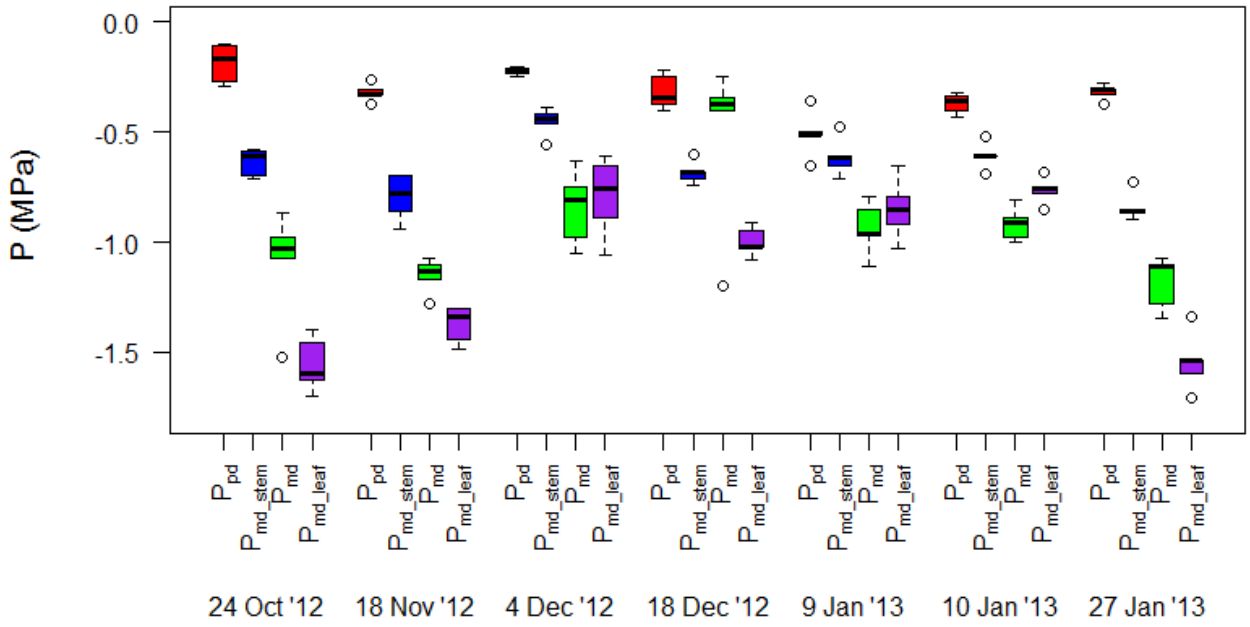

Figure 3.15: A comparison of various measures of water potential for *P. repens* collected for a separate study from October 2012 to January 2013. Predawn shoot water potential (P_{pd}) was consistently lower (i.e. less negative) than midday stem water potential (P_{md_stem}), providing support for its use as a lower bound estimate of PLC in the stem. Midday shoot water potential (P_{md}) was consistently higher (i.e. more negative) than P_{md_stem}, providing support for its use as an upper bound estimate of PLC in the stem.

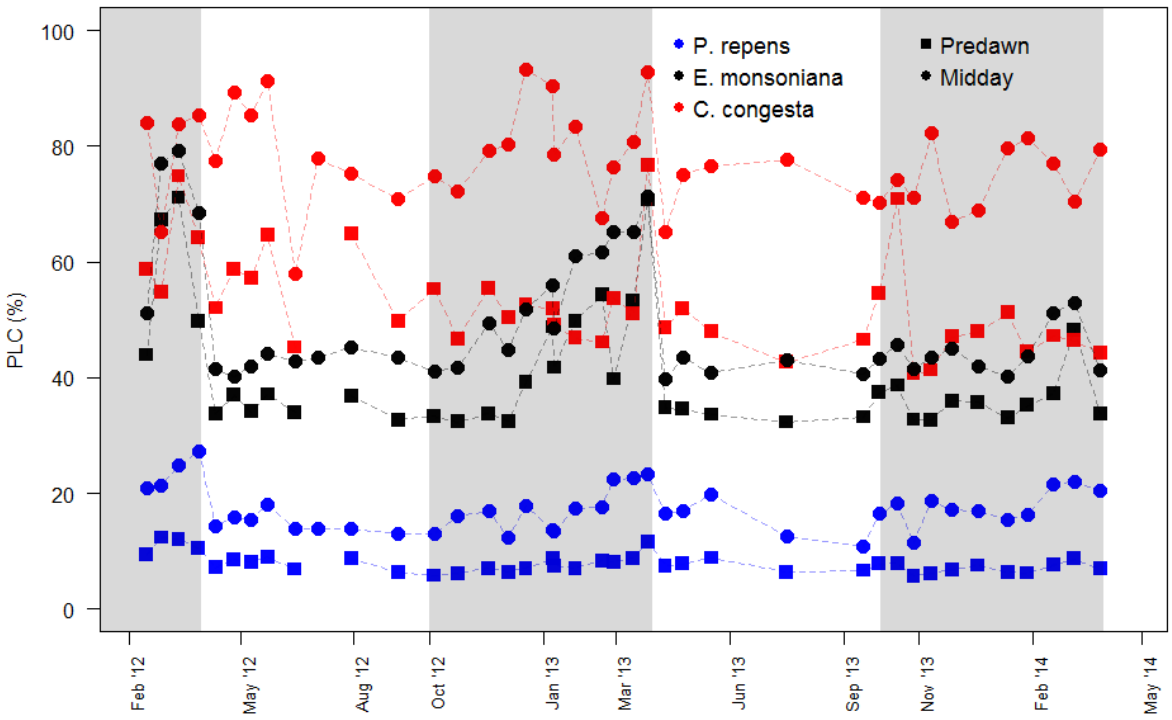

Figure 3.16: Timeline of the envelope of PLC in situ for the three study species calculated using the vulnerability curves and mean predawn and midday water-potentials. The shaded grey bars are six-month intervals between 1 October and 31 March each year. During this period, the study site experiences relatively hot and dry conditions compared with the remaining six months.

Response to summer rainfall events

The response to summer rainfall events varied between species. A comparison of sapflow before and after a rain event during the summer of 2012/13 showed that *E. monsoniana* increased sapflow by more than 60% from pre-rain-event levels (Fig. 3.17 & 3.18). Species in which stomatal conductance is limited primarily by low xylem water potential may recover rapidly following rehydration (Brodribb & McAdam, 2013). By contrast, *P. repens* and *C. congesta* did not appear to respond strongly to these events (Fig. 3.17 & 3.18). It is likely that *P. repens* and *C. congesta* did not respond to this rainfall event as they were both relatively well hydrated and already transpiring at close to maximum values (Fig. 3.1 & 3.3). Alternatively transpiration rate may remain relatively constant even when a plant is able to take up moisture and increase xylem conductance if the difference between soil and leaf water potential (Δ P) decreases.

Carbon uptake during drought events

All three species displayed reductions in leaf-level carbon gain during the dry summer periods (Fig. 3.19). The summer of 2012/13 was worse for all three species than the mild summer of 2013/14 (Fig. 3.18). *E. monsoniana* and *P. repens* both experienced leaf-level carbon deficit during summer drought periods (Fig. 3.19). The worst of these occurred during the summer drought of 2012/13, when *P. repens* experienced up to several days and *E. monsoniana* over a month without leaf-level carbon gain. Although *P. repens* displayed relatively consistent water potential values over the course of the study, the sensitive stomatal response to desiccation resulted in periods of net carbon loss during both summers. In *E. monsoniana*, the stomatal response was less sensitive, but water potentials declined enough to ensure periods of stomatal closure and limited carbon uptake. Although *C. congesta* maintained positive leaf-level carbon uptake throughout the entire study period, it showed declines in periods of moisture deficit.

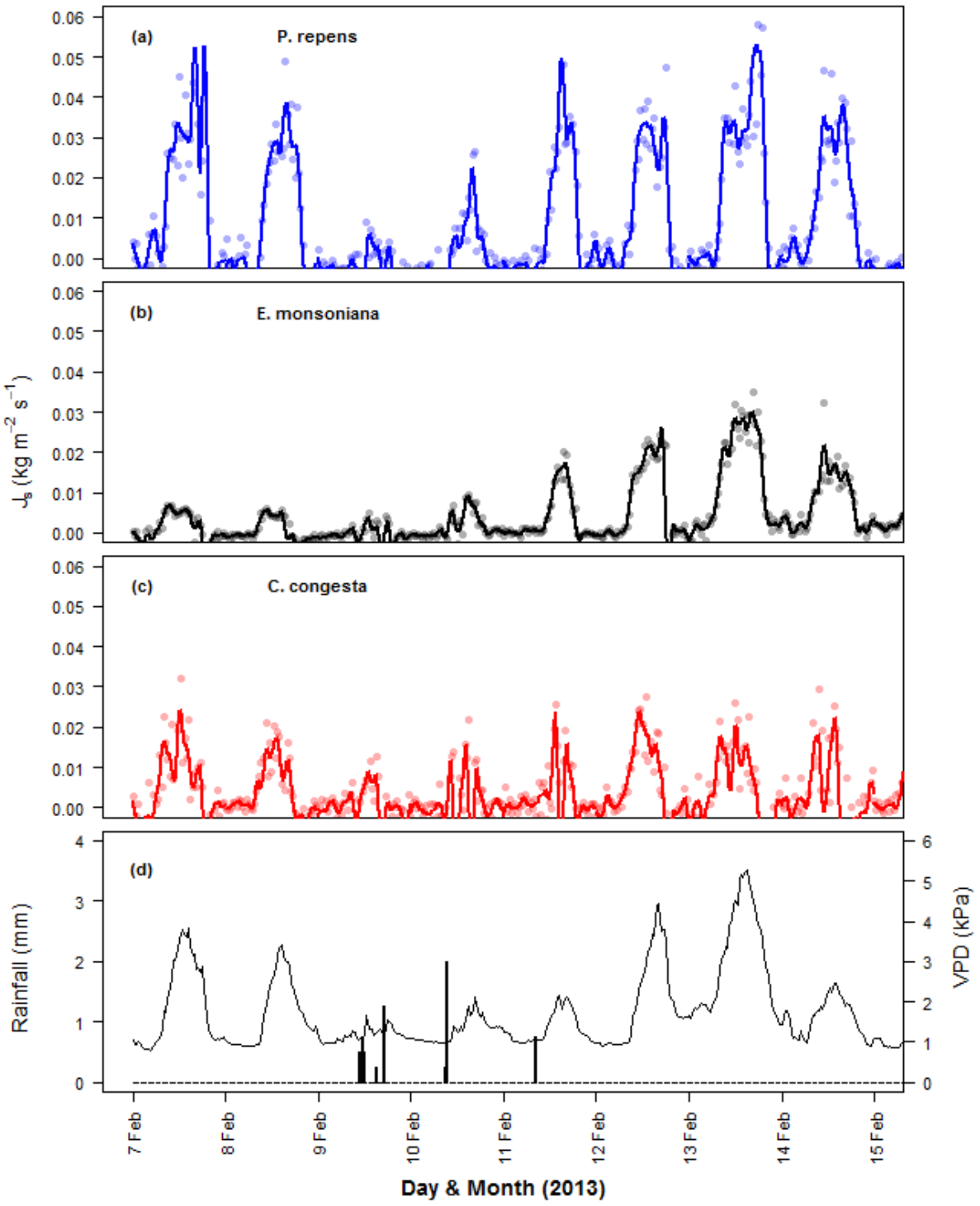

Figure 3.17: Diurnal courses of sapflow response for eight consecutive days in the 2012/13 summer season for (a) *P. repens*, (b) *E. monsoniana* and (c) *C. congesta* showing how each species responded to a pulse rainfall event (d).

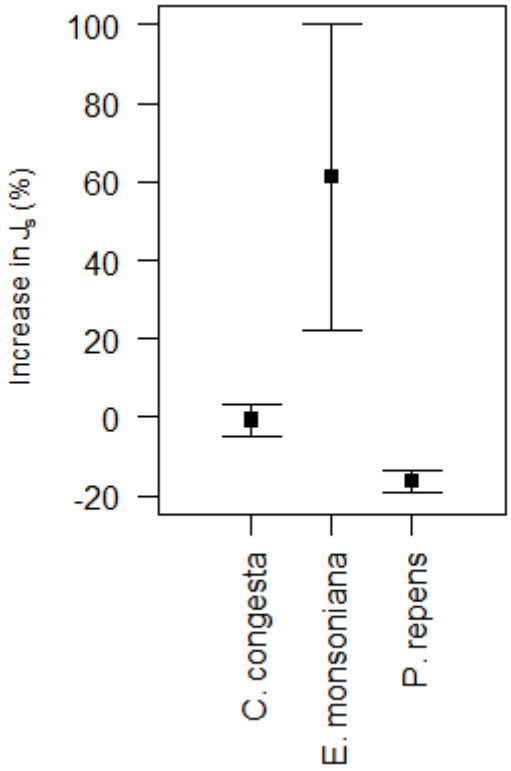

Figure 3.18: Percentage change in total daily sapflow two days after a rainfall event relative to two days prior to the event during the 2012/2013 summer season for each of the three study species.

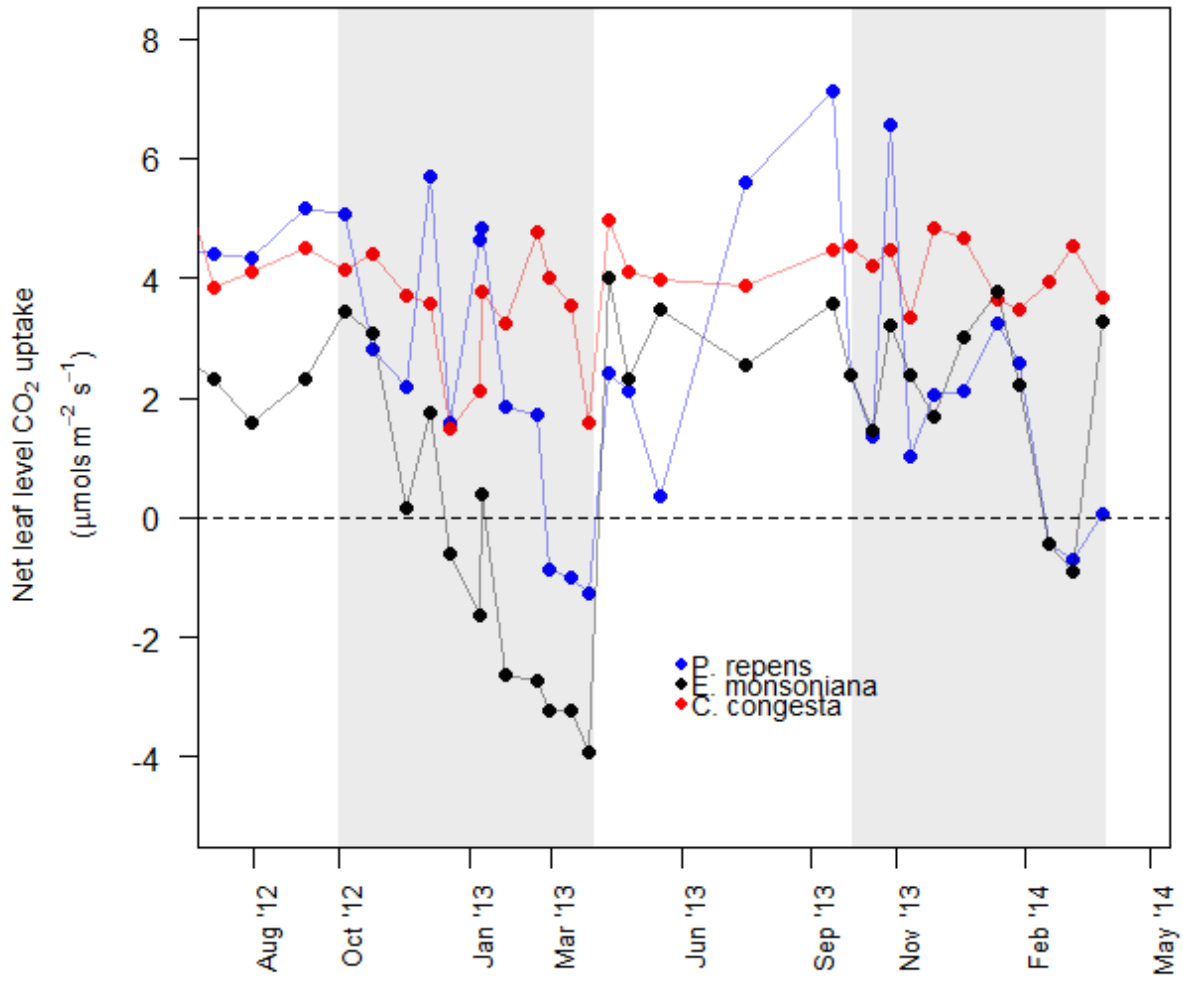

Figure 3.19: Timeline of net leaf-level photosynthetic carbon gain over the study period for each of the three study species. Leaf-level carbon gain in each species was estimated by combining *in situ* predawn water potential values with a modelled relationship between assimilation rate and water potential (see "*Methods—Modelling carbon gain and seasonal PLC*" for details)

Discussion

Detailed assessment of physiological responses and functional trait variability revealed distinct hydraulic regulation strategies in response to major environmental drivers within mountain fynbos communities. Consistently high water potential and rapid declines in stomatal conductance with declining water potential observed in *P. repens* are strongly consistent with isohydric water potential regulation. By contrast, the observation of large seasonal differences in water potential and the relatively gradual decrease of stomatal conductance in *E. monsoniana* are strongly indicative of an anisohydric response. Although *C. congesta* maintained relatively high predawn water potentials throughout periods of seasonal drought, it displayed low stomatal regulation of water potential and high loss of xylem conductivity. The results of this study are highly consistent with a previous investigation into the hydraulic regulation strategies of fynbos functional types conducted on different species at a field site far removed (>100 km) from our present study location (West *et al.*, 2012). This allows us to extend our results beyond the species in this study and to comment more broadly about hydraulic regulation strategies of fynbos functional types. Significantly, our findings support the notion that proteoid species adopt isohydric water regulation, while ericoid species are mostly anisohydric. Since contrasting hydraulic regulation strategies may have implications for mechanisms of mortality (McDowell *et al.*, 2008; West *et al.*, 2012), this finding may be crucial for predicting vulnerability to future climate-change-type drought events within fynbos communities.

Importantly, our study went beyond merely describing hydraulic regulation strategies in fynbos communities. We explored associations between physiological responses, key functional traits and environmental variables to gain deeper insight into physiological mechanisms operating in these species. Significantly, we found strong support for our hypothesis that isohydric species should be more sensitive to VPD than anisohydric species. Our data also illustrate how knowledge of rooting depth and stem hydraulic vulnerability is crucial to understanding the mechanisms underlying inter- and intra-species seasonal differences. In turn, this provides greater insight into which environmental variables are crucial to the persistence of each species. The case seems to be clearest in *P. repens*. This species displayed significant reductions in sapflow in the latter stages of the summer of 2013/14 and slight reductions in 2013/14. However, the water potential and vulnerability-curve data showed that the mechanism underlying these distinct responses was not a loss of

hydraulic conductance. Instead, we propose that the mechanism underlying reductions in sapflow was stomatal closure to prevent cavitation. This is supported by evidence that *P. repens* was more sensitive to VPD than the anisohydric *E. monsoniana*. Greater sensitivity to VPD rather than soil moisture could provide an early signal to close stomata and to, consequently, avoid cavitation (Jones & Sutherland, 1991). As such, *P. repens* is not likely to suffer drought-induced hydraulic failure during severe drought events, nor does it rely heavily on summer rainfall for maintaining hydraulic conductance. Future increases in temperatures might, however, lead to further reductions in stomatal conductance and impose greater carbon limitations on this species.

E. monsoniana displayed a contrasting seasonal response to drought in comparison to *P. repens*. This response was more characteristically anisohydric. In particular, *E. monsoniana* experienced declining minimum midday water potentials during the summer drought periods. These resulted in decreases in seasonal sapflow, presumably caused by stomatal closure (Tyree & Sperry, 1988, 1989). Vulnerability-curve data indicated that those water potentials experienced *in situ* were sufficient to induce large seasonal losses of stem hydraulic conductance. Importantly, water potentials came close to exceeding P_{88}, a critical point from which many angiosperms fail to recover (Urli *et al.*, 2013; Choat, 2013). These data suggest that *E. monsoniana* is highly vulnerable to hydraulic failure during future summer drought events (Tyree & Sperry, 1988). This is consistent with observations of mortality of E. monsoniana individuals occurring at Jonaskop following the drought period of 2012/2013 (Plate 3.2).

Continuous measurements also showed that *E. monsoniana* has the ability to recover hydraulic conductance relatively rapidly following summer rainfall events. Since the period of recovery was a matter of days and presumably too short for new xylem to have developed, we infer that the increase in total daily sapflow was caused by a refilling event (Scoffoni *et al.*, 2012). This is the first time that a refilling event has been documented in mountain fynbos, further highlighting the importance of continuous measurement for deciphering physiological mechanisms. Although we are uncertain of the exact mechanism of recovery in *E. monsoniana*, plausible options are positive root pressure or osmotic redistribution (Salleo *et al.*, 2004). Irrespective of the exact mechanism, a reliance on summer precipitation events for recovery of hydraulic conductance may make *E. monsoniana* highly susceptible to future climate change.

The response of *C. congesta* was slightly more complex than that of the other two species. Field water potentials did not decline below −2 MPa and (apparent) stomatal conductance was also highly sensitive to VPD. Yet, vulnerability curves indicated that this species experienced significant losses of stem hydraulic conductance. *C. congesta* also displayed relatively constant total daily transpiration rates and smaller seasonal differences in sapflow than the other two species. These observations may be explained by anisohydric regulation of stomatal conductance and regular refilling of xylem embolism throughout summer (Scoffoni *et al.*, 2012). We provide several independent lines of evidence showing that *C. congesta* is able to take up moisture from dew events. These events occur frequently at Jonaskop, providing a potentially valuable source of moisture during dry periods. This is consistent with previous studies on restioid species indicating that they are able to take up cloud moisture (Marloth, 1903, 1905; West *et al.*, 2012). This response is not easily classified by either isohydric or anisohydric water potential regulation, but might be closer to isohydry.Could it be given a different or new term? Alternative terminology has been developed for isohydrodynamic species: those that maintain a relatively constant difference between predawn and midday water potential (Franks *et al.*, 2007). However, we feel that this term does not adequately describe the response of *C. congesta*, which does not exhibit a constant difference between predawn and midday water potential. Instead, the relatively insensitive stomatal response in addition to regular refilling and constant predawn water potential could be referred to as “anisodynamic”. This mechanism fits with phenological observations of growth and flowering in the species (pers. obs.). Rapid growth and flowering in *C. congesta* occurs almost concurrently in early spring when water is available (Plate 3.3). From that point onward the mature culm becomes highly cavitated and transpiration may gradually decline. After one or two seasons the culm is discarded (Plate 3.4). Further study might be necessary to determine whether this response is unique enough to warrant a new term. Nevertheless, the response is certainly different from that of the other species in this study, which provides further evidence for the existence of hydraulic niche separation within fynbos communities.

Finally, we speculate that carbon limitation may be an important mechanism of mortality in fynbos species. During the summer drought period of 2012/13, *P. repens* and *E. monsoniana* both experienced periods of carbon deficit, suggesting that they are vulnerable to carbon limitation during summer drought periods. *E. monsoniana* is of particular concern, since its shallow rooting resulted in longer periods of moisture stress and, consequently, lengthier

periods without carbon accumulation. However, it is important to note that our measure of net carbon uptake is not necessarily representative of the total availability of carbon, as it does not incorporate stored carbon reserves or changes in the metabolic rates of these species, precluding us from making strong statements about carbon starvation in these species at present. The role of carbon limitation in plant mortality is currently a hot topic in plant ecophysiology (Sala & Hoch, 2009; Adams *et al.*, 2009; Sala, 2009; Sala *et al.*, 2010, 2012; Mitchell *et al.*, 2014) and the need to address our ignorance with respect to its role in fynbos mortality is urgent.

Plate 3.2: Evidence of mortality: a dead *E. monsoniana* individual at Jonaskop during spring 2013. Photograph by Robert Skelton. 5 October 2013.

Plate 3.3: Flowering display on a newly emerged culm of a male *C. congesta* individual at Jonaskop during spring 2013. Photograph by Robert Skelton. 5 October 2013.

Plate 3.4: Culm mortality of *C. congesta* individuals at Jonaskop during spring 2013. Photograph by Robert Skelton. 5 October 2013.

Chapter Four: Using functional traits to predict the vulnerability to drought of forty species from Mediterranean-type shrubland communities of South Africa.

Abstract

Background/Questions/Methods

Attempts to understand the mechanisms underlying plant mortality during drought have led to the emergence of a hydraulic framework describing distinct hydraulic strategies. This framework distinguishes species that respond to dehydration by rapidly decreasing stomatal conductance (g_s), thereby maintaining high water potential (isohydric), from those that maintain positive gs, thereby maintaining carbon assimilation albeit at the cost of hydraulic dysfunction (anisohydric). However, portraying the hydraulic framework as a dichotomy between isohydry and anisohydry may obscure important continuous variation in hydraulic regulation, particularly in complex communities with high functional-trait diversity. The purpose of this study was to investigate the range of hydraulic strategies present across a large sample of species from a diverse community. Using stomatal response curves from laboratory-based drydowns for forty species from South Africa's Cape Floristic Region (CFR) together with vulnerability curves, we developed a novel framework that assessed co-ordination between measures of vulnerability (the water potential inducing 50% loss of conductivity, P_{50}, and the minimum water potential, P_{min}) and the water potential inducing stomatal closure (P_{g12}). We used the differences between P_{g12} and $P_{50,}$ and P_{g12} and P_{min} as proxies for stomatal regulation of cavitation and carbon limitation, respectively, and the percentage loss of conductivity (PLC) at P_{min} as a proxy for hydraulic dysfunction.

Results/Conclusions

Our data showed that species varied in the degree to which they regulated cavitation through stomatal closure and experienced seasonal declines in water potential and that these differences resulted in distinct predictions of mechanisms of mortality. Restioids had combinations of high vulnerability to embolism, low P_{g12} and low P_{min} that led to high levels of hydraulic failure. Proteoids avoided hydraulic failure and carbon limitation by maintaining relatively high P_{min}. Ericoid species varied in vulnerability and seasonal PLC, resulting in two distinct predictions of mortality within this functional type. *Erica* species had a combination

of P_{g12} and P_{min} that led to both high hydraulic failure and carbon limitation, while species of Asteraceae displayed more negative P_{50} values and, consequently, were predicted to suffer carbon limitation only. We also showed that a continuum existed in the degree to which diverse species in our Mediterranean-type community regulated cavitation through stomatal closure. There was strong agreement between predictions from our framework and those from long-term field-based studies in the same communities. This, together with the relative ease with which trait data can be produced, suggests that our novel framework will be valuable for predicting the response of diverse communities to future climate-change-type drought events.

Introduction

Increased frequency of plant mortality is predicted in response to global climate-change-induced drought events (Allen *et al.*, 2010; McDowell, 2011). Such a threat has resulted in attempts to understand the precise mechanisms underlying plant mortality and to determine which species are more vulnerable than others (McDowell *et al.*, 2008; Choat, 2013). A hydraulic framework describing distinct hydraulic regulation strategies and the influence of these on carbon balance and the integrity of the soil-plant hydraulic pathway during drought periods has emerged (Zimmermann, 1983; Tyree & Sperry, 1988; Jones & Sutherland, 1991; Tyree & Ewers, 1991; Sperry *et al.*, 1998; McDowell *et al.*, 2008). This framework distinguishes between species that respond to dehydration by rapidly decreasing stomatal conductance, thereby maintaining relatively high plant water potential and those that maintain relatively high stomatal conductance in response to dehydration, thereby maintaining carbon assimilation (Tardieu & Simonneau, 1998). The framework builds on the paradigm of grouping species as either drought-avoiding (isohydric) species or drought-tolerating (anisohydric) species (Tardieu & Simonneau, 1998; McDowell *et al.*, 2008). Most importantly, it has utility in understanding current patterns of drought-induced mortality, which will enhance predictions of future responses (McDowell *et al.*, 2008).

Under severe drought conditions, drought tolerators are likely to suffer hydraulic failure as the water column in the soil-plant-atmosphere continuum comes under increasing tension (Tyree & Sperry, 1988, 1989; Tyree & Ewers, 1991; Sperry *et al.*, 1998). Conversely, during prolonged drought events, drought avoiders may suffer carbon starvation due to stomatal closure or leaf shedding (Tyree *et al.*, 1993; Sevanto *et al.*, 2013), although the precise manner in which this operates remains contentious (Sala & Hoch, 2009; Adams *et al.*, 2009; Sala, 2009; Sala *et al.*, 2010, 2012). Currently, the primary example of where the hydraulic framework has allowed accurate assessment and prediction of drought mortality is in the Piñon-Juniper woodlands of the eastern United States, a system composed of two dominant species (Breshears *et al.*, 2005; West *et al.*, 2007a,b; McDowell *et al.*, 2008; Plaut *et al.*, 2012). Here, the isohydric *Pinus edulis* experienced large-scale mortality induced by long-term carbon limitation during recent drought events, while the anisohydric *Juniperus monosperma* and *J. osteosperma* were largely unaffected (Breshears *et al.*, 2005, 2009; West *et al.*, 2007b, 2008). However, the utility of the hydraulic framework has yet to be thoroughly examined in highly diverse communities where it is unclear to what extent species separate

out into the isohydric-anisohydric dichotomy or form a continuum of hydraulic strategies. In functionally diverse communities, the significant variety in other key hydraulic functional traits, such as rooting depth (West *et al.*, 2012), may promote greater diversity of stomatal regulation strategies and reveal unique pathways to mortality. For example, shallow-rooted species that close stomata early in response to drought to avoid hydraulic failure may still reach low water potentials as the soil dries out and, therefore, suffer loss of conductivity during protracted drought periods. This leads to the possibility that shallow-rooted species with sensitive stomatal response risk both carbon limitation and hydraulic failure. Here we describe a novel trait-based system for predicting hydraulic strategies and mortality mechanisms designed to expand the role of the hydraulic framework within diverse communities.

The primary objectives of this study were to describe the range of stomatal response strategies in a diverse community and to predict likely mechanisms of mortality using associations between functional traits. The relationship between stomatal response and xylem vulnerability is fundamental to understanding the range of hydraulic strategies within a community and for predicting the likely mechanism of mortality of each individual species (Brodribb & Jordan, 2008; Meinzer *et al.*, 2009). In isolation, vulnerability to cavitation does not necessarily equate to risk of embolism *in situ,* since tight stomatal regulation of water potential might prevent its occurrence (McDowell *et al.*, 2008). Several species have been shown to close their stomata prior to the onset of cavitation, suggesting a primary role of stomata in those species of preventing embolism (Tyree & Sperry, 1988; Jones & Sutherland, 1991; Sperry & Pockman, 1993; Sparks & Black, 1999; Brodribb & Holbrook, 2003; Froux *et al.*, 2005; Brodribb & Jordan, 2008). However, this is not the case for all species; many tolerate some degree of hydraulic failure *in situ* prior to stomatal closure (Tardieu & Simonneau, 1998; West *et al.*, 2008; Plaut *et al.*, 2012). The concept of a safety margin describes this variation between species (Meinzer *et al.*, 2009; Johnson *et al.*, 2011; Choat *et al.*, 2012). Safety margins are usually assessed as the difference between a critical point on the vulnerability curve (e.g. the water potential at 50% loss of conductivity, P_{50}) and the minimum seasonal water potential, P_{min} (Meinzer *et al.*, 2009; Choat *et al.*, 2012). Large positive differences imply a relatively conservative stomatal response, while small differences (or even negative differences) suggest a hydraulically risky response.

Here, we use the concept of a safety margin to define the hydraulic strategy of each species with two slight modifications. Implicit in the definition of a safety margin presented earlier is the notion that stomata regulate P_{min}. While this is probably true for many species, other traits, such as rooting depth, may also influence P_{min} (Fig. 4.1 & 4.2). Shallow-rooted species that close stomata early in response to drought to avoid hydraulic failure may still reach low water potentials as the soil dries out (Fig. 4.1 & 4.2). To account for this, we included critical points from stomatal-conductance water-potential response curves in addition to P_{min} values into our concepts of safety margins (Fig. 4.1 & 4.2).

Species also vary in the degree of hydraulic failure from which they can recover (Brodribb & Cochard, 2009; Blackman *et al.*, 2009; Urli *et al.*, 2013). To account for this, we included multiple critical water potential values into our trait-based system. The air-entry point (P_e or the water potential at 12% loss of conductivity) is frequently used as a measure of the onset of drought-induced cavitation (Jones & Sutherland, 1991; Sparks & Black, 1999; Domec & Gartner, 2001), while the water potential at 50% and 88% loss of conductivity (P_{50} and P_{88}) are widely used to represent points of rapid and almost complete loss of conductivity, respectively (Maherali *et al.*, 2004, 2006; Cochard *et al.*, 2013). Although P_{50} is the most commonly used point (Choat *et al.*, 2012; Pivovaroff *et al.*, 2014), P_{88} is perhaps the most appropriate for a community of angiosperm species (Urli *et al.*, 2013). This is because the hydraulic "point of no return", the water potential at which a species fails to recover, has been shown to vary in major groups of land plants, with angiosperms more likely to suffer mortality once they reach P_{88}, compared to P_{50} for gymnosperms (Blackman *et al.*, 2009; Urli *et al.*, 2013; Choat, 2013).

To assess the likely mechanism of drought-induced mortality for each species, we developed novel combinations of functional traits based primarily on those shown in Figure 4.1 (Fig. 4.2). We used the difference between the point of stomatal closure (P_{g12}) and minimum seasonal water potential in the field (P_{min}) as a proxy for the degree to which species incur carbon limitation (Fig. 4.2). We reasoned that P_{g12} would provide a reasonable estimate of the onset of leaf-level carbon limitation since maximum assimilation rate is linearly related to stomatal conductance (Wong *et al.*, 1979; Farquhar & Sharkey, 1982). The difference between P_{g12} and P_{min} would provide an indication of the degree to which a species would have to endure carbon limitation *in situ*. To assess the degree to which a species may suffer hydraulic failure during drought conditions, we calculated the PLC at P_{min}. We reasoned that

P_{min} would integrate both rooting depth and hydraulic strategy. P_{min} is determined by rooting depth and stomatal regulation through their influences on water availability (Sperry *et al.*, 1998, 2002; Jackson *et al.*, 2000) and loss (Jarvis, 1976), respectively.

A secondary objective of this study was to determine whether stem density could provide a relatively simple, yet effective, way of describing vulnerability and, hence, have utility in describing variation in species' response patterns. Stem density has previously been shown to be related to vulnerability to cavitation (Jacobsen *et al.*, 2007; Nardini *et al.*, 2014). We quantified the relationship between stem density and P_{50} within the community and then compared the relationship between stem density and P_{g12} to that between P_{50} and P_{g12}.

We tested our system in highly diverse mountain fynbos communities from the Mediterranean-type shrubland of South Africa (the CFR). The CFR presents an excellent system in which to explore these questions and examine the suitability of the hydraulic framework in understanding how complex communities might respond to drought events. It contains an exceptionally diverse flora composed of several discernible functional groups (van der Heyden & Lewis, 1989; Goldblatt & Manning, 2002; Linder, 2003). Furthermore, West *et al.* (2012) showed the existence of drought-avoiding and drought-tolerating strategies in a mountain fynbos community by assessing the response of six species to long-term rainfall exclusion treatment.

We quantified the response of stomatal conductance to changes in water potential and related the point of stomatal closure to various standardised measures of vulnerability for a wide range of species. To address the practical difficulty of identifying the degree of stomatal regulation in response to dehydration without conducting a long-term field study, rainfall-exclusion manipulation or laboratory drought experiment, we assessed the efficacy of a reasonably simple benchtop dehydration technique. The accuracy of these stomatal conductance dehydration response curves were assessed by comparing them to the data obtained from long-term field measurements in Chapter Three.

We show that our traits based framework is helpful in identifying contrasting hydraulic regulation strategies. For example, it allows us to distinguish species in which the stomatal closure is relatively insensitive to declining water potential but which differ in the extent to which they incur low water potentials and hence cavitation. This framework also allows us to make predictions about likely mechanisms of mortality within highly diverse communities.

Methods and materials

Study sites and species

Species were sampled from three different study sites located in the south-western corner of South Africa's Western Cape Province. These sites were at Jonaskop in the Riviersonderend mountain range (33° 15′ 48.34″ S, 19° 31′ 33.97″ E, elevation 981 m), the Kogelberg Biosphere (34° 19′ 02.57″ S, 18° 57′ 39.74″ E, elevation 61 m) and the Silvermine (34° 06′ 26.45″ S, 18° 26′ 31.37″ E, elevation 375 m) and Cape Point (34° 15′ 48.34″ S, 18° 25′ 55.15″ E, elevation 90 m) sections of the Table Mountain National Park. These study sites were chosen as they contain particularly diverse floral communities that have been the focus of previous ecophysiological studies, including assessments of the variation in vulnerability of stem xylem to cavitation across a range of species and a long-term rainfall exclusion experiment (Aston, 2007; Jacobsen *et al.*, 2007; Pratt *et al.*, 2012; West *et al.*, 2012). Although there is a degree of microsite variability between sites, all sites are exposed to winter rainfall regimes and are situated on sands derived from the underlying quartzitic arenite of the Table Mountain Group. Annual rainfall was above 1000 mm at the Kogelberg and TMNP sites and approximately 600 mm at the Jonaskop site. Mountain fynbos, the most abundant vegetation type in the fynbos biome, was the predominant vegetation type in all these areas.

Gas exchange and water potential of plants in situ

Field-based measurements of xylem or shoot water potential and g_s were taken for nine species over a period of three consecutive years as part of two separate long-term monitoring studies. Six species were monitored in the Silvermine section of the TMNP between 2007 and 2009 (West *et al.*, 2012) and three at Jonaskop between 2011 and 2014 (see Chapter Three). The six species sampled at Silvermine were *Leucadendron laureolum*, *Diastella divaricata*, *Hypodiscus aristatus*, *Staberoha cernua*, *Erica subcapitatum* and *Erica ericoides*. We will briefly report the important details of this measurement campaign, as they have been reported elsewhere (West *et al.*, 2012). Stomatal conductance was measured using a Li-Cor 6400 infra-red gas analyser (Li-Cor, Lincoln, Neb., USA) at midday during spring and late-summer measurement campaigns, over three years. Light intensity in the cuvette was set at 1500 μmol m^{-2} s^{-1}, humidity was maintained just below ambient and CO_2 was held constant at 400 ppm. Stomatal conductance was expressed on a per-leaf-area basis. Water potential

was measured at the same time using a Scholander pressure chamber (PMS Instrument Company, Albany, OR, USA). At Jonaskop, we sampled *Protea repens* (L.) L. (Proteaceae), *Erica monsoniana* L.f. (Ericaceae) and *Cannomois congesta* Mast. (Restionaceae). Details of this study have been reported in Chapter Three. Again, stomatal conductance was measured at midday approximately every two weeks during summer dry periods and monthly during winter. The light intensity in the cuvette was set at 1500 μmol m^{-2} s^{-1}, humidity was maintained just below ambient and CO_2 was held constant at 400 ppm. Stomatal conductance was expressed on a per-leaf-area basis. Water potential was measured at the same time using a Scholander pressure chamber (PMS Instrument Company, Albany, OR, USA).

Stomatal response to dehydration

The relationship between stomatal conductance, g_s, and shoot water potential, P_s, was examined using a benchtop dehydration method. We termed these relationships "stomatal dehydration response curves" (Fig. 4.3). Stems or branches of forty-five species were cut under water in the field and subsequently transported back to the laboratory in water (see supporting material Table S1 for full list of species). Each stem was placed on a benchtop in a temperature- and light-controlled chamber and allowed to dry for varying periods of time to a range of water potentials. Stomatal conductance was measured using an infra-red gas analyser (Li-Cor 6400, Lincoln, Neb., USA) and expressed per leaf area. Light intensity was kept constant at 1500 μmol m^{-2} s^{-1} and humidity was maintained slightly below ambient using a dessicant. Immediately following the g_s measurement, the target shoot was cut and P_s was measured using a Scholander pressure chamber (PMS Instrument Company, Albany, OR, USA). A Weibull function was fitted to the stomatal conductance dehydration response curve for each species using non-linear models:

$$g_s\ (\%\ \text{of}\ g_{max}) = 100 - (100 / (1 + e^{(a\,(x\,-\,b))})) \qquad \text{(Eq. 4.1)}$$

where a is a fitted parameter describing the slope of the curve and b is the water potential at 50% loss of stomatal conductance (Pammenter & Vander Willigen, 1998). Similarly to the analysis of Domec and Gartner (2001), we parameterised this model and extracted several standardised values describing the sensitivity of g_s to P_s. Specifically, we found the derivative of equation 4.1:

$$d\ PLC_g / d\ P = -a\ (e^{a\,(P\,-\,b)})\ 100 / (1 + e^{a\,(P\,-\,b)})^2 \qquad \text{(Eq. 4.2)}$$

which provides the slope of the tangential line to equation 4.1 at each P. We used this derivative to find the slope of the tangential line at the P-inducing 50% loss of stomatal conductance (i.e. 50% of g_{max}). Subsequently, this was used to calculate the point where the tangential line intercepted the water potential axis with the following equation:

$$P_{g12} = 2 / a + b \quad \text{(Eq. 4.3)}$$

This point was termed P_{g12} and we used it as a proxy of the water potential at which stomatal closure occurs (Fig. 4.3).

Vulnerability curves

We obtained the PLC in response to declining water potential (i.e. vulnerability curves) for eighteen species (see Table 4.1 for a list of species). To obtain vulnerability curves for as many species as possible, we measured vulnerability curves using both the benchtop-dehydration method (Sperry & Saliendra, 1994) and the air-injection method (Sperry & Ikeda, 1997; Cochard *et al.*, 2013) and also gathered data from published studies (see Table 4.1 for the studies in which vulnerability curve data were presented). We assessed the comparativeness of these measures by comparing the vulnerability curve of *P. repens* obtained using the benchtop-dehydration method to that obtained using the air-injection method and found strong agreement (see Chapter Three).

We used the benchtop-dehydration method for *P. repens*, *E. monsoniana* and *C. congesta*. For each species, we first determined the maximum vessel length to inform the minimum stem length needed to avoid any open vessels. We cut five stems under water in the field. In a laboratory setting, we placed tubing on one end, connected it to an air tank and made successive cuts from the opposite end. The mean length at which bubbles first emerged was taken as the maximum vessel length for each species. For each species, stems were cut under water in the field and subsequently dried to a range of water potential values by placing them on a laboratory work bench. Once the target water potential had been obtained, the stems were sealed in plastic bags and placed in a dark room for at least an hour to equilibrate. A shoot was cut from each stem and water potential was measured using a Scholander pressure chamber (PMS Instrument Company, Albany, Or, USA). The remaining stem was placed under water and cut into an unbranched segment under water. Several cuts were made at each end to ensure that the xylem tension relaxed. Native flow rate was measured by connecting each stem to tubing attached to a pressure head of < 15kPa containing KCl solution (20 mM).

Water was collected from the distal end of the stem and weighed on a balance. Once a consistent flow rate had been achieved and measured, the stems were removed and immediately connected to tubing connected to a high pressure, filtered KCl solution. Stems were flushed for a period of at least an hour to remove any embolism. After this, the stems were reconnected to the pressure head and flushed flow rate was measured. Native and flushed–stem-specific conductivity (K_n and K_{max} respectively) were calculated by expressing flow rate per pressure head per stem length per second. PLC at each water potential value was calculated using the following formula:

$$PLC = 100 ((K_{max} - K_n) / K_{max}) \quad \text{(Eq. 4.4)}$$

where K_{max} was the flushed conductivity and K_n was the native conductivity.

We also quantified vulnerability curves of two species using the air-injection method. These species were *H. aristatus* and *L. laureolum*. Stems of these two species were collected in the field and placed in air sleeves connected to a pressure tank after being scored slightly with a razor blade. The distal end of each stem was connected to tubing connected to a pressure head containing filtered 20 mM KCl solution. Flow rate was measured by periodically measuring the weight of vials connected to the axial end of the stem. Embolism was induced in the stem by applying different pressures to the sleeve for ten minutes at a time. After each pressure treatment, the pressure was released and the stable flow rate was determined. PLC was calculated as before using equation 4.4.

Vulnerability curves were modelled for each species using the Weibull function. Briefly, we used the following formula:

$$PLC = 100 / (1 + e^{(a (P - b))}) \quad \text{(Eq. 4.5)}$$

where a and b were parameters found using least-squares regression analysis.

Table 4.1: List of species for which the P_{50} has been examined and the study in which it was reported.

Family	Species	Study	Abbreviation
Asteraceae	*Metalasia densa*	Jacobsen et al. (2007)	Mden
	Osmitopsis asteriscoides	Aston (2007)	Oast
Bruniaceae	*Brunia alopecuroides*	Aston (2007)	Balo
Ericaceae	*Erica plukenetii*	Jacobsen et al. (2007)	Eplu
	E. vestita	Jacobsen et al. (2007)	Ev
	E. monsoniana	Current study	Emon
	E. perspicua	Aston (2007)	Eper
	E. baccans	Aston (2007)	Ebac
Fabaceae	*Aspalathus hirta*	Jacobsen et al. (2007)	Ahir
	A. pachyloba	Jacobsen et al. (2007)	Apac
Proteaceae	*Leucadendron laureolum*	Current study	Llau
	L. laureolum	Jacobsen et al. (2007)	
	L. salignum	Jacobsen et al. (2007)	Lsalig
	L. salicifolium	Aston (2007)	Lsalic
	L. xanthoconas	Aston (2007)	Lxan
	L. argenteum	Aston (2007)	Larg
	Mimetes hirtus	Aston (2007)	Mhir
	M. cucullatus	Aston (2007)	Mcuc
	Protea repens	Jacobsen et al. (2007) and current study	Prep
Restionaceae	*Hypodiscus aristatus*	Current study	Hari
	Cannomois congesta	Current study	Ccon
Rosaceae	*Cliffortia ruscifolia*	Jacobsen et al. (2007)	Crus

P_{min} and stem density

Minimum seasonal water potential in the field (P_{min}) was collected for nine species during summer dry periods. Since these data were initially collected as part of long-term periodic water potential campaigns, we have confidence that these represent close to actual P_{min} values in the absence of extreme drought. For each species, shoot water potential of at least five shoots was sampled at midday using a Scholander pressure chamber (PMS Instrument Company, Albany, OR, USA). We also extracted P_{min} values from Jacobsen et al. (2007) and Aston (2007) for the remaining species.

Stem density was measured for forty-five species (Table S4.1) by calculating the dry mass (in kilograms) divided by volume (in m^3). At least five stems of each species were collected in the field and kept under water for at least an hour to rehydrate. Both ends of each stem were cut under water until we had attained an unbranched segment approximately 10 cm in length. The bark and pith (where possible) of each stem were removed and the volume was determined using the displacement of water quantified with a measuring cylinder. Stems were then placed in a drying oven for at least seventy-two hours and their dry weight was recorded. For the Restionaceae species, we assessed culm density using the method outlined above. These species did not have bark, so we measured the volume and dry mass of entire sections of culms.

Trait correlations

We assessed the correlations between various traits using regression analysis for species where these were available (Table 4.2). We also calculated several different safety margins based on relationships between traits. The stomatal regulation safety margin was calculated as the difference between P_{50} and P_{g12} (Fig. 4.2). We used this as a proxy for hydraulic regulation strategy. Large positive differences occurred when stomatal closure was initiated after large losses of conductivity and were interpreted as anisohydric regulation. Negative differences occurred when stomatal closure was initiated prior to P_{50} and were interpreted as isohydric regulation. The water-potential safety margin was calculated as the difference between P_{50} and P_{min} (Fig. 4.2). This measure assessed the degree to which species incur > 50% loss of conductivity in the field during seasonal drought conditions (Fig. 4.2). P_{g12} and P_{min} were used to obtain an indication of the degree of stomatal regulation. Negative differences indicated that species maintained water potential by means other than stomatal

closure, while positive differences indicated that stomatal closure was ineffective as a means of regulating water potential (Fig. 4.2).

We used these measures as proxies for carbon limitation and hydraulic failure. To assess the degree to which species may incur carbon limitation during drought conditions in the field, we calculated the difference between the point of stomatal closure (P_{g12}) and minimum seasonal water potential in the field (P_{min}) (Fig. 4.2). To assess the degree to which a species may suffer hydraulic failure during drought conditions, we calculated the PLC at P_{min} using species vulnerability curves and termed this seasonal PLC. Although pressure chamber measurements on previously transpiring shoots are likely overestimate the tension that was present in the xylem, which might lead to an overestimate of native loss of conductivity, this effect is likely to be similar for all species (Melcher *et al.*, 2001). For this reason we emphasise relative changes in seasonal PLC rather than absolute measures to gain insight into likely mechanisms of mortality.

To investigate the suitability of stem density as a measure of vulnerability, we found the relationship between stem density and P_{min}, P_{50} and P_{88}. We subsequently assessed the relationship between P_{g12} and P_{50} calculated from stem density and compared these results to the relationship between P_{g12} and actual P_{50}

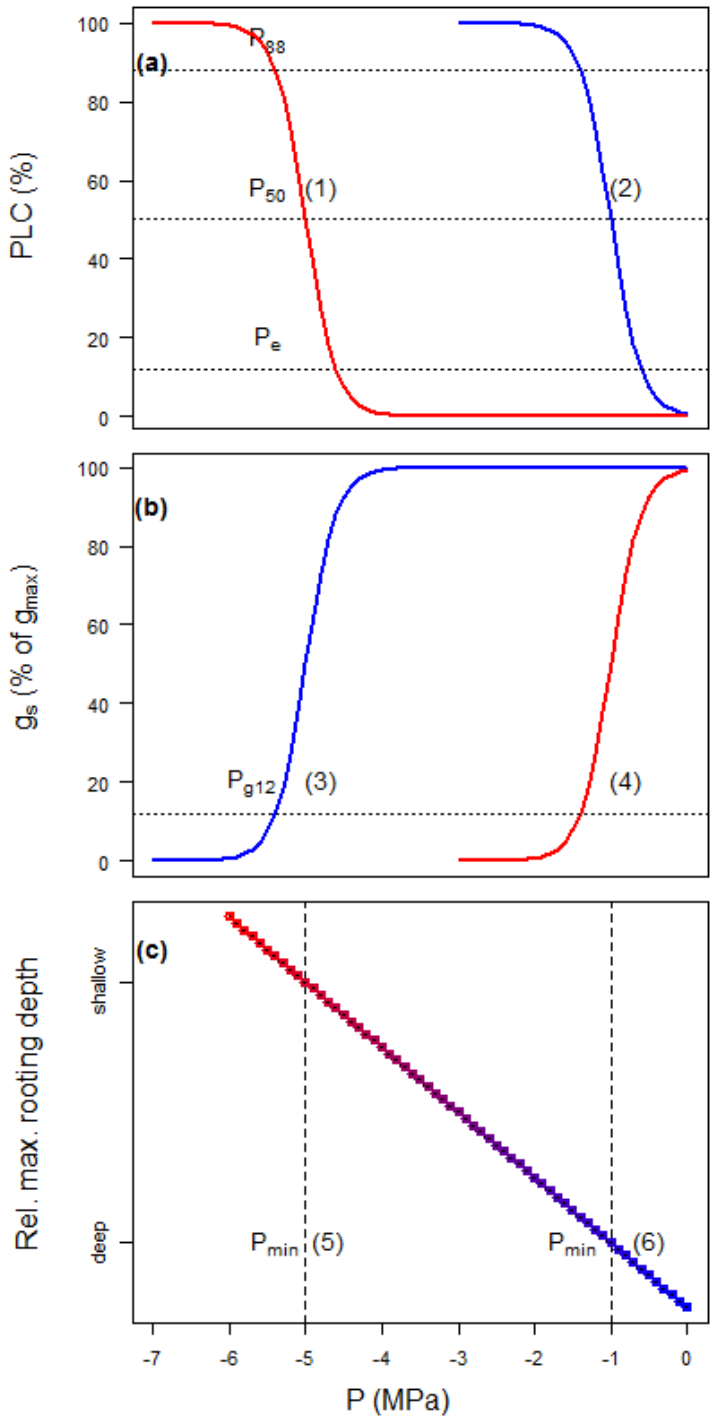

Figure. 4.1: Physiological traits used to describe the (a) vulnerability of xylem to embolism, (b) stomatal regulation strategy and (c) degree to which individuals experience low water potentials during seasonal drought. In each case, we have illustrated two extreme responses: (a) a relatively vulnerable species (blue) and a less vulnerable species (red), (b) isohydric stomatal response (blue) and anisohydric stomatal response (red) and (c) deep-rooted species (blue) and shallow-rooted species (red).

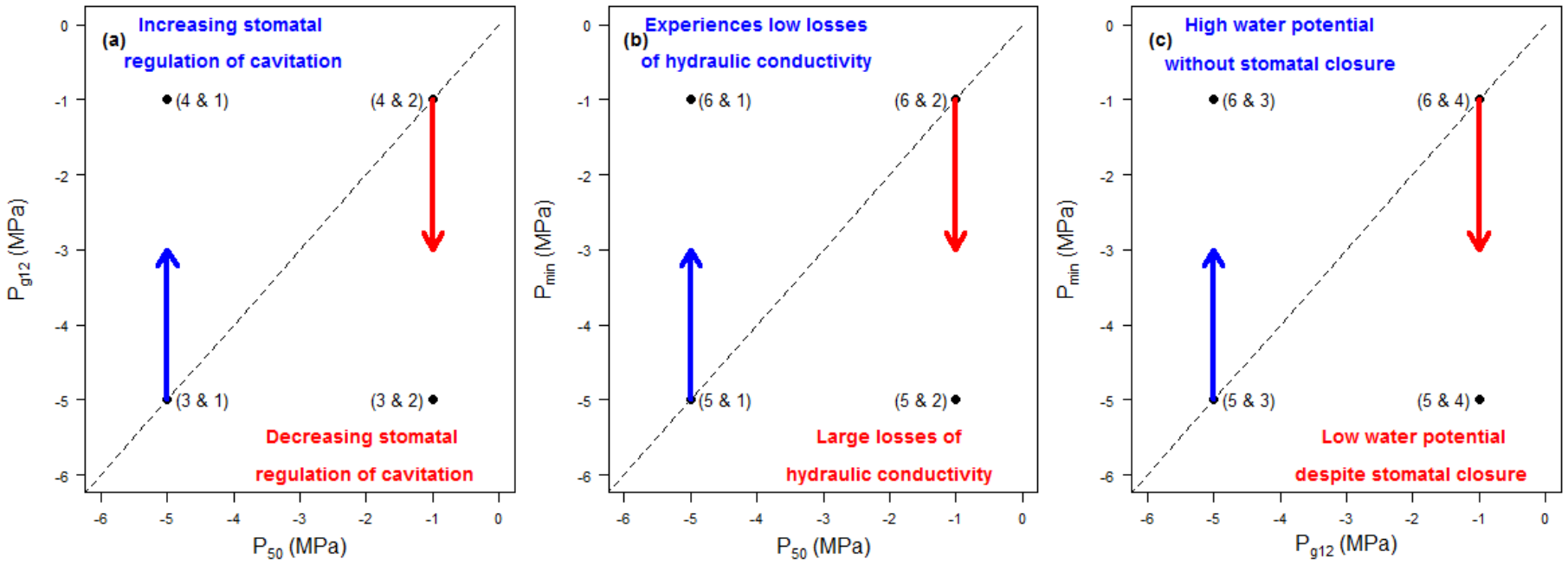

Figure 4.2: Combinations of key hydraulic traits shown in Figure 4.1. We use these relationships to infer (a) the degree of stomatal regulation of xylem embolism, (b) the amount of xylem embolism experienced *in situ* during seasonal drought periods and (c) the extent to which stomatal closure regulates water potential *in situ*.

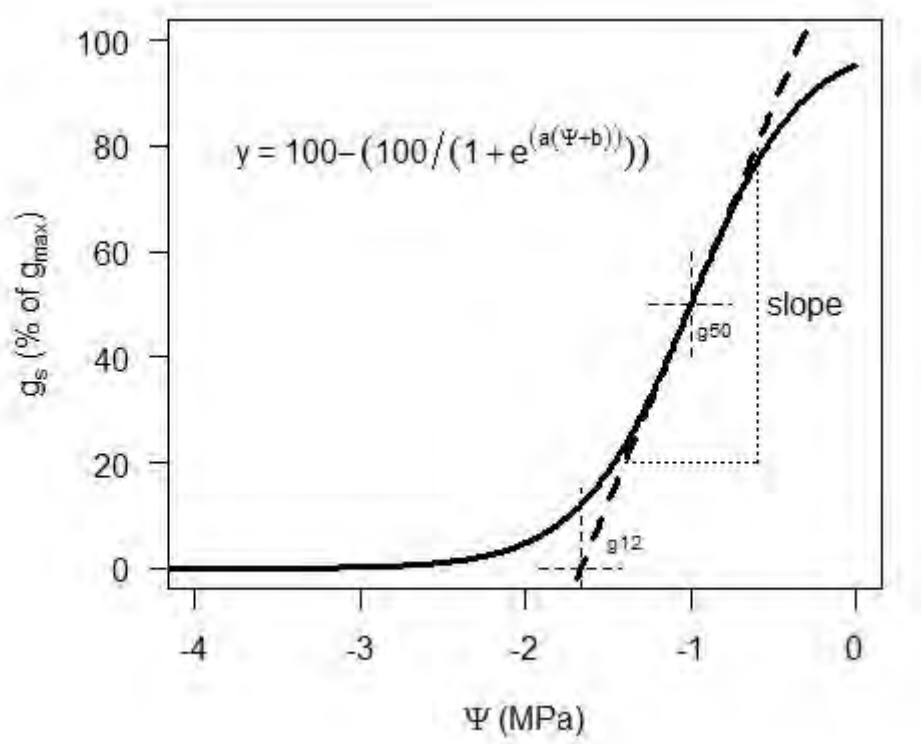

Figure 4.3: A sigmoidal function was fitted to the stomatal conductance dehydration response curves (Eq. 4.1) and various parameters were extracted from this (see "*Method and materials—Stomatal response to dehydration*" above for details).

Table 4.2: Results of correlation analysis between functional traits. Significant results are indicated in bold and the significance level is denoted by the asterisks (see notes below). Degrees of freedom are shown in brackets.

Trait	P_e	P_{50}	P_{88}	P_{min}	***Stem density***
P_e	-	-	-	-	-
P_{50}	**0.39***** (14)	-	-	-	-
P_{88}	0.13 (13)	**0.83****** (13)	-	-	-
P_{min}	< 0.01 (12)	0.24* (14)	**0.42**** (12)	-	-
Stem density	0.13 (12)	**0.64****** (14)	**0.73****** (11)	**0.54****** (21)	-
P_{g12}	0.06 (13)	< 0.01 (15)	0.02 (12)	0.08 (22)	0.03 (37)

****: p < 0.1***

*****: p < 0.05***

******: p < 0.01***

*******: p < 0.001***

*******: P < 0.0001***

Results

There was generally very good agreement between stomatal conductance dehydration response curves obtained using the benchtop dehydration method and the data collected in the field (Fig. 4.4). There was significant variation in stomatal response to declining water potential between species. Some species displayed reductions in stomatal conductance at water potentials < −1 MPa (e.g. *Mimetes hirtus*, Fig. 4.5), whilst others closed stomata at > −2 MPa (e.g. *E. monsoniana*, Fig. 4.5). There did not appear to be a consistent association between the water potential at the initiation of stomatal closure and different metrics of xylem vulnerability. Certain species reduced stomatal conductance at similar water potentials to P_e (e.g. *L. laureolum*, Fig. 4.5), whilst for others this point was closer to P_{50} (e.g. *Osmitopsis asteriscoides*, Fig. 4.5).

Explicit comparison between P_{g12} and P_e revealed that most species tolerated some degree of cavitation (Fig. 4.6a). *Metalasia densa* was the only species able to close stomata prior to the onset of air entry. The comparison between P_{g12} and P_{50} showed that approximately half of all species had initiated stomatal closure prior to 50% loss of conductivity (Fig. 4.6b). Although this might not accurately reflect the absolute values of PLC tolerated by each species, it shows that there is considerable variation in the relative extent to which species are likely to experience PLC in situ. There seemed to be some degree of consistency within families, with most members of the Proteaceae and Fabaceae displaying stomatal closure prior to P_{50} while all members of the Restionaceae and Ericaceae incurred 50% loss of conductivity. Most species had closed stomata prior to P_{88} (Fig. 4.6c). The exceptions were members of the Restionaceae: *H. aristatus* and *C. congesta* (Fig. 4.6c).

We found a continuum in the degree of stomatal regulation of cavitation among the sixteen species sampled (Fig. 4.7). Species ranged from *C. congesta*, which displayed the greatest tolerance of incurring 50% loss of conductivity, to *M. densa*, which exhibited stomatal closure approximately 4 MPa prior to P_{50}.

The relationship between P_{g12} and P_{min} showed the range in the degree to which species exhibit stomatal closure in the field during drought conditions (Fig. 4.8a). Species above the 1 : 1 line exhibited increasingly early stomatal closure, while those below the 1 : 1 line displayed little stomatal response to desiccation in the field. The relationship between P_{50} and P_{min} showed the range in the degree to which species exhibit > 50% cavitation in the field

(Fig. 4.8b). The majority of species did not experience low water potential in the field relative to P_{50} (i.e. those that fell below the 1 : 1 line). Four species experienced > 50% loss of cavitation during drought conditions.

Species displayed significant variation in the degree to which they were likely suffer carbon limitation and hydraulic failure during drought periods in the field (Fig. 4.9). The majority of species exhibited little risk of carbon limitation (difference close to the zero line) and low seasonal PLC. *M. densa* exhibited a strong risk of carbon starvation, but limited PLC. *C. congesta* exhibited high risk of hydraulic failure. *Erica plukenetii* and *E. monsoniana* exhibited high risk of carbon limitation and high seasonal PLC. Although *H. aristatus* exhibited little stomatal regulation, it did not incur > 50% seasonal PLC.

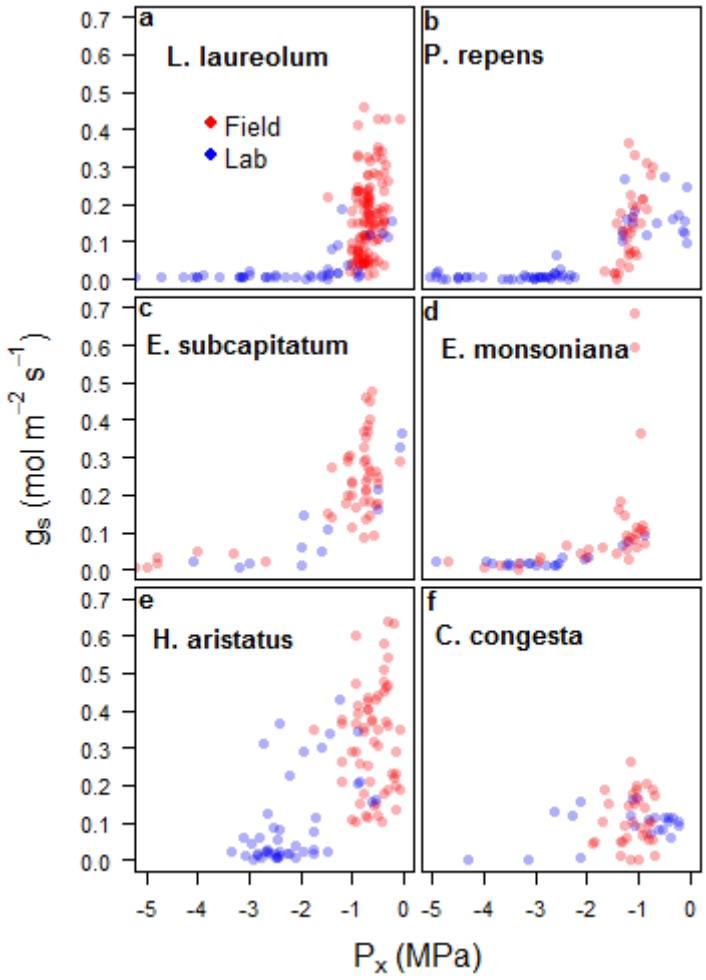

1522

Figure 4.4: Comparison of the stomatal conductance water potential dehydration response curve data collected in a laboratory-based (blue) and field-based (red) setting for six species.

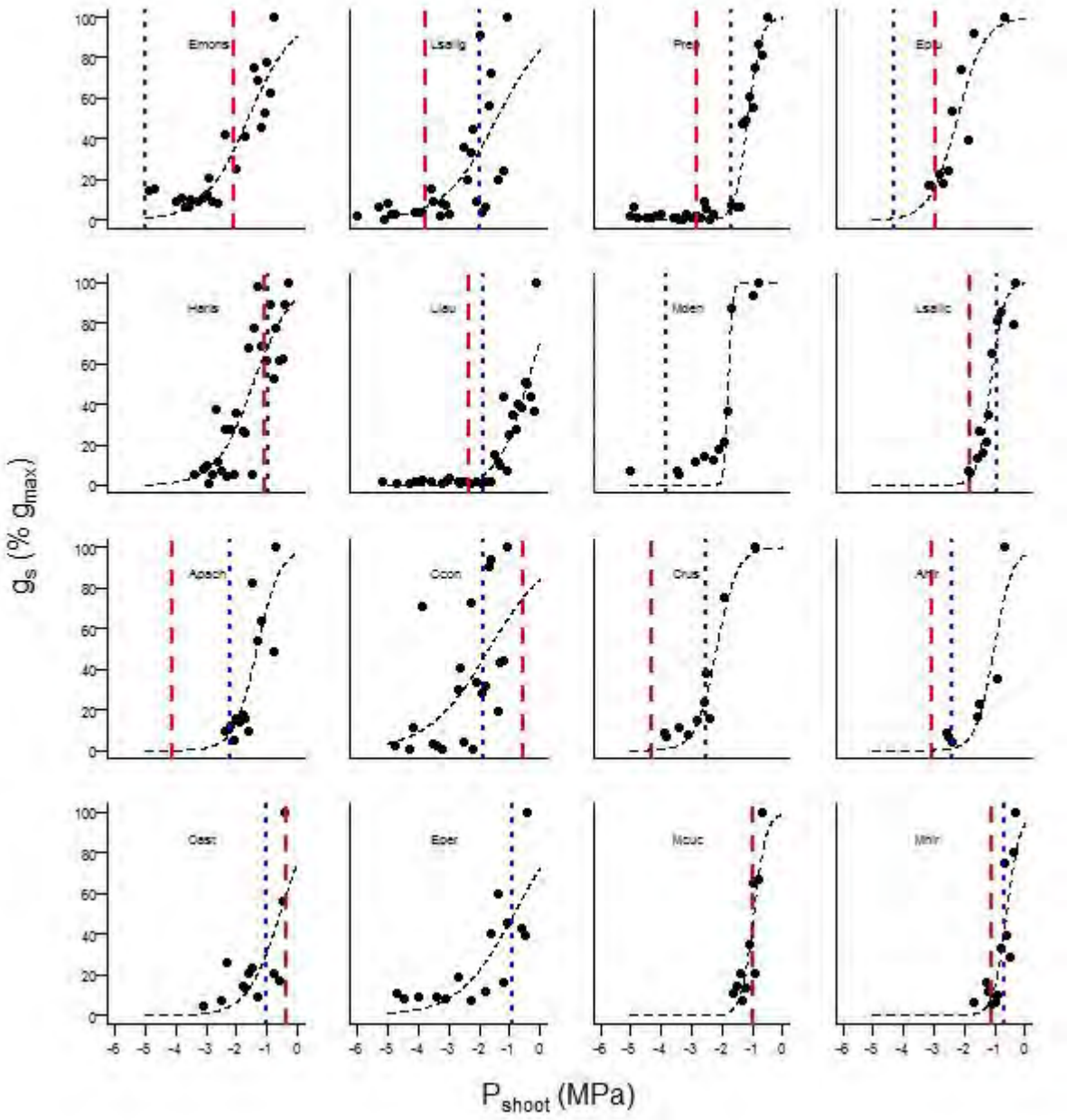

Figure 4.5: Stomatal-conductance water-potential response curves for diverse fynbos species, showing changes in stomatal conductance with declining shoot water potentials. Vertical lines are P_{50} (dashed red) and P_{min} (dotted blue) for each species. Species abbreviations are shown in Table 4.1 and Table S1.

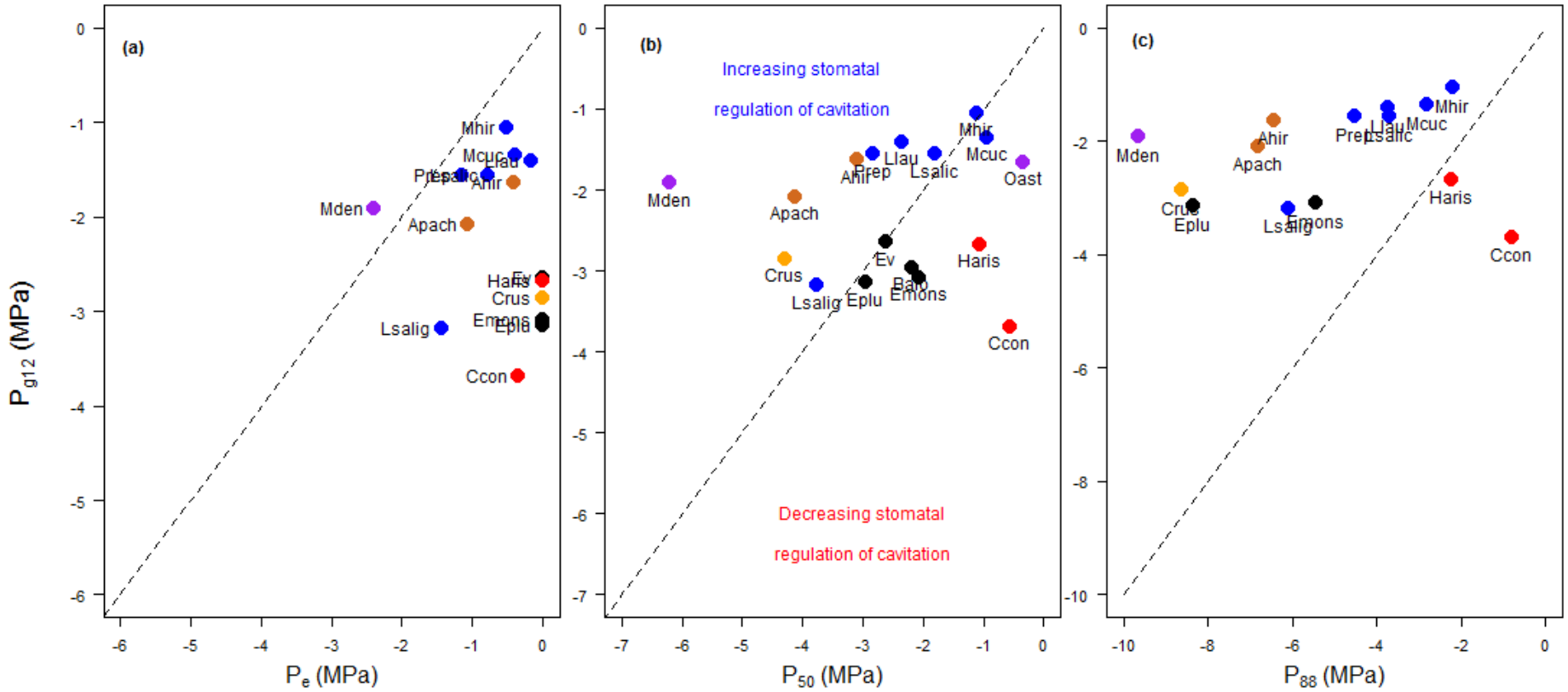

Figure 4.6: Relationship between water potential at stomatal closure (P_{g12}) and (a) air-entry point (P_e), (b) water potential at 50% loss of conductivity (P_{50}) and (c) water potential at 88% loss of conductivity (P_{88}) for fynbos species. Species are coloured by family.

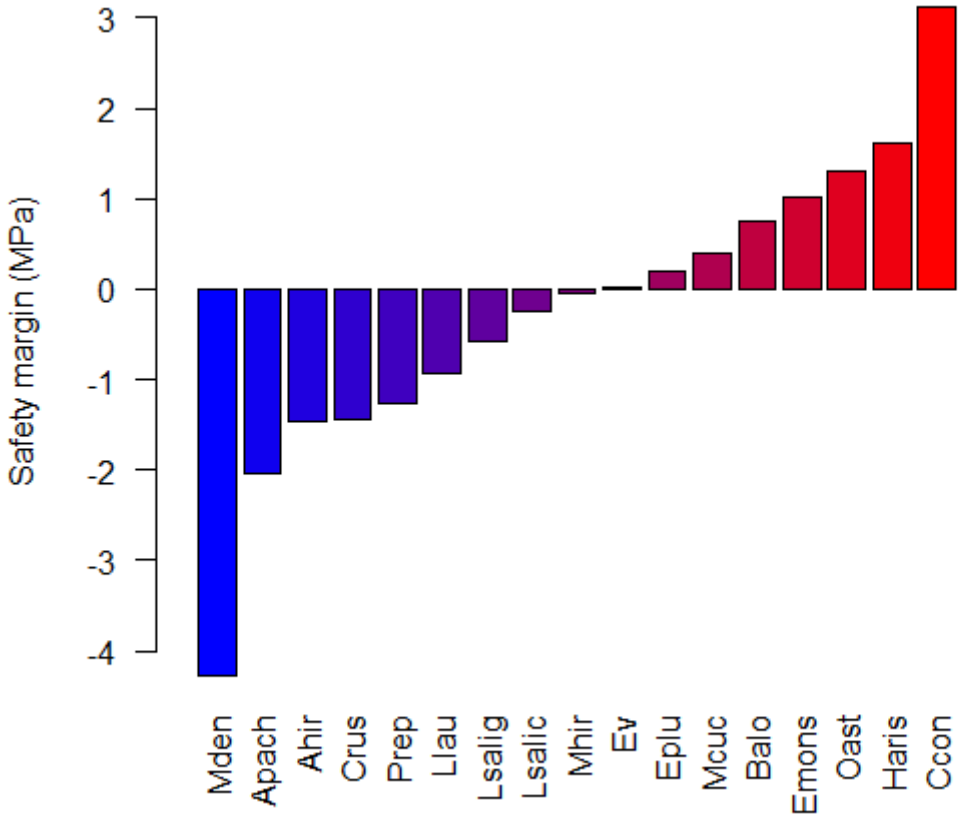

Figure 4.7: Safety margins of seventeen mountain fynbos species showing the range of stomatal regulation strategies in fynbos communities. Safety margin was defined as the difference between P_{g12} and P_{50}. Red bars indicate increasing anisohydric regulation while blue bars indicate increasing isohydric regulation.

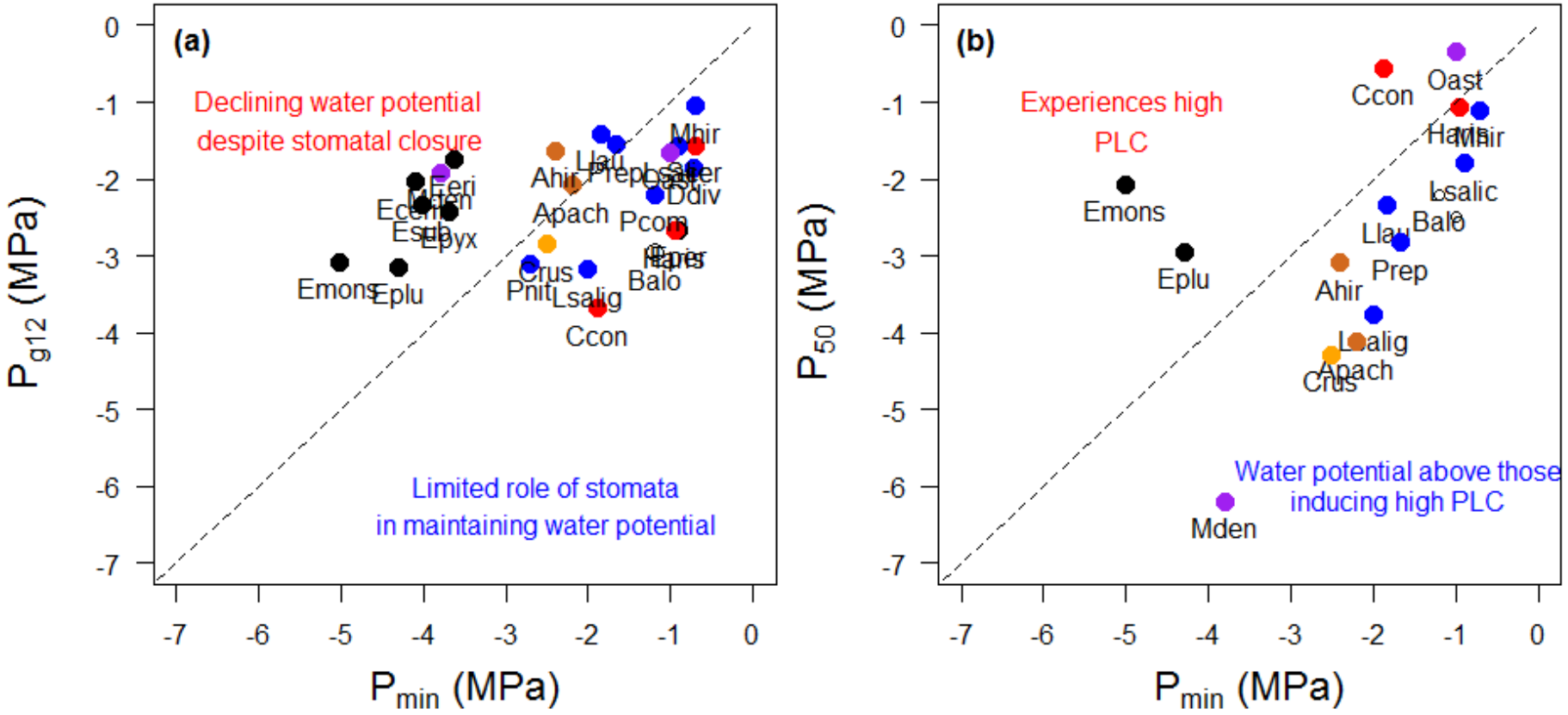

Figure 4.8: Relationship between minimum water potential in the field (P_{min}) and the water potential at (a) stomatal closure (P_{g12}) and (b) 50% loss of conductivity (P_{50}) for diverse species in fynbos communities.

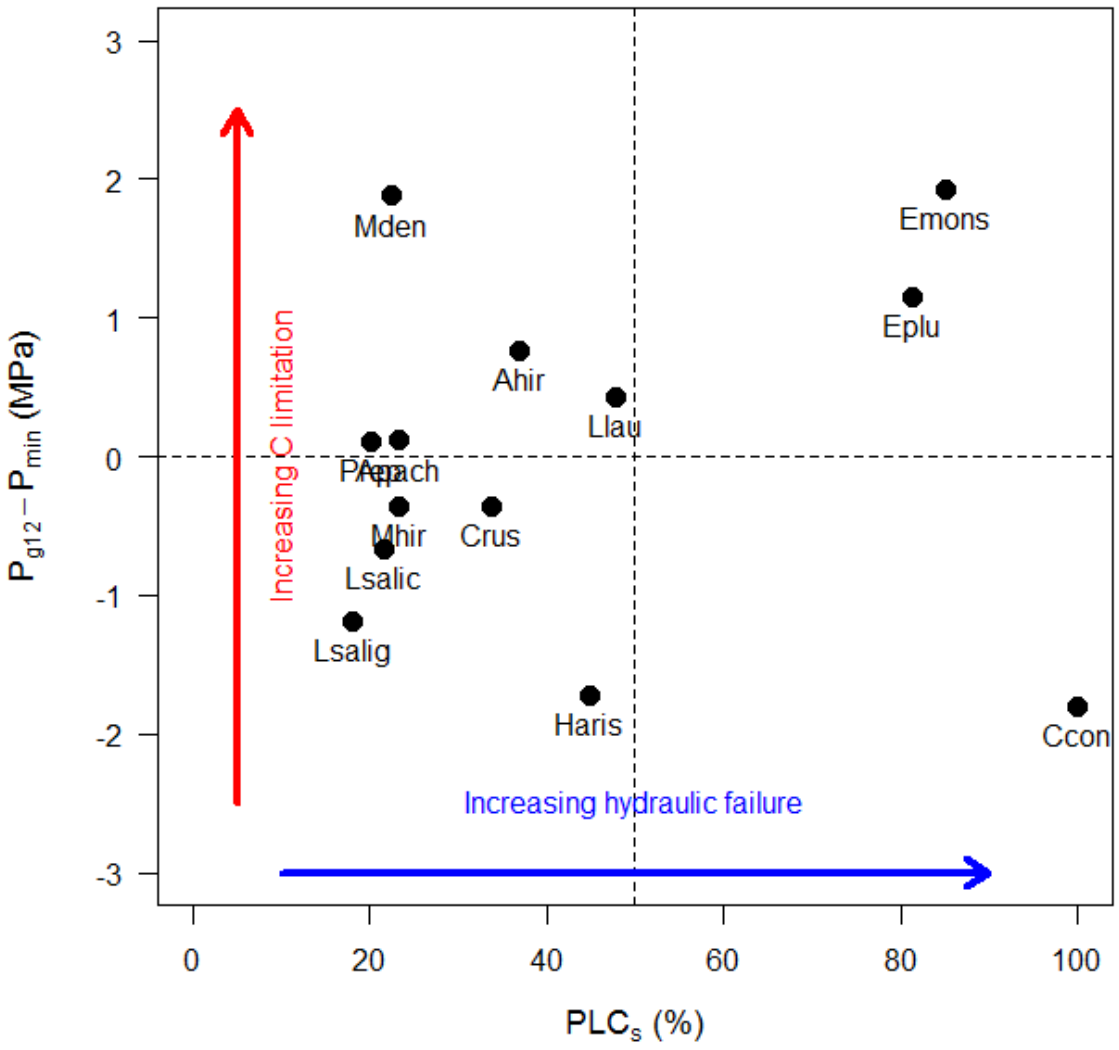

Figure 4.9: Relationship between stomatal safety margin ($P_{g12} - P_{min}$) and seasonal loss of conductivity (PLC_s) for diverse fynbos species.

There were linear relationships between stem density and all three measures of critical water potential values for diverse fynbos species (Fig. 4.10). Species with highly dense stems experienced lower P_{min} values, but were also less vulnerable to drought-induced cavitation (Fig. 4.10). *E. monsoniana* had a lower P_{50} values than expected from its stem density (Fig. 4.10), supporting our finding from Chapter Three that this species has highly variable vulnerability to cavitation. The strong linear relationships between stem density and the critical water potential values also support the use of stem density as a proxy for xylem vulnerability (Jacobsen *et al.*, 2007).

The use of stem density as a proxy for P_{50} was further validated when plotted against P_{g12} (Fig. 4.11). A comparison between the relationship between P_{50} and P_{g12} (Fig. 4.6) and stem density and P_{g12} (Fig. 4.11) showed that only two species fell on different sides of the 1 : 1 lines. The inability of stem density to capture P_{50} for *E. monsoniana* has already been shown. The only other species to fall on the opposite side of the 1 : 1 line was *L. laureolum*. This species was shown to have lower stem density than predicted by its P_{50} value. Despite this, the relationship between P_{50} and P_{g12} could be accurately assessed for the majority of species based on the relationship between stem density and P_{g12} (Fig. 4.12).

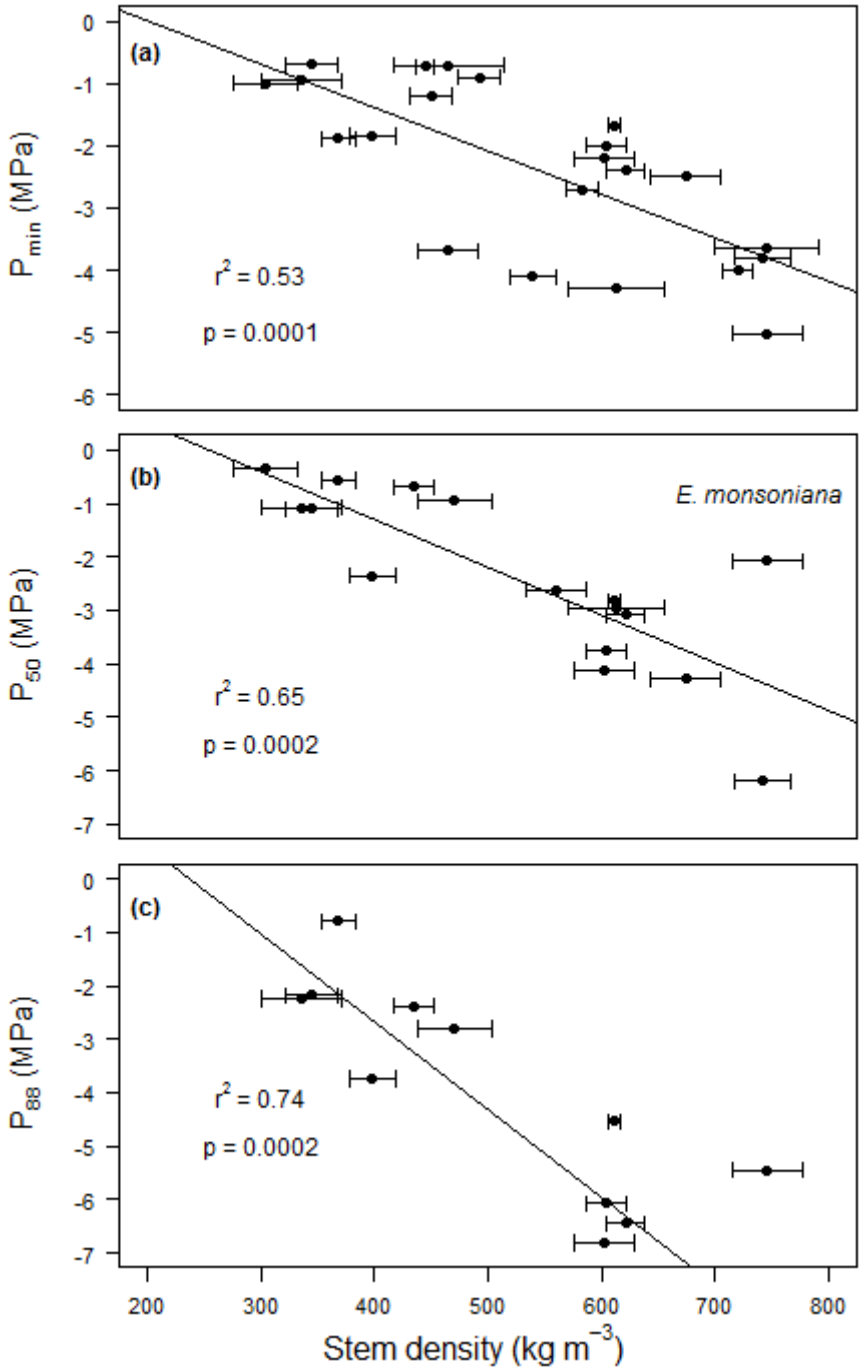

Figure 4.10: Relationship between stem density and (a) minimum seasonal water potential (P_{min}) and the water potential at (b) 50% loss of conductivity (P_{50}) and (c) 88% loss of conductivity (P_{88}) for diverse fynbos species.

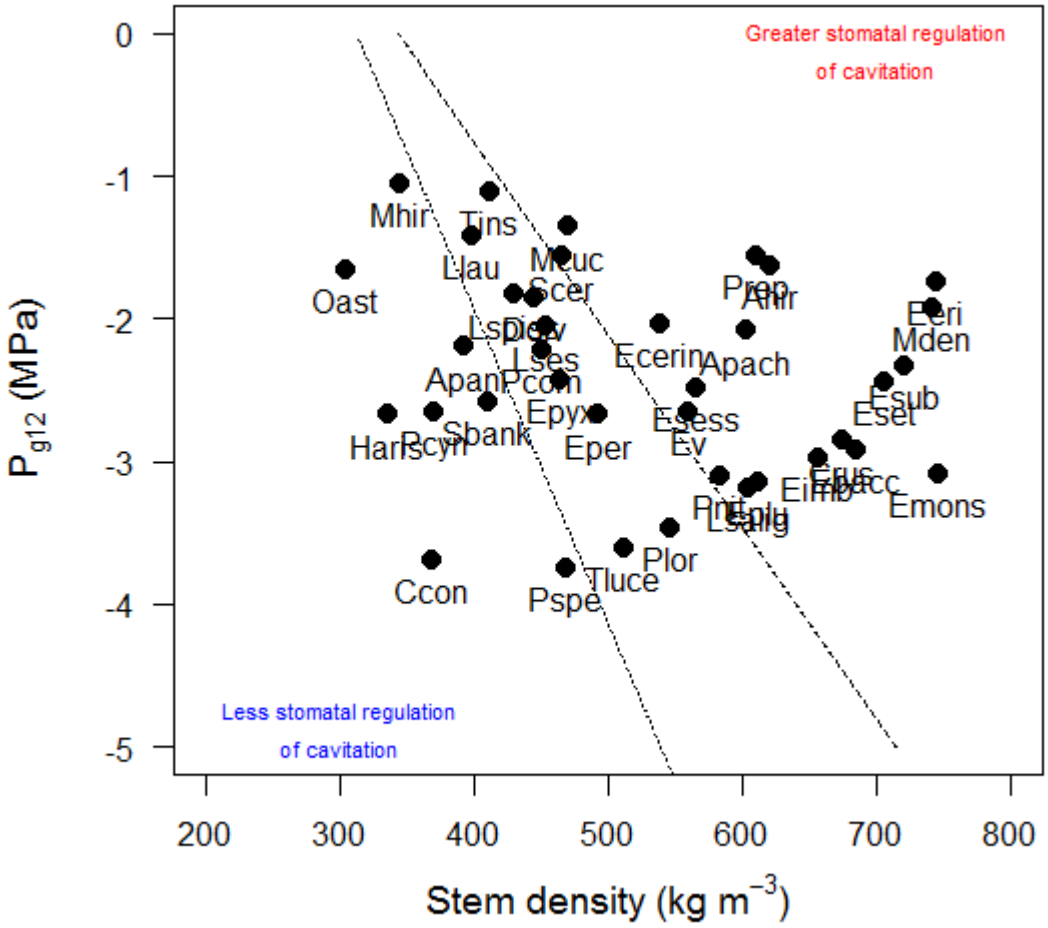

Figure 4.11: Relationship between water potential at stomatal closure (P_{g12}) and stem density (sd) for diverse fynbos species. The dashed line represents the 1 : 1 between P_{g12} and the predicted P_{50} based on the linear relationship between sd and P_{50} established in Figure 4.10, while the dotted line is the same relationship but for P_{88}.

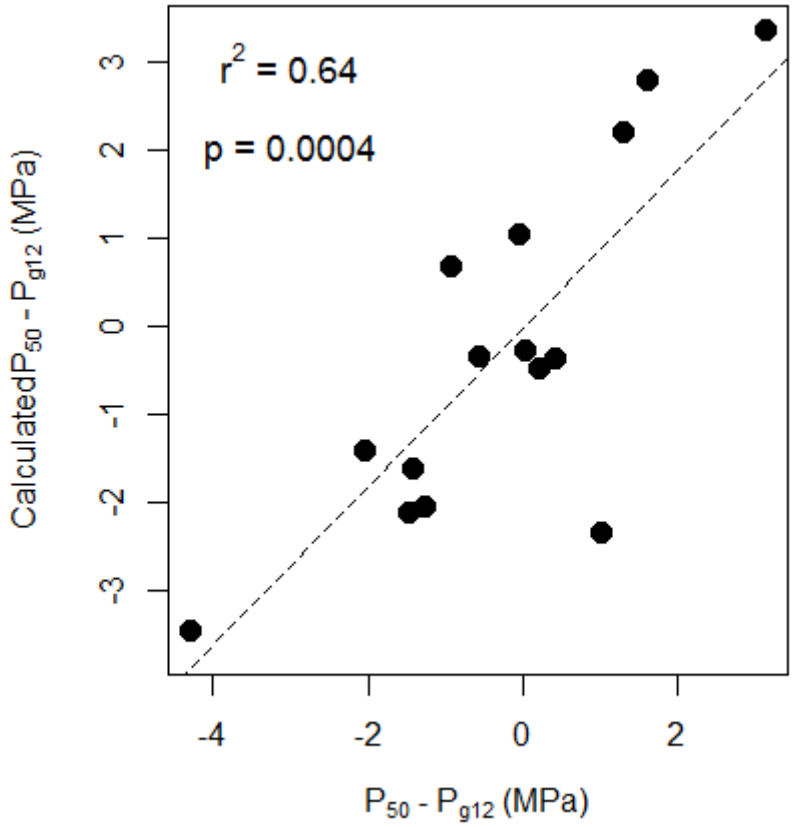

Figure 4.12: Relationship between the safety margin calculated as the difference between P_{g12} and actual P_{50} and that calculated as the difference between P_{g12} and the predicted P_{50} obtained from the stem density for sixteen species.

Discussion

We presented a system in which functional traits can be incorporated into the hydraulic framework to provide valuable insights into the range of hydraulic strategies present in diverse communities. This trait-based approach allows predictions of the likely mechanisms of mortality to be made and produced testable hypotheses for future studies. This approach may prove valuable for rapid assessment of the vulnerability of diverse communities to future drought events. Our results showed that a diverse range of stomatal responses exists in mountain fynbos communities, with species varying in the extent to which they tolerated large losses of conductivity. This represents the first study to show a continuum of the degree of stomatal regulation of cavitation within a single community. These findings lend support to evidence that species occupy distinct water regulation and utilisation niches in mountain fynbos communities and further highlight the importance of water relations in community composition (Miller *et al.*, 1983; Silvertown *et al.*, 1999, 2012; West *et al.*, 2012; Vilagrosa *et al.*, 2014).

Most species displayed some degree of stomatal regulation of cavitation, closing stomata prior to 88% loss of conductivity. Exceptions included members of the Restionaceae, which displayed stomatal closure at lower water potentials than P_{88}. This lends support both to the primary role of stomata in preventing xylem cavitation (Jones & Sutherland, 1991; Sperry *et al.*, 2003) and to the significance of P_{88} as the point of hydraulic failure in angiosperms (Choat *et al.*, 2012; Urli *et al.*, 2013; Choat, 2013). However, over 40% of species experienced minimum water potentials *in situ* that were lower than those inducing stomatal closure during drought conditions. This suggests that stomatal closure is insufficient in preventing loss of conductivity in mountain fynbos communities. It is important to note that of those species that displayed lower P_{min} values compared to P_{g12} over 90% were ericoid. These species are known to have shallow rooting depths (Higgins *et al.*, 1987; West *et al.*, 2012) and small leaves with rolled margins (Campbell & Werger, 1988). Although shallow rooting has been shown to promote the uptake of episodic rainfall (Chapter Three), it also exposes these species to low minimum soil water potential values during seasonal drought periods (Sperry *et al.*, 2002). The ericoid leaf form may be an adaptation to enhance water conservation under dry conditions by increasing the boundary layer thickness (McDonald *et al.*, 2003).

Our study provides further support for our finding in Chapter Three that the extent of cavitation in proteoids and restioids is determined by a combination of stomatal regulation and alternative means of maintaining maximum water potential. The majority of proteoids experienced P_{min} values that were greater than P_{g12}, further supporting the notion that they avoid desiccation partly by being deep rooted (Higgins *et al.*, 1987; West *et al.*, 2012). Although the shallow-rooted restioid *H. aristatus* did not close its stomata prior to P_{88}, neither did it experience minimum water potentials lower than P_{50}, providing further evidence that it is able to take up cloud moisture or dew (West *et al.*, 2012).

This study also highlighted unusual combinations of functional traits, which point toward alternative functional strategies present in this mountain fynbos community. These results provide testable hypotheses regarding the functionality of individual species and provide a strong stimulus for future ecophysiological investigations. Importantly, the inclusion of P_{min} and P_{g12} into measures of safety margins provided valuable insight into distinct hydraulic strategies. It allowed us to distinguish between species that regulate water potential through stomatal closure but still experience greater than 50% loss of conductivity from those that effectively regulate water potential through stomatal closure. In this study, the former condition was observed in *E. monsoniana* and *E. plukenetii*, while *M. densa* provided an example of the latter. Although these three species are shallow-rooted ericoid species, a key difference between them is that *M. densa* had a significantly lower P_{50}. This suggests that, even within functional types, species segregate out in key functional traits. The driving force behind this variability might be a trade-off between hydraulic vulnerability and hydraulic efficiency (Maherali *et al.*, 2006), which has previously been shown to occur in mountain fynbos communities (Maherali *et al.*, 2006; Jacobsen *et al.*, 2007; Pratt *et al.*, 2007, 2012).

The use of P_{min} also allowed us to distinguish contrasting strategies of water potential in species in which the stomatal sensitivity to declining water potential is relatively low. Several of these species experienced very negative minimum water potentials and are likely to incur a relatively high degree of cavitation. Other species with less sensitive stomatal responses did not incur low water potentials in situ, and are less likely to incur large losses of hydraulic conductance. Examples of these distinct strategies are found in *C congesta* and *H. aristatus*. The low likelihood of experiencing large losses in conductance in combination with a relatively insensitive stomatal response for *H. aristatus* points toward an alternative means of

water potential regulation. This is consistent with previous findings that restioids are able to take up dew or cloud moisture (Chapter Three).

Combinations of functional traits also allowed us to explore how potential mechanisms of mortality differed between species. We identified several species that displayed conservative stomatal regulation patterns, as determined by the difference between P_{g12} and P_{min}. The three species found to be at greatest risk of carbon limitation within a season were *M. densa*, *E. monsoniana* and *E. plukenetii*. Although this measure provides an indication of the extent of stomatal limitation to carbon assimilation, it does not necessarily mean that these species will suffer carbon starvation (Sala, 2009; Sala *et al.*, 2010, 2012). Whether carbon starvation is likely to occur within a species remains a complex issue since it is highly dependent on a multitude of factors in addition to assimilation rate (Körner, 2003; Adams *et al.*, 2009; Sala, 2009; McDowell & Sevanto, 2010; Sala *et al.*, 2012; Sevanto *et al.*, 2013; Mitchell *et al.*, 2014).To come to any meaningful conclusion about the risk of carbon starvation in a species, it is important to quantify the assimilation of carbon, the availability of, and ability to redistribute, stored carbon reserves and seasonal adjustments in metabolic demand (McDowell & Sevanto, 2010; Sevanto *et al.*, 2013; Mitchell *et al.*, 2014). This is beyond the scope of our trait-based system and, consequently, limits our current analysis to making inferences about potential carbon limitation rather than risk of mortality *per se*.

We were also able to identify those species at risk of hydraulic failure, as determined by estimating the PLC at P_{min} for each species. The three species found to be most at risk were *E. monsoniana*, *E. plukenetii* and *C. congesta*. Remarkably, *E. monsoniana* and *E. plukenetii* appear to be vulnerable to both carbon starvation and hydraulic failure, making them highly susceptible to drought mortality. This is consistent with observations of mortality in *E. monsoniana* at Jonaskop during the study period (see Plate 3.2). Alternatively, these species may have developed alternative strategies to coping with drought, such as xylem refilling, osmotic adjustment or hydraulic segmentation and leaf shedding. *E. plukenetii* is a resprouting species, raising the possibility that it might be adapted to recovery from drought-induced crown dieback (Vilagrosa *et al.*, 2014). If culms of restioids can be considered to be functionally equivalent to leaves in woody species, it raises the possibility that hydraulic segmentation (Scoffoni *et al.*, 2012; Pivovaroff *et al.*, 2014) may also occur in *C. congesta*. Restioids such as these possess underground rhizomes from which they resprout each year. If rhizomes are less vulnerable compared to the culms, the whole-plant strategy might be to

tolerate loss of culm conductivity while maintaining rhizome integrity (Chapter Three and Plate 3.3). The physiology of restioids has received little attention, yet offers up intriguing potential and deserves further investigation. Xylem refilling has been shown to occur in several species even under negative pressures (Stiller *et al.*, 2005; Meinzer & Mcculloh, 2013; Sperry, 2013), although it has yet to be shown in mountain fynbos communities. To make more robust conclusions about the potential for hydraulic failure to induce mortality in fynbos communities, this should also be further investigated, particularly in *Erica* species.

Stem density was shown to be useful as a predictor of xylem vulnerability to cavitation. Since P_{g12} and stem density were both reasonably simple to quantify, this allowed us to evaluate the relationship between P_{g12} and a proxy of P_{50} and P_{88} for a large number of species. Our findings were consistent for those species for which we had both stem density and P_{50}, suggesting that results drawn from this comparison were valid. This supports previous findings of the relevance of stem density as a determining factor in vulnerability (Hacke *et al.*, 2001; Bhaskar *et al.*, 2007; Jacobsen *et al.*, 2007; Pratt *et al.*, 2007). Importantly, our data supported the earlier finding that species vary in the sensitivity of their stomatal closure response and hence in the degree to which they regulate loss of conductance. Since the accuracy of our absolute measure of PLC is contingent on bulk shoot water potential being comparable to stem water potential, we must be cautious not to conclude that these are exact measures for each species. Despite this, our method allows for comparison of relative differences between species. In particular, we feel it is valid to conclude that different species are more or less likely to incur large losses in PLC. The majority of species closed stomata prior to the onset of 50% loss of conductance (i.e. incurred large losses) and only 12.5% of all species sampled tolerated a loss of conductance greater than 88%. The latter group of species might be particularly vulnerable to cavitation in severe drought events. It is relevant to note that the two *Protea* species that tolerated a high degree of loss of conductance are resprouting species, again suggesting that hydraulic segmentation and recovery through osmotic adjustment might be important for this functional type.

A drawback of using measures extracted from xylem vulnerability curves, such as P_{50}, is that these curves are difficult to collect. This practical hindrance limits our ability to describe variation in important hydraulic traits and to characterise hydraulic trade-offs between species. Easily quantifiable traits, such as stem density, provide a simple, yet effective way of describing xylem vulnerability. In turn this allows us to incorporate hydraulic strategies into

the worldwide trait spectra, which relies upon the principle that easily measured plant functional traits may explain differences in growth and survival and thus help explain patterns of community composition and dynamics (Reich, 2014). We think the system that we presented in this study may be helpful in making predictions about potential vulnerability of different species to future drought events.

Supplementary material

Table S4.1: List of species for which stomatal dehydration response curves and stem density were quantified.

Family	Genus	Species	Abbreviation	P_{50}	P_{88}	P_e	P_{min}	Stem density (kg m^{-3})
Asteraceae	*Metalasia*	*densa*	Mden	−6.20	−9.65	−2.39	−3.8	740.89
Asteraceae	*Osmitopsis*	*asteriscoides*	Oast	−0.35	NA	NA	−1	304.49
Bruniaceae	*Brunia*	*alopecuroide*	Balo	−2.2	NA	NA	−1.2	448.87
Ericaceae	*Erica*	*baccans*	Ebacc	NA	NA	NA	NA	684.71
Ericaceae	*E.*	*cerinthoides*	Ecerin	NA	NA	NA	−4.1	539.58
Ericaceae	*E.*	*coccinea*	*Ecoc*	*NA*	*NA*	*NA*	*NA*	701.61
Ericaceae	*E.*	*ericoides*	*Eeri*	*NA*	*NA*	*NA*	−3.63	745.20
Ericaceae	*E.*	*imbricata*	*Eimb*	*NA*	*NA*	*NA*	*NA*	656.07
Ericaceae	*E.*	*monadelpha*	*Emona*	*NA*	*NA*	*NA*	*NA*	NA
Ericaceae	*E.*	*monsoniana*	Emons	−2.07	−5.45	0	−5.02	745.43
Ericaceae	*E.*	*perspicua*	Eper	NA	NA	NA	−0.9	492.24
Ericaceae	*E.*	*plukenetii*	Eplu	−2.95	−8.34	0	−4.3	612.66
Ericaceae	*E.*	*pyxidiflora*	*Epyx*	*NA*	*NA*	*NA*	−3.68	464.76
Ericaceae	*E.*	*sessiliflora*	*Esess*	*NA*	*NA*	*NA*	*NA*	565.50
Ericaceae	*E.*	*setacea*	*Eset*	*NA*	*NA*	*NA*	*NA*	705.32
Ericaceae	*E.*	*subcapitatum*	*Esub*	*NA*	*NA*	*NA*	−4.01	720.00
Ericaceae	*E.*	*vestita*	Ev	−2.62	NA	0	NA	559.73
Fabaceae	*Aspalathus*	*hirta*	Ahir	−3.09	−6.44	−0.41	−2.4	620.79
Fabaceae	*A.*	*pachyloba*	Apach	−4.12	−6.81	−1.06	−2.2	602.47
Proteaceae	*Diastella*	*divaricata*	*Ddiv*	*NA*	*NA*	*NA*	*−0.7*	444.5
Proteaceae	*Leucadendron*	*argenteum*	*Larg*	*−0.6*	*−2.3*	*0*	NA	*NA*

Proteaceae	*L.*	*laureolum*	Llau	−2.35	−3.74	−0.16	−1.84	398.58
Proteaceae	*L.*	*salicifolium*	Lsalic	−1.8	−3.69	−0.77	−0.9	NA
Proteaceae	*L.*	*salignum*	Lsalig	−3.76	−6.08	−1.44	−2	604.07
Proteaceae	*L.*	*sessile*	*Lses*	*NA*	*NA*	*NA*	*NA*	453.65
Proteaceae	*L.*	*spissifolium*	*Lspiss*	*NA*	*NA*	*NA*	*NA*	429.42
Proteaceae	*L.*	*xanthoconas*	Lxan	−2.5	−4.32	−0.69	−1	NA
Proteaceae	*Mimetes*	*cucullatus*	Mcuc	−0.95	−2.8	−0.39	NA	470.24
Proteaceae	*M.*	*hirtus*	Mhir	−1.1	−2.18	−0.51	−0.7	344.91
Proteaceae	*Protea*	*compacta*	Pcom	NA	NA	NA	−1.2	450.43
Proteaceae	*P.*	*cynaroides*	*Pcyn*	*NA*	*NA*	*NA*	*NA*	370.42
Proteaceae	*P.*	*lorifolia*	*Plor*	*NA*	*NA*	*NA*	*NA*	546.65
Proteaceae	*P.*	*nitida*	Pnit	NA	NA	NA	−2.7	583.44
Proteaceae	*P.*	*repens*	Prep	−2.83	−4.53	−1.14	−1.67	610.55
Proteaceae	*P.*	*speciosa*	*Pspe*	*NA*	*NA*	*NA*	*NA*	468.27
Restionaceae	*Askidiosperma*	*paniculatum*	*Apan*	*NA*	*NA*	*NA*	*NA*	392.71
Restionaceae	*Cannomois*	*congesta*	Ccon	−0.56	−0.79	−0.34	−1.88	368.47
Restionaceae	*Chondropetalu*	*tectorum*	*Cpet*	*NA*	*NA*	*NA*	*NA*	NA
Restionaceae	*Hypodiscus*	*aristatus*	Hari	−1.07	−2.24	0	−0.95	335.98
Restionaceae	*Staberoha*	*banksii*	*Sbank*	*NA*	*NA*	*NA*	*NA*	410.57
Restionaceae	*S.*	*cernua*	*Scer*	*NA*	*NA*	*NA*	−0.71	465.47
Restionaceae	*Thamnochortus*	*erectus*	*Terec*	*NA*	*NA*	*NA*	*NA*	NA
Restionaceae	*T.*	*insignis*	*Tins*	*NA*	*NA*	*NA*	*NA*	411.77
Restionaceae	*T.*	*lucens*	*Tluce*	*NA*	*NA*	*NA*	*NA*	511.4
Restionaceae	*T.*	*spicigerus*	*Tspici*	*NA*	*NA*	*NA*	*NA*	506.76
Rosaceae	*Cliffortia*	*ruscifolia*	Crus	−4.29	−8.61	0	−2.5	674.28

Chapter Five: The mechanistic view from the Cape: simulating drought response of fynbos communities.

Abstract

Background/Questions/Methods

Despite evidence that increased plant mortality is being caused by global-change type-drought events, our ability to predict the response of diverse communities remains limited. Nowhere is this more of a concern than in global biodiversity hotspots, regions of the world containing remarkable concentration of species. Predictions from South Africa's Cape Floristic Region (CFR) have previously been based mostly on climate-envelope models, which suffer from a lack of a mechanistic basis. Recently, a hydraulic framework has emerged describing contrasting hydraulic regulation strategies and their effects on likely mechanism of mortality. We set out to incorporate these contrasting regulation strategies into the Campbell soil-plant-atmosphere continuum (SPAC) model designed to simulate plant transpiration and water potential. We modified the model to include xylem vulnerability curves, which allowed us to investigate the role of stomatal versus xylem effects on plant response. We tested the modified model in a highly diverse mountain fynbos community using detailed measurements of water potential and transpiration data collected during a long-term study. We were then able to examine the likely mechanisms of mortality present in this community using combinations of functional traits, also collected from previous studies.

Results/Conclusions

Our data confirmed that species varied in the degree to which they regulated cavitation through stomatal closure and experienced seasonal declines in water potential and that these differences resulted in distinct predictions of mechanisms of mortality. Shallow-rooted, isohydric ericoids were shown to be highly susceptible to leaf-level carbon limitation, but not hydraulic failure. Shallow-rooted anisohydric species, such as *Erica monsoniana* L.f. (Ericaceae) were shown to be vulnerable to hydraulic failure. Although deep-rooted proteoids avoided hydraulic failure for over six months of drought, they were frequently carbon limited. Our model was unable to capture the response of restioid species, possibly due to uptake of dew or cloud moisture. Despite this, there was generally strong agreement between predictions from our model and those from both long-term field-based studies and trait-based

studies in the same communities. This, together with the relative ease with which simulations can be produced, suggests that our model will be valuable for predicting the response of diverse communities to future climate-change-type drought events.

Introduction

An alarming increase in the number of reports of widespread tree die-off in biomes across the world has been documented (Allen *et al.*, 2010). There is strong evidence that this increasing mortality is being caused by global climate-change-type drought events (Breshears *et al.*, 2009; Allen *et al.*, 2010). Understanding and predicting the response of ecosystems remains a grand challenge of fundamental importance for effective management and conservation of biodiversity. Nowhere is this challenge greater than in global biodiversity hotspots in Africa. Alarmingly, "work on species-level responses to climate change factors is lacking in Africa, despite its high concentration of endemic species" (Thuiller *et al.*, 2008). Models can assist greatly in our understanding of how communities are likely to respond to future drought (Hannah *et al.*, 2005; Yates *et al.*, 2010a; Midgley & Thuiller, 2010). For example, climate-envelope models have been effectively utilised to predict the vulnerability of species to extinction (Hannah *et al.*, 2002; Midgley *et al.*, 2002; Thomas *et al.*, 2004; Thuiller *et al.*, 2008). These models use the current geographic distribution of a species to infer its environmental requirements, which then allows prediction of its range under future (or past) climate scenarios (Thomas *et al.*, 2004; Hijmans & Graham, 2006). Although such studies are useful, they have been hampered by the confounding effects of other factors that influence species ranges, such as biotic interactions and human habitat destruction (Pearson & Dawson, 2003). If populations are not in equilibrium with current climate, these models may inaccurately predict potential distributions (Hijmans & Graham, 2006). Another important consideration is that climate-envelope models are most useful at global, continental or regional scales where climate is the predominant factor in determining species distribution (Pearson & Dawson, 2003). At the local or site-specific level, other factors, such as land use and soil type, become significant drivers. Here, a more nuanced, mechanism-based modelling approach is appropriate (Pearson & Dawson, 2003). This is particularly true if the primary interest is in the response to a single factor, such as drought.

Soil-plant-atmosphere continuum (SPAC) models are a primary resource for site-specific modelling and for predicting the vulnerability of local communities to future drought (Campbell, 1985; Tyree & Sperry, 1988; Sperry *et al.*, 1998). The analysis of soil-plant hydraulics can be used to predict patterns of water use for different species and may be useful in determining when hydraulic thresholds are surpassed (Tyree & Ewers, 1991; Sperry *et al.*, 1998). Importantly, these models have advanced our understanding of the physiological

mechanisms underpinning plant death, the consequence of which has been the development of a predictive framework for how communities are likely to respond to drought (McDowell *et al.*, 2008; Plaut *et al.*, 2012; Sevanto *et al.*, 2013). Two of the likeliest mechanisms of mortality to have emerged are carbon starvation and hydraulic failure (McDowell *et al.*, 2011), although we may be some way off from a complete understanding of these (Sala *et al.*, 2010). During drought, the water column in the xylem comes under increasing tension and as a result cavitation may occur (Tyree & Sperry, 1988). Over time, cavitation may become widespread, eventually leading to hydraulic failure (Tyree & Sperry, 1988; Sperry *et al.*, 1998, 2002). During a drought, carbon assimilation may also decline as a result of stomatal closure (Jones & Sutherland, 1991). If the drought persists, carbon reserves may become depleted and an individual may eventually suffer carbon starvation (Sevanto *et al.*, 2013). There are several advantages to site-specific, physiology-based models. Firstly, this modelling approach can provide species-specific predictions of vulnerability for highly diverse or complex communities (Thuiller *et al.*, 2006; West *et al.*, 2007b, 2012; McDowell *et al.*, 2008). Secondly, these models incorporate variation in key functional traits, such as stomatal regulation and rooting depth, which may provide testable hypotheses and generalisable ecological trends (Sperry *et al.*, 2003; McGill *et al.*, 2006).

The objective of this study was to develop a biophysical model that could accurately describe water relations of diverse fynbos functional types. This model was based primarily on soil properties and equations from Campbell (1985). The primary outputs of the model were leaf-level transpiration rate, leaf-water potential and soil moisture content. Once we had shown that the model was able to adequately capture plant response, we used it to simulate a drought and to assess the response of a community of highly diverse mountain fynbos species. Species within this community have been shown to vary in three major hydraulic functional traits: rooting depth, stomatal sensitivity to declining water potentials and xylem vulnerability to embolism (Higgins *et al.*, 1987; Jacobsen *et al.*, 2009; Chapters Three and Four). We used the results of this simulation to infer which species were most likely to succumb to drought mortality under future climate change scenarios and to test hypotheses for the likely mechanism. Our first hypothesis was that deep-rootedness and isohydry would make species less prone to hydraulic failure during simulated summer drought than shallow-rootedness and anisohydry (Table 5.1). Our second hypothesis was that shallow-rootedness and isohydry would induce carbon limitation earlier in response to drought than deep-rootedness and anisohydry (Table 5.1).

Table 5.1: *A priori* predictions of the likely mechanisms of mortality based on combinations of functional traits.

		Hydraulic regulation	
		Isohydric	*Anisohydric*
Rooting depth	*Shallow*	C-limitation (High risk)	Hydraulic failure (High risk)
	Deep	C-limitation (Low risk)	Hydraulic failure (Low risk)

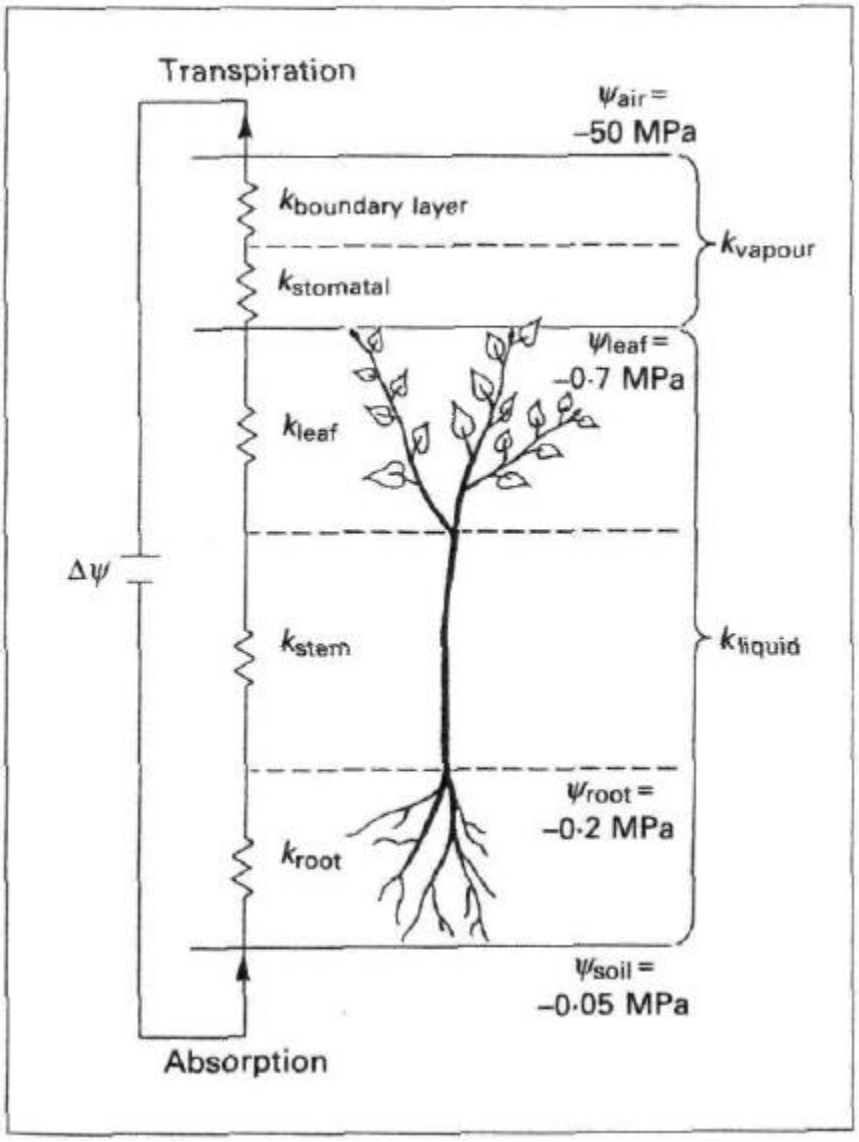

Figure 5.1: The electrical analogy of soil-plant systems, illustrating how the soil-plant system can be treated as a series of resistors with variable conductivities (k). Transpiration is equivalent to the current and is driven by differences in water potentials (Δ P) between the soil and the atmosphere. Figure from Tyree & Ewers (1991).

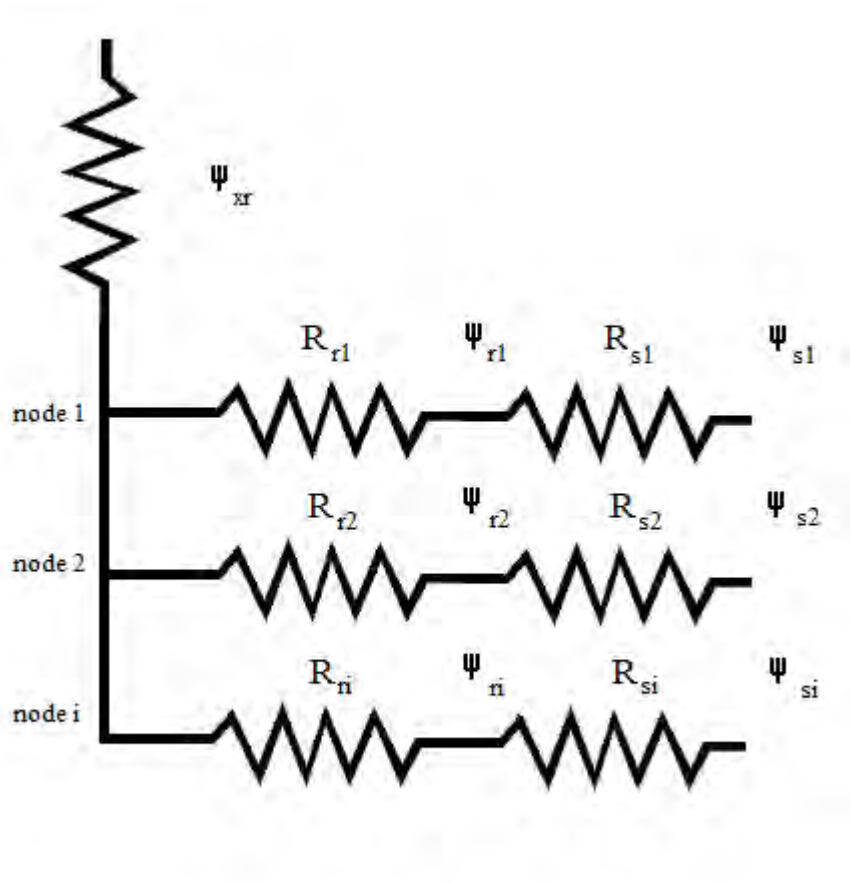

Figure 5.2: The electrical circuit analogue of the soil-root system showing three soil-root layers (nodes) and the resistances (R_s and R_r), and water potential (Psi_s and Psi_r) associated with each of these (Campbell, 1985).

Table 5.2: Standard hydraulic properties of some common soils used in the model. P_e is the air-entry water potential, b is the soil-texture parameter based on mean particle size and K_s is the saturated hydraulic conductivity (Campbell, 1985).

Texture	Silt fraction	Clay fraction	P_e (kPa)	b	K_s (kg s m^{-3})
Sand	0.05	0.03	−0.6	2.2	130.8
Loamy sand	0.12	0.07	−0.79	2.64	75.1
Sandy loam	0.25	0.1	−0.91	3.31	53.2
Loam	0.4	0.18	−0.88	6.58	12.7
Clay	0.2	0.6	−0.98	14.95	1.69

The original Campbell SPAC model

The SPAC model used in this study was based on that of Campbell (1985). Here, I present an overview of the essential components of the model, the details of which can be found by consulting Campbell (1985). SPAC models treat the soil-plant system as analogous to an electrical circuit, where gradients in water potential between circuit components provide the driving force for water uptake or loss (Fig. 5.1). This is in accordance with Darcy's Law where water flux (J_w) is equivalent to the product of water-potential gradient and hydraulic conductivity, K (Campbell, 1985):

$$J_w = K\,(P)\,(\Delta P) \qquad \text{(Eq. 5.1)}$$

The model works by solving equation 5.1 for a range of processes of water uptake and water loss and by checking that these are balanced at each time interval (Campbell, 1985). The relevant principle here is that the difference between the amount of water that flows into a layer and the amount that flows out must equal the amount that is stored in that layer (Campbell, 1985). Important processes for determining the water budget of soils are infiltration of water, redistribution of water between soil layers, evaporation of water directly to the atmosphere and transpiration from plants (Campbell, 1985). Thus, the model works by solving the following equation (Box 5.1):

$$\rho_w L\, d\theta / dt = J_{wi} - J_{wd} - E_s - E_p \qquad \text{(Eq. 5.2)}$$

where ρ_w is the density of water, L is the soil depth , θ is the water content, J_{wi} and J_{wd} are infiltration and redistribution of water in the soil and E_s and E_p are losses due to evaporation and transpiration (Campbell & Norman, 1998). The major difficulty in solving Darcy's Law for soil-plant systems is that K in soils and plants is a function of P (Campbell & Norman, 1998; Sperry *et al.*, 2002). For soils, a simple equation based on soil physical properties that approximates conductivity is (Campbell & Norman, 1998):

$$K\,(P_m) = K_s\,(P_e / P_m)^{2 + 3/b} \qquad \text{(Eq. 5.3)}$$

where P_m is the matric water potential, K_s is saturated conductivity, P_e is the air-entry water potential and b is the exponent of the soil moisture release equation. Both P_e and b rely on soil physical properties such as texture and standard values of these can be found in most soil physics textbooks (Table 5.2). The rates of infiltration and redistribution are dependent on

gradients in matric and gravitational potentials (P_g) along depths of soil, z. Returning to Darcy's Law, these rates can be expressed as (Campbell & Norman, 1998):

$$J_w = - K (P_m) (dP_m / dz) - K(P_m) (dP_g / dz) = -K (P_m) (dP_m / dz) - K (P_m) g \quad \text{(Eq. 5.4)}$$

Solutions to these differential equations are determined for each node by converting them to algebraic equations Campbell (1985). Campbell (1985) showed that by separating the variables and integrating equation 5.4 one can obtain algebraic equations for each of these processes:

$$J_{wd} = - (k_{i+1} P_{i+1} - k_i P_i) / [(z_{i+1} - z_i) (1 - n)] \quad \text{(Eq. 5.5)}$$

where n = 2 + 3/b and:

$$J_{wi} = g (k_i) \quad \text{(Eq. 5.6)}$$

Evaporation is incorporated by calculating vapour fluxes (E_s) for each node. These fluxes are dependent on vapour concentration (c_v), humidity (h) and vapour diffusivity in soil (D_v) according to the following equation (Campbell, 1985):

$$E_{si} = D_v c_v (h_{i+1} - h_i) / (z_{i+1} - z_i) \quad \text{(Eq. 5.7)}$$

Transpiration, E_p, is determined by assessing differences in water potential between soil (P_s) and plant (P_{xr}) and resistance to flow (R) along the soil-root system (Fig. 5.2):

$$E_i = (P_{si} - P_{xri}) / (R_{si} + R_{ri}) \quad \text{(Eq. 5.8)}$$

If axial resistances are assumed to be negligible (Fig. 5.2), equation 5.8 can be solved for P_{xr}:

$$P_{xr} = \{ - E_p + \sum [P_{si} / (R_{si} + R_{ri})]\} / \sum [1 / (R_{si} + R_{ri})] \quad \text{(Eq. 5.9)}$$

Then, if xylem resistance is assumed to be negligible, and R_l is leaf resistance, the leaf water potential, P_l, is given by:

$$P_l = P_{xr} - E_p R_l \quad \text{(Eq. 5.10)}$$

Substituting equation 5.9 into equation 5.10 produces the following:

$$P_l = \sum[P_{si} / (R_{si} + R_{ri})] / \sum [1 / (R_{si} + R_{ri})] - E_p / \sum[1 / (R_{si} + R_{ri})] - E_p R_l \quad \text{(Eq. 5.11)}$$

At this stage, the model works by inputting an initial water potential and subsequently finds a stomatal resistance and water potential which balance water uptake with water loss for that time period. This is achieved using the Newton-Raphson method (see Box 5.1). In this case, the mass balance, F, is the difference between soil and leaf potential minus transpiration rate times the total resistance (Campbell, 1985; Campbell & Norman, 1998):

$$F = P_s - P_l - E_{pmax} \cdot (R_l + R_s + R_r) / [1 + (P_l / P_c)^s] \quad \text{(Eq. 5.12)}$$

When transpiration and leaf water potential are correct, F will be zero. These values for E_p and P_l are then used to calculate actual transpiration rate according to:

$$E_p = E_{pmax} / [1 + (P_l / P_c)^s] \quad \text{(Eq. 5.13)}$$

where P_c is the water potential at which stomata reach twice their minimum and s is the slope of the closure response curve. Once E_p has been determined for each node, these losses become sink terms in the mass balance equation (Eq. 5.2). To solve equation 5.2, the Newton-Raphson method (Box 5.1) is used. This process iteratively finds water potential values at each node until it establishes those that ensure mass balance. Importantly, the water potentials that force the mass balance to zero at each node are those which ensure overall mass balance (Campbell, 1985). Once convergence for each node is satisfied, total flux and change in soil profile water are calculated and water contents are updated. These are then used as starting values for the next time period and the process can be repeated (for more details see Box 5.2).

Box 5.1: *How the Newton-Raphson method works to determine mass balance in soil-plant systems:*

The Newton-Raphson method is often used to solve non-linear equations. Specifically, it is used to find the value of x for which F(x) = 0 (or for which F(x) is less than a set value). The method works by equating the slope of F(x) at x^1 to the derivative $F^1(x)$ to find x^2. $F(x^2)$ is then evaluated and, if it is less than the predetermined value, provides a solution to the equation.

Mathematically:

$$\Delta y / \Delta x = F^1 (x^1) \qquad \text{(Eq. 5.i)}$$

Therefore:

$$F^1 (x^1) (x^1 - x^2) = F (x^1) \qquad \text{(Eq. 5.ii)}$$

Solving for x^2:

$$x^2 = - F (x^1) / F^1 (x^1) / x^1 \qquad \text{(Eq. 5.iii)}$$

If $F(x^2)$ is less than a predetermined value, x^2 is a solution, otherwise solve for x^3 using x^2 as the starting point.

For the purposes of the soil-plant system, we need to use simultaneous equations, where the mass balance, F, across multiple nodes tends to zero. Instead of the single solution of equation 5.ii, we need to find multiple solutions (i.e. solutions for each node). To do this, we use matrix algebra to find solutions to multiple simultaneous equations. A coefficient matrix is needed, which is made up of partial derivatives of F at each node with respect to each x. The solution can then be written in matrix notation (Campbell 1985) and solved iteratively until $F_1 + F_2 + \ldots + F_i = 0$:

$$\begin{bmatrix} dF_1/dx_1 & dF_1/dx_2 & dF_1/dx_3 \\ dF_2/dx_1 & dF_2/dx_2 & dF_2/dx_3 \\ dF_3/dx_1 & dF_3/dx_2 & dF_3/dx_3 \end{bmatrix} \begin{bmatrix} x_1^{p+1} - x_1^{p} \\ x_2^{p+1} - x_2^{p} \\ x_3^{p+1} - x_3^{p} \end{bmatrix} = \begin{bmatrix} F_1 \\ F_2 \\ F_3 \end{bmatrix}$$

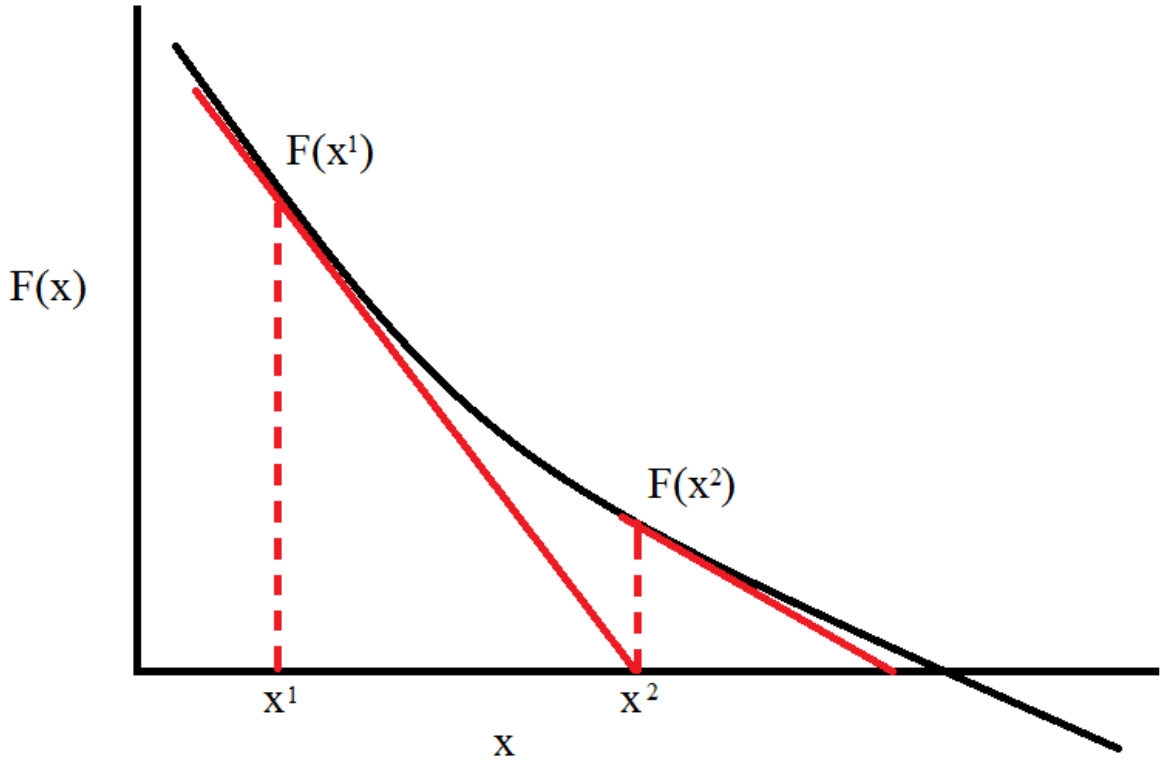

Figure B5.1: The Newton-Raphson method can be used to solve non-linear equations.

Incorporating xylem embolism and loss of conductance into the model

We modified the model to incorporate variable xylem resistance caused by cavitation. We did this by adding xylem resistance, R_x, to equation 5.10:

$$P_l = P_{xr} - E_p (R_l + R_x) \quad \text{(Eq. 5.14)}$$

This is valid since R_x and R_l are in series. Substituting equation 5.9 into equation 5.14 instead of equation 5.10 produces the following:

$$P_l+ = \sum [P_{si} / (R_{si} + R_{ri})] / \sum [1 / (R_{si} + R_{ri})] - E_p / \sum [1 / (R_{si} + R_{ri})] - E_p (R_l + R_x) \quad \text{(Eq. 5.15)}$$

We then had to modify mass-balance equation (Eq. 5.12). We did this by including the relationship between loss of xylem conductance with declining water potential (vulnerability curves) into the relationship between E_{pmax} and E_p, changing it from equation 5.13 to:

$$E_p = E_{pmax} / [(1 + (P_l / P_c)^s) + (1 + (P_l / P_d)^v)] \quad \text{(Eq. 5.16)}$$

where P_d is the point at which resistance reaches twice its maximum (i.e. P_{50}) and v is the slope of the vulnerability curve at P_{50}. The mass balance, F, is then calculated as the difference between soil and leaf potential minus transpiration rate times the total resistance (which includes xylem resistance) (Campbell, 1985; Campbell & Norman, 1998):

$$F = P_s - P_l - E_{pmax} \cdot (R_l + R_s + R_r + R_x) / [1 + (P_l / P_c)^s + (1 + (P_l / P_d)^v)] \quad \text{(Eq. 5.17)}$$

As before, when transpiration and leaf water potential are correct, F will be zero. These values for E_p and P_l are then used to calculate the actual transpiration rate according to equation 5.16 and, once E_p has been determined for each node, these losses become sink terms in the mass-balance equation (Eq. 5.2).

The model was implemented in R (R Development Core Team, 2013) and scripts are available on request.

Box 5.2: *How the SPAC model uses the Newton-Raphson method to solve the overall balance equation:*

At each node, i = 1 to m, we need to find values for P which will make $F_i = 0$. The mass-balance equations at each node are given by:

$$F_i = J_{wdi-1} - J_{wdi} + J_{wii-1} - J_{wii} + \rho_w (\theta_i^{j+1} - \theta_i^j) (z_{i+1} - z_{i-1}) / 2 \Delta t - E_p - E_s \qquad \text{(Eq. 5.2a)}$$

Using the algebraic equations for each process described in the methods we can show that the mass-balance equation at each node is given by:

$$F_i = (k_i P_i - k_{i-1} P_{i-1}) / [(z_i - z_{i-1}) (1 - n)] - (k_{i+1} P_{i+1} - k_i P_i) / [(z_{i+1} - z_i)$$

$$(1 - n)] + g (k_{i-1} - k_i) + \rho_w (\theta_i^{j+1} - \theta_i^j) (z_{i+1} - z_{i-1}) / 2 \Delta t - E_{pi} - E_{si} \qquad \text{(Eq. 5.2b)}$$

The Newton-Raphson method is used to find a water potential that is a solution to this equation for each node (i.e. that P which makes $F_i = 0$). To produce the appropriate matrix, we need to find partial derivatives of each term on the right of the mass-balance equation with respect to each P influencing it. These equations are as follows (Campbell, 1985):

$$dF_i / dP_i = k_i / (z_i - z_{i-1}) + k_i / (z_{i+1} - z_i) - ng\, k_i / P_i + \rho_w \theta_i (z_{i+1} - z_{i-1}) /$$

$$2 b P_i \Delta t + M_w (h_i - h_{i-1}) k_v / (RT) \qquad \text{(Eq. 5.2c)}$$

where M_w is the molar mass of water, R is the universal gas constant, T is temperature in Kelvin and k_v is vapour conductance. The latter term is calculated from the following equation:

$$k_v = 0.66 D_v c_v h_r M_w / R\theta \qquad \text{(Eq. 5.2d)}$$

where D_v is the vapour diffusivity in soil, c_v is the soil vapour concentration.

$$dF_i / dP_i - = - k_i - / (z_i - z_{i-1}) + ng\, k_{i-1} / P_{i-1} \qquad \text{(Eq. 5.2e)}$$

$$dF_i / dP_{i+1} = - k_{i+1} / (z_{i+1} - z_i) \qquad \text{(Eq. 5.2f)}$$

These equations are then used to form the required matrix, which allows us to iteratively solve F for each node. The new estimates of P at the end of the time step are those that make F = 0 for all nodes.

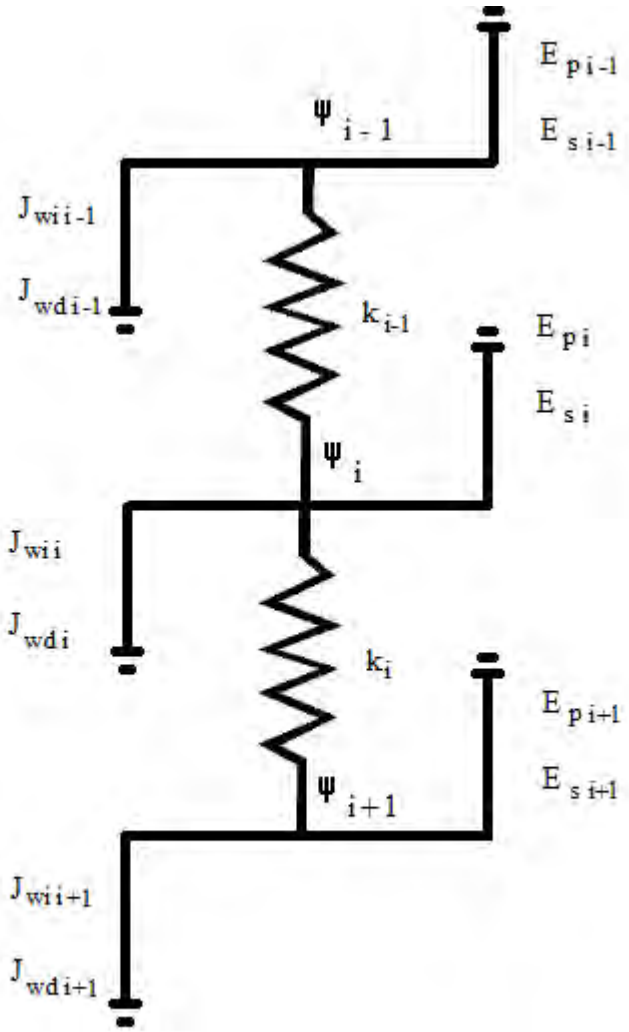

Figure B5.2: Nodes, water potentials (P), conductivities (k) and fluxes (J and E) used in the Newton-Raphson procedure to solve the overall water-balance equation (Campbell, 1985).

Verifying the model with field data

We used field data from Chapters Two and Three, as well as previously published findings, for rooting depth (Higgins *et al.*, 1987) to validate and parameterise the SPAC model.

Sapflow

Sapflow was monitored for three species at the study site at Jonaskop in the Western Cape as outlined in Chapters Two and Three of this thesis. Briefly, miniature external heat-pulse gauges (Skelton *et al.*, 2013) captured sapflow every thirty minutes. Sapflow was converted to transpiration rate using the methods outlined in Chapters Two and Three.

Water potential and gas exchange measurements

As outlined in Chapter Three, predawn and midday shoot water potential were measured at the study site. We measured five individuals of each species using a Scholander pressure chamber. Stomatal conductance was measured at the same time on the same five individuals. These measurements allowed us to construct stomatal-conductance water-potential response curves for the three species. We fitted the following curves to these data to provide estimates of critical water potential (P_c) and slope of the response, s, as required by the model:

$$G_s = 100 / [1 + (P_l / P_c)^s] \quad \text{(Eq. 5.18)}$$

Rooting depth

As outlined in Chapter Three, we assumed that rooting depth for ericoid, proteoid and restioid functional types were similar to those reported by Higgins *et al.* (1987). Without a detailed assessment of rooting depths at the study site, we cannot say for certain that this assignment is correct. However, the relative rooting depths agree with those shown in Chapter Three and with results from previous studies on these functional types (West *et al.*, 2012).

Soil moisture

As outlined in Chapter Three, Volumetric soil moisture was measured at the study site using the EnviroSmart Soil Water Content Profile Probes (Campbell Scientific, Logan Utah, US) . Measurements were taken every hour at depths of 20 cm, 40 cm and 50 cm.

Vulnerability to simulated drought in fynbos communities

We simulated a major drought event in fynbos communities by running the model without any rainfall inputs for an extended period of time. Rainfall is predicted to decline in the western part of the CFR throughout the twenty-first century (Bomhard *et al.*, 2005; Hewitson & Crane, 2006; Lumsden *et al.*, 2009). Winter-dominated rainfall results in seasonal flooding of the water table or at least very wet conditions where evaporation far exceeds potential evapotranspiration. Thus, even a reduction in rainfall with climate change would still be insufficient to cause drought throughout the winter. Rather, the effects of reduced winter rainfall would be felt in extended summer drought. We therefore simulated a drought event that lasted less than a year (approximately 290 days). Our goal was to assess how long it took for critical thresholds to be surpassed for various species during a single drought event. For each species, we extracted two critical water-potential values, which were extracted from the vulnerability curves and the stomatal-conductance water-potential response curves presented in Chapters Three and Four. Rooting depths were assumed to be constant within functional types.

Critical water potential values

We defined two critical water-potential values for each species: the point of carbon-uptake limitation and hydraulic failure. The first point was the water potential at stomatal closure (P_{g12}) obtained from the stomatal-conductance water-potential response curves presented in Chapter Four. The second point was the water potential at almost complete loss of stem-level hydraulic conductivity (P_{88}). We used these two water potential values to provide estimates of the onset of carbon limitation and of hydraulic failure. P_{88} was chosen instead of P_{100} as this has been suggested to be the onset of runaway cavitation and the point of no return for angiosperms (Meinzer & Mcculloh, 2013; Urli *et al.*, 2013; Choat, 2013). Few species that reach 88% loss of conductivity during drought events are able to recover sufficiently (Urli *et al.*, 2013).

Results

Comparison of original SPAC model with model incorporating xylem vulnerability

Our modified SPAC model incorporated variable xylem resistance into simulations of transpiration and water potential (Fig. 5.3 & 5.4). The new model showed that xylem

cavitation may have significant effects on plant transpiration and water potential. Without increasing resistance caused by xylem embolism, plant water potential decreased rapidly and transpiration remained high until the point of stomatal closure (Fig. 5.4; blue lines). Incorporating xylem resistance meant that water potential decreased at the point of air entry (P_e), which reduced the maximum transpiration rate (Fig. 5.4). This is consistent with results from previous SPAC models, which have shown the role of xylem resistance in limiting transpiration (Tyree & Sperry, 1988; Sperry & Pockman, 1993; Sperry *et al.*, 1998, 2003; Sperry, 2000). Our model allowed us to test two different scenarios regarding stomatal regulation of water potential (Fig. 5.3). Isohydric plants are defined as those where stomatal closure was induced prior to P_{50} for the xylem, while anisohydric plants were those that initiated closure subsequent to P_{50} for the xylem (Fig. 5.3) (Jones & Sutherland, 1991; McDowell *et al.*, 2008). Our model was able to simulate isohydric responses, where individuals maintained high water potentials as a consequence of stomatal closure (Fig. 5.4). Total daily transpiration of these individuals was the lowest of the three scenarios (Fig. 5.4). Our model was also able to simulate anisohydric responses, where stomata remained open and water potential continued to decline until hydraulic failure (Fig. 5.4). Transpiration of these individuals was slightly higher than in isohydric individuals, but lower than in individuals with resistant xylem (Fig. 5.4).

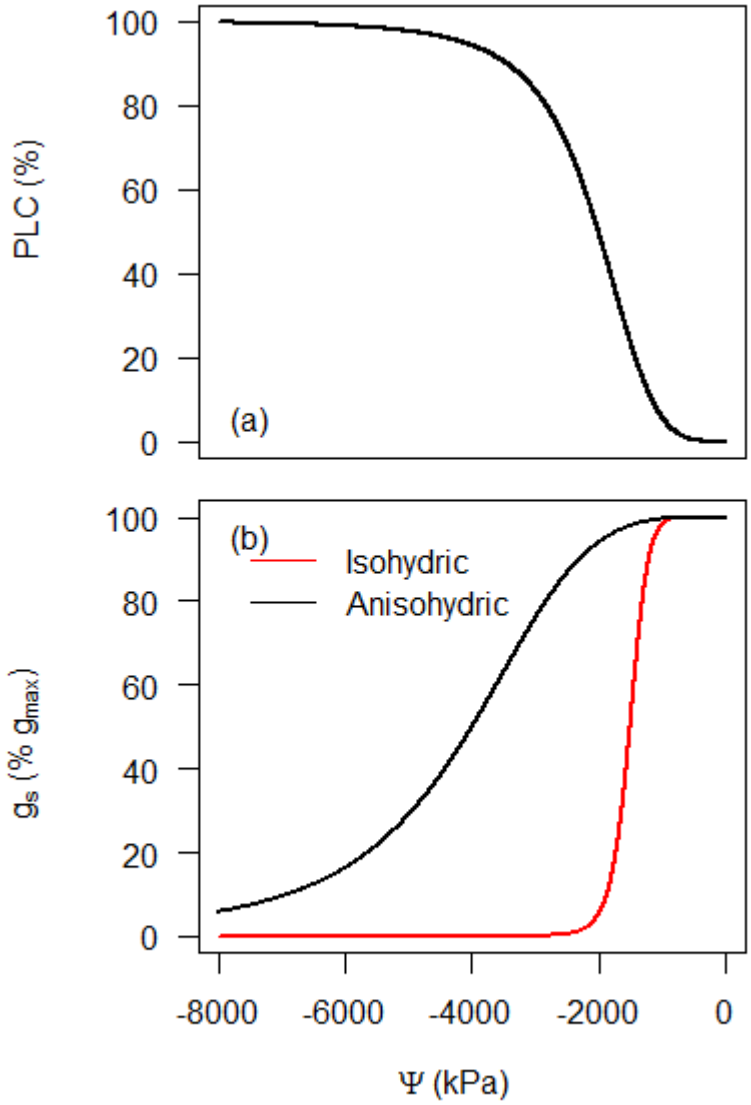

Figure 5.3: Variable xylem resistance was incorporated into the model using vulnerability curves. To test the model, two different assumptions were made regarding stomatal control of cavitation: Isohydric species were assumed to initiate closure of stomata prior to the onset of xylem embolism, while anisohydric species were assumed to have some degree of xylem embolism prior to the onset of stomatal closure.

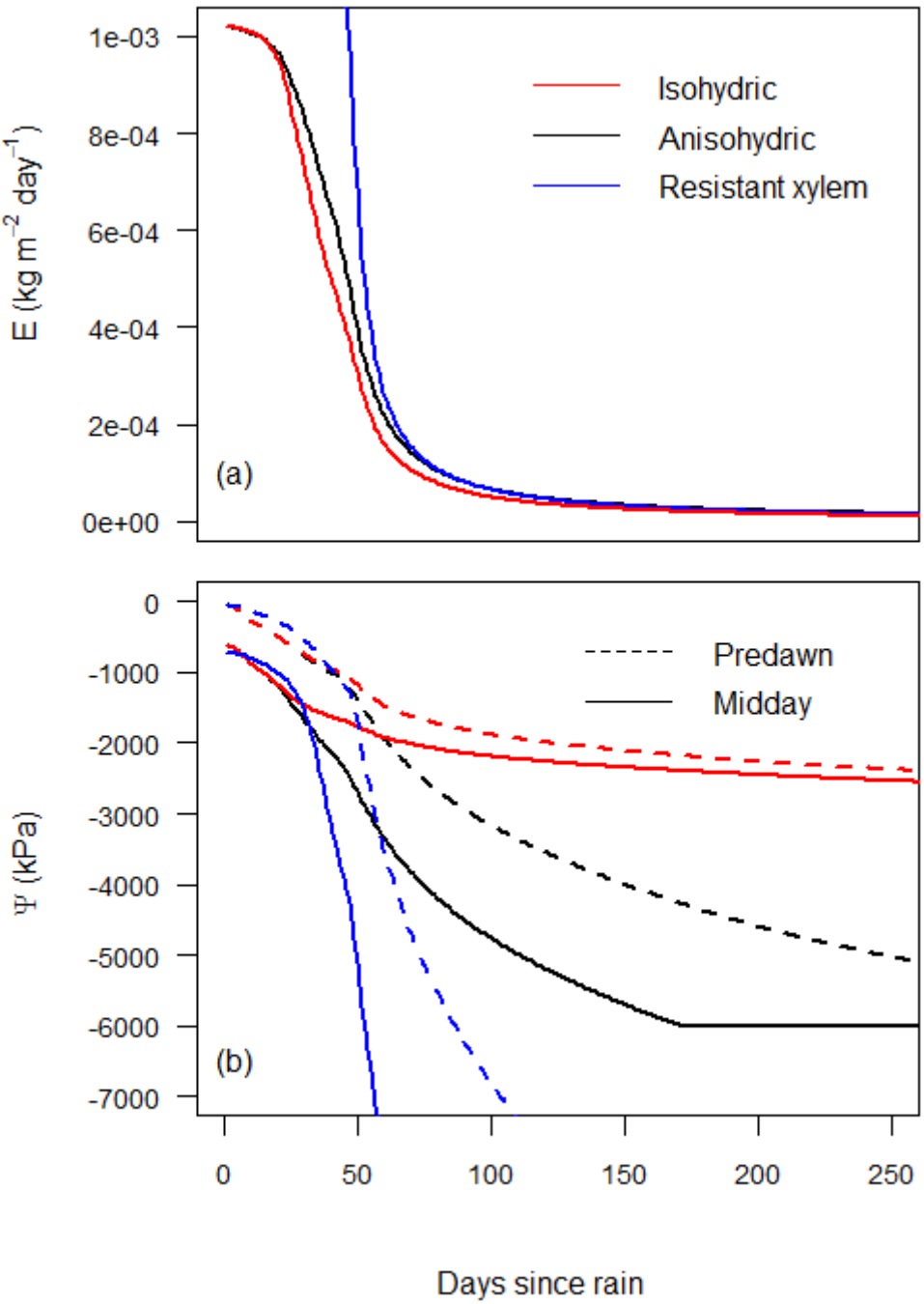

Figure 5.4: Simulated total daily transpiration (a) and minimum predawn and midday water potential (b) from models with three different assumptions: the model with resistant xylem was the original model without xylem vulnerability (Campbell, 1985); the isohydric model incorporated xylem vulnerability, but with stomatal closure initiated prior to xylem embolism; and the anisohydric model incorporated xylem vulnerability with stomatal closure initiated subsequent to the onset of xylem cavitation (see Fig. 5.3).

How well does the model perform against field data?

The model accurately simulated soil moisture at several different depths, as shown by a comparison to field data from Jonaskop (Fig. 5.5). Soil moisture in layers < 2 m showed declining soil moisture over the course of the summer, until significant rainfall events toward the latter stages (Fig. 5.5). We compared field data for transpiration and water potential from Chapter Three to simulated values for each species under two different assumptions: without rainfall and with both rainfall and dew. Since the model simulated drought conditions, we used data from the relatively dry summer of 2012/13 (Fig. 5.6). The capacity of the model to quantify plant response was species specific (Fig. 5.6). Without rainfall events, the SPAC model effectively simulated transpiration and water potential for *Erica monsoniana* L.f. (Ericaceae) and *Protea repens* (L.) L. (Proteaceae) (Fig. 5.6). The model was able to accurately quantify daily transpiration and predawn and midday water potential over the course of the summer. Actual transpiration for *E. monsoniana* was greater than that predicted by the model toward the end of summer (Fig. 5.6a). This is consistent with our previous finding that *E. monsoniana* can refill embolised vessels during summer. When we ran the model including rainfall events during the summer of 2012/13, the model was able to capture this response (Fig. 5.7). This provides strong support for our previous finding that *E. monsoniana* relies upon summer moisture (Chapter Three).

The model performed similarly with and without rainfall events for *P. repens* (Fig. 5.6 & 5.7). In both cases, the model underestimated transpiration during the latter stages of the summer and displayed lower water-potential values than were observed in the field. A possible explanation for this is that deeper roots may be contributing more to water-potential regulation than the model predicts. Although our simulations used rooting densities that were based on field observations (Fig. 5.8) (Higgins *et al.*, 1987), the authors of that study did note that the proteoids that they sampled may have had roots extending beyond the maximum values reported. The model including rainfall captured the recovery in transpiration following a large rainfall event in late summer (Fig. 5.7). However, *P. repens* did not appear to respond to smaller summer rainfall events (Fig. 5.7). This supports our previous inference that *P. repens* responds to large rainfall events during autumn and winter.

The model excluding rainfall or dew was unable to effectively quantify transpiration and water potential for *Cannomois congesta* Mast. (Restionaceae) (Fig. 5.6). The point of hydraulic failure was set at P_{88} in the model based on findings indicating that this is the point

of hydraulic no return for angiosperms (Choat *et al.*, 2012; Urli *et al.*, 2013). The consequence of this for *C. congesta* was that it was predicted to be fully cavitated soon after a drought event was initiated (Fig. 5.6). Despite this, *in situ* predawn water potential for *C. congesta* remained above the threshold of hydraulic failure throughout the summer (Fig. 5.6). However, when we included dew events in the model by increasing the soil moisture in shallow layers every eight days, it captured the response more accurately (Fig. 5.7). This is consistent with our previous interpretation that *C. congesta* is able to maintain high water potentials despite being shallow rooted by refilling most nights using dew (Chapter Three). The model therefore supports the explanation that *C. congesta* is able to recover from high levels of embolism and loss of xylem conductivity despite experiencing water potentials lower than P_{88} (Chapter Three). That the model varied in its ability to capture plant water-potential response underscores the remarkable diversity of hydraulic regulation strategies present in fynbos communities.

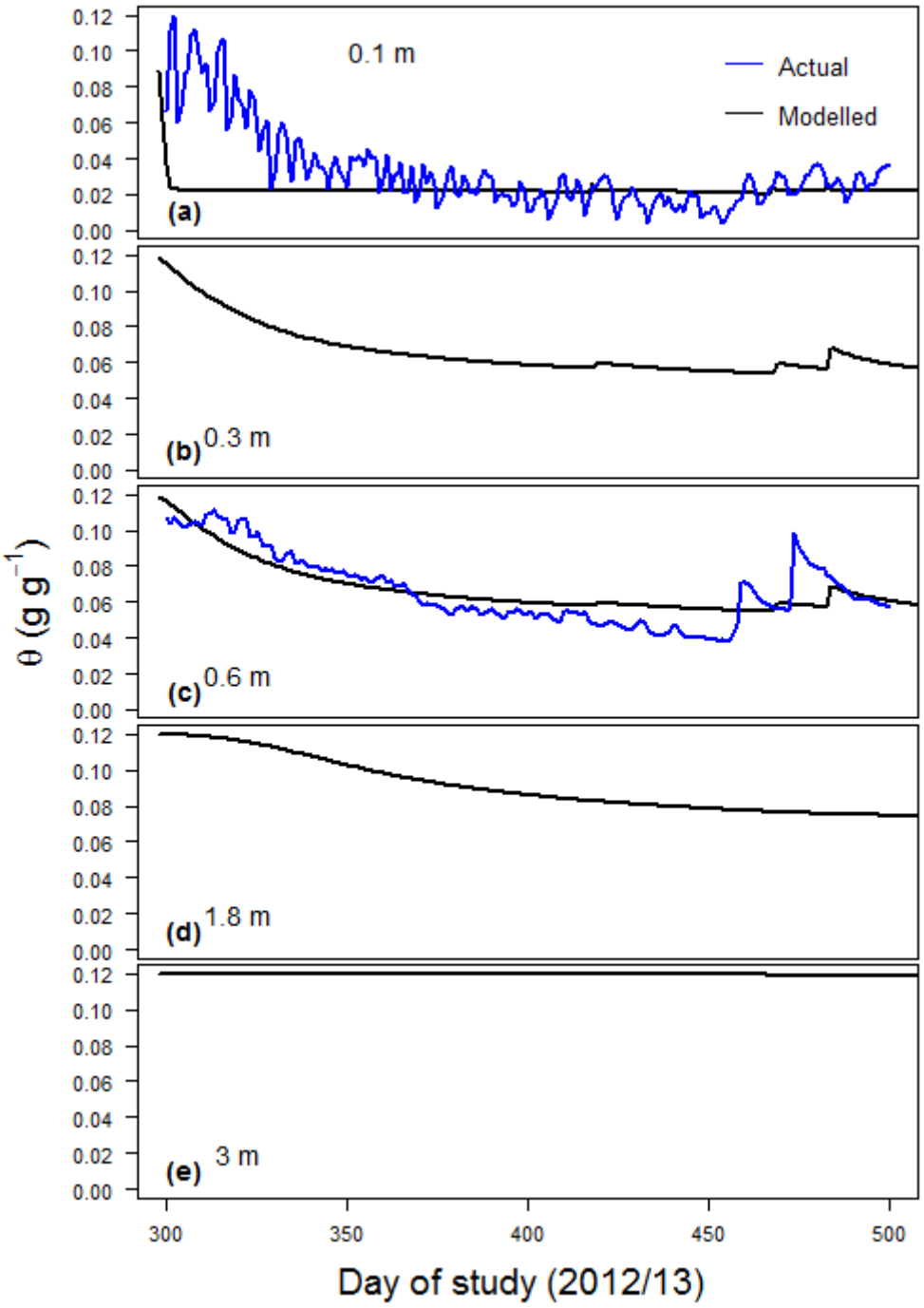

Figure 5.5: Timeline of soil moisture for different depths simulated by the model and, where possible, from the soil-moisture probe.

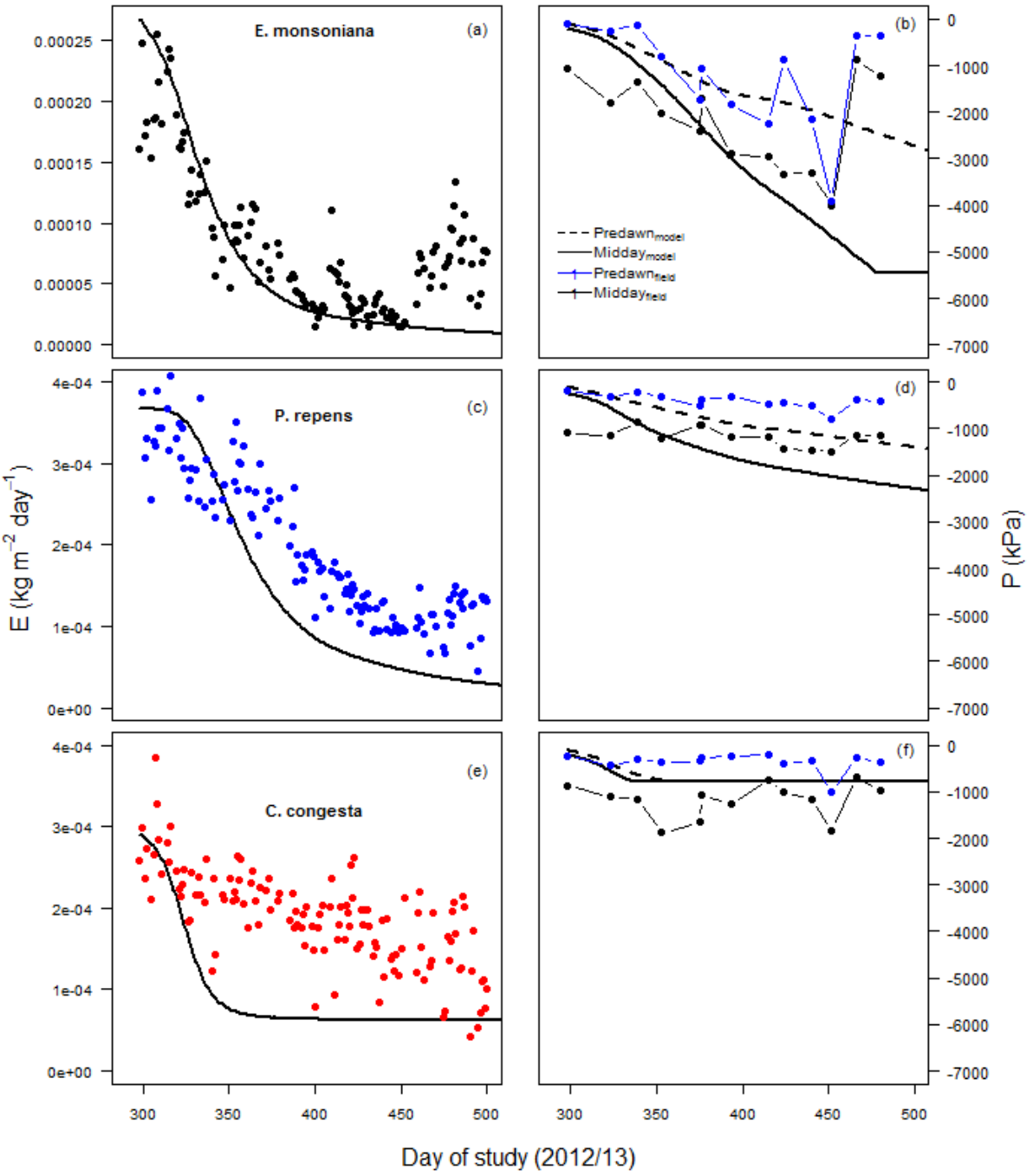

Figure 5.6: Comparison between modelled transpiration and transpiration ((a), (c) and (e)) and modelled water potential and actual water potential ((b), (d) and (f)) for three species occurring at Jonaskop.

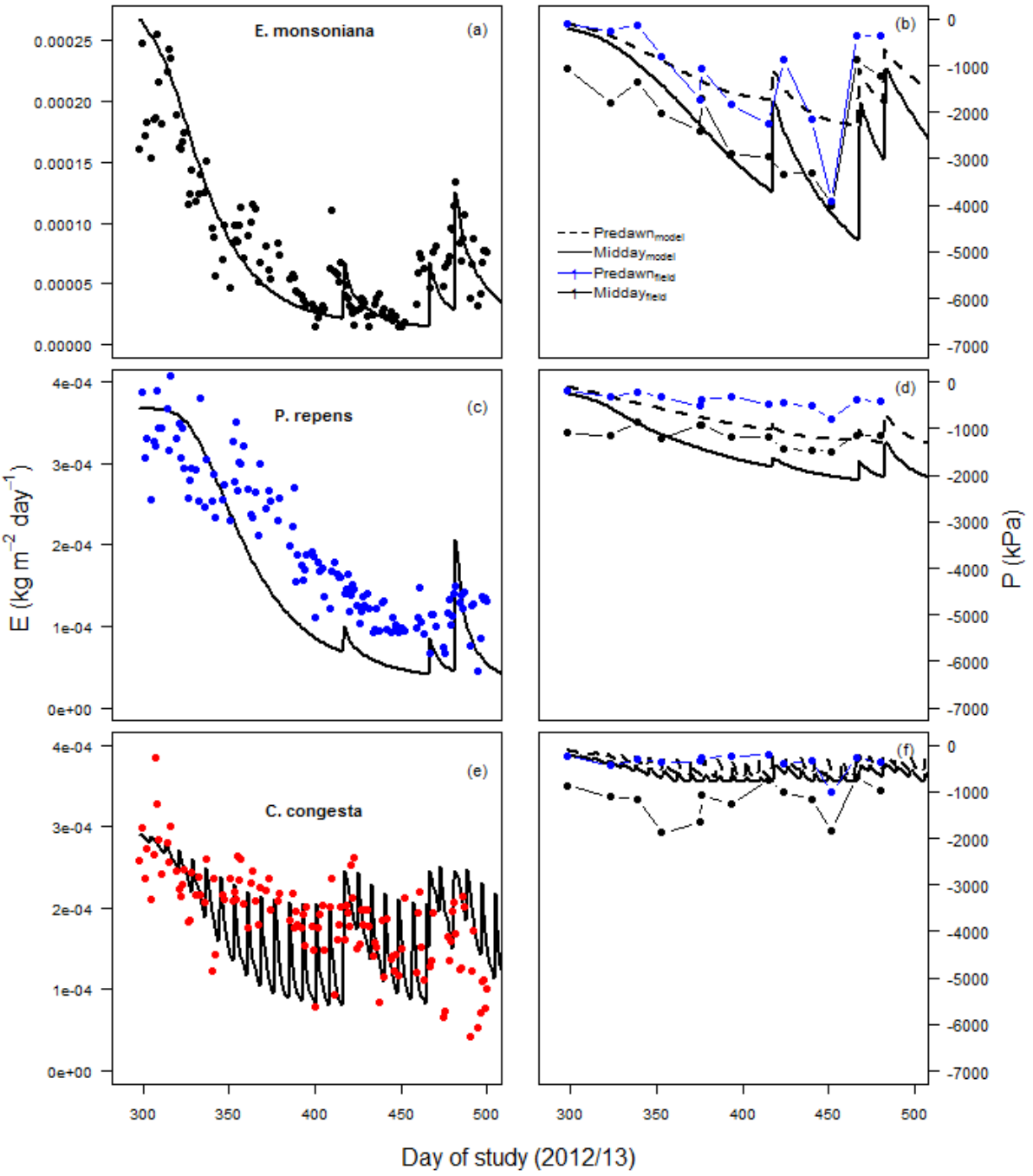

Figure 5.7: Comparison between modelled transpiration and transpiration ((a), (c) and (e)) and modelled water potential and actual water potential ((b), (d) and (f)) for three species occurring at Jonaskop when rainfall and dew events are included in the model.

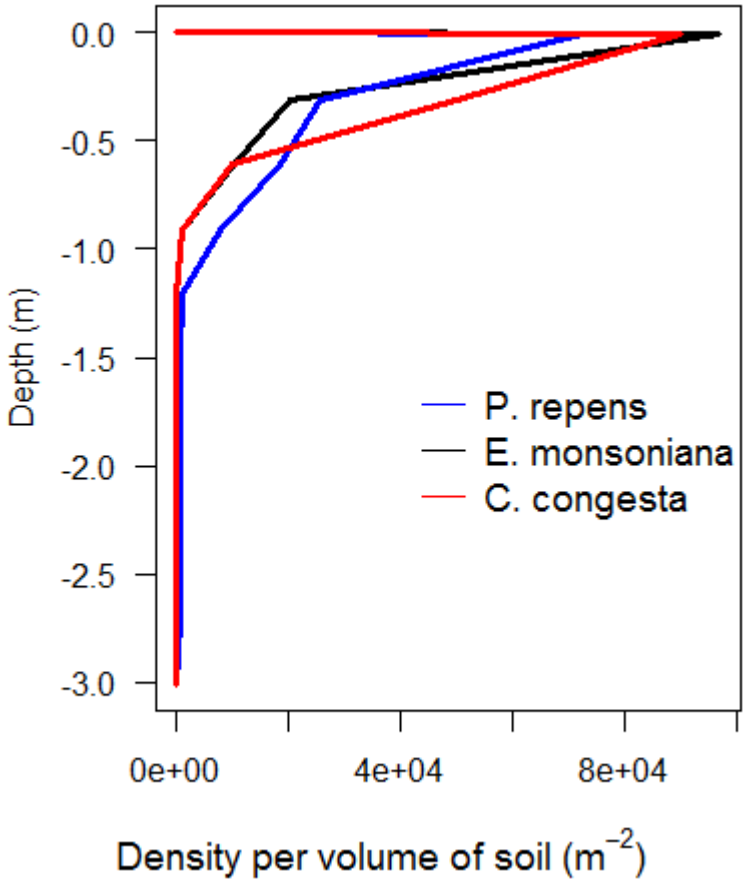

Figure 5.8: Rooting densities of each of the three species for different soil layers (Higgins *et al.*, 1987).

Predicting future response

We used the model to simulate a drought event lasting over nine months for fourteen species for which we had both vulnerability and stomatal-conductance water-potential response curve data (Table 5.3). Four of the fourteen species were predicted to surpass P_{88} and suffer hydraulic failure during this period (Table 5.4). *C. congesta* and *Hypodiscus aristatus* were predicted to pass this point of no return relatively early in response to the drought event. Remarkably, *C. congesta* was predicted to surpass P_{88} after approximately forty days without rainfall (or dew). The remaining individuals were predicted to succumb to hydraulic failure towards the end of the drought period (Table 5.4). *E. monsoniana* was the only ericoid predicted to suffer hydraulic failure, the prediction being death after a period of approximately 181 days. Twelve of the fourteen species from the mountain fynbos community were predicted to endure some form of carbon limitation during the drought (Table 5.4). Water potentials dropped below P_{g12} within three months for half of the fourteen species (Table 5.4). Predicted mechanisms of mortality were also highly consistent within functional types (Table 5.4). Restioids were predicted to fare worst, which suggests that they are heavily dependent on dew or cloud moisture. The majority of ericoid species reach water potentials inducing stomatal closure around a period of two months from the start of the simulated drought (Table 5.4). Proteoids fared slightly better in terms of being carbon limited, with most species reaching P_{g12} after three to four months (Table 5.4). A single proteoid, *Leucadendron salignum*, was predicted to suffer hydraulic failure toward the end of the drought period, after eight to nine months without rainfall (Table 5.4).

Predictions of the mechanism of mortality from the model were largely in agreement with those made *a priori* based on the combination of hydraulic regulation strategy and rooting depth (Table 5.1). Our prediction that shallow-rooted, isohydric species would suffer carbon limitation relatively early following the onset of drought was borne out by the response of several ericoid species (Table 5.4). The response of *Metalasia densa* exemplifies this in that, of the ericoids, it is predicted to endure leaf-level carbon limitation earliest after the onset of drought. Deep-rooted isohydric species were predicted to endure some form of carbon limitation during protracted drought events, but this was initiated much later in comparison to shallow-rooted species. Of the two species that were anisohydric and shallow-rooted, *E. monsoniana* was predicted to be susceptible to hydraulic failure and carbon limitation. *E. plukenetii* managed to avoid hydraulic failure by having much lower vulnerability to

cavitation, but was predicted to suffer carbon limitation (Table 5.4). There were no deep-rooted anisohydric species for which we had vulnerability curve data.

Table 5.3: Critical values obtained from vulnerability curves and stomatal-conductance water-potential response curves used in the model for each species.

Species	Stomatal response curves			Vulnerability curves		
	P_{g50} (MPa)	Slope	P_{g12}	P_{50} (MPa)	Slope	P_{88} (MPa)
Protea repens	−1.03	4.14	−1.52	−2.77	3.24	−4.53
Leucadendron salignum	−1.43	2.37	−3.19	−3.64	3.16	−6.08
L. salicifolium	−1.13	5.86	−1.56	−1.71	2.63	−3.69
L. laureolum	−0.35	1.31	−1.41	−1.72	2.13	−3.74
Mimetes cucullatus	−0.93	4.97	−1.35	−0.82	1.88	−2.80
M. hirtus	−0.57	2.87	−1.05	−1.11	3.17	−2.18
Erica monsoniana	−0.56	1.76	−2.17	−1.58	1.04	−5.45
E. plukenetii	−2.21	5.02	−3.14	−0.28	0.55	−8.34
Aspalathus hirta	−0.97	3.79	−1.63	−2.65	2.04	−6.44
A. pachyloba	−1.28	3.48	−2.08	−3.53	2.54	−6.81
Cliffortia ruscifolia	−2.16	6.59	−2.85	−3.09	1.27	−8.61
Metalasia densa	−1.79	26.5	−1.92	−5.80	3.23	−9.65
Cannomois congesta	−1.03	1.56	−2.17	−0.54	3.36	−0.79
Hypodiscus aristatus	−1.33	2.29	−2.67	−0.90	1.49	−2.24

Table 5.4: Time taken to reach critical water potentials for a range of species from diverse mountain fynbos communities. The plausible mechanism of mortality is shown in bold. If both mechanisms were found to be plausible, they are underlined.

Functional type	Genus	Species	Hydraulic strategy *	Relative rooting depth **	Time to P_{g12} (days since last rainfall)	Time to P_{88} (days since last rainfall) ***
Proteoid	*Protea*	*repens*	Iso	D	**85**	-
	Leucadendron	*salignum*	Iso	D	**119**	**268**
		laureolum	Iso	D	**130**	**-**
		salicifolium	Iso	D	**94**	-
	Mimetes	*cucullatus*	Iso	D	**110**	**-**
		hirtus	Iso	D	**98**	**-**
Ericoid	*Erica*	*monsoniana*	Aniso	S	**75**	**181**
		plukenetii	Aniso	S	**75**	-
	Aspalathus	*hirta*	Iso	S	**48**	-
		pachyloba	Iso	S	**46**	-
	Cliffortia	*ruscifolia*	Iso	S	**49**	-
	Metalasia	*densa*	Iso	S	**41**	-
Restioid	*Cannomois*	*congesta*	Aniso	VS	**-**	**40**
	Hypodiscus	*aristatus*	Aniso	VS	**-**	**60**

***** Iso = isohydric Aniso = anisohydric stomatal regulation. Assignments were based on physiology as explained in Chapters Three and Four.

****** D > 2 m, S < 1.5 m and VS < 50 cm.

******* - indicates that the water potential did not drop below P_{88} during the drought event.

Discussion

Incorporating xylem vulnerability into the SPAC model developed by Campbell (1985) allowed us to more accurately simulate plant response to drought events. Tests of the model showed that it can accurately capture the response of species that can be categorised by the classic isohydric-anisohydric framework (McDowell *et al.*, 2008). Results were also consistent with the physiological findings from previous chapters (Chapter Three). For example, the model accurately simulated the response of *E. monsoniana* and *P. repens*, species known to display anisohydric and isohydric water-potential regulation, respectively (Chapter Three). It showed that *E. monsoniana* is susceptible to large declines in water potential during summer drought periods and that *P. repens* is able to maintain water potential through stomatal closure, preventing xylem embolism. The model with rainfall or dew performed well when simulating the water potential and transpiration of *C. congesta*, which provides strong support for our finding that it is able to recover from cavitation experienced during the day by taking up cloud moisture or dew (Chapter Three). This further supports the role of detailed physiological investigations in deciphering the response of mountain fynbos species to drought events (Hannah *et al.*, 2005; West *et al.*, 2012).

The modified SPAC model presented here also enabled us to test predictions about the vulnerability of diverse mountain fynbos species to future drought events. By simulating a drought event, we were able to determine the time limits required to surpass physiological thresholds that induced hydraulic failure or stomatal closure. Our simulations confirmed *a priori* hypotheses regarding the role of key functional traits and mortality. In particular, our results showed that shallow-rooted isohydric species were highly susceptible to carbon limitation during drought events and that shallow-rooted anisohydric species were susceptible to hydraulic failure. These respective responses were exemplified by *M. densa* and species within *Aspalathus* and by *E. monsoniana*. Deep-rooted proteoid species were shown to be resilient to hydraulic failure during severe drought events lasting up to nine months. The most susceptible of these was *L. salignum*, which was predicted to experience hydraulic failure after approximately eight months. The consistency of responses within functional types enabled us to make further predictions about the susceptibility of diverse fynbos functional types to drought events.

Our results suggest that ericoids are most threatened by future climate-change-type drought events. This is consistent with previous studies within mountain fynbos communities (West *et*

al., 2012). Although a single proteoid was shown to be susceptible to hydraulic failure after protracted periods of drought, of greater concern is the prediction that this functional type would incur carbon limitation during extended periods of drought. Although the significance of a once-off period of limited carbon assimilation might be negligible, multiple periods have been shown to weaken plant defences and enhance the risk of mortality by disease (Breshears *et al.*, 2005; Allen *et al.*, 2010; McDowell *et al.*, 2011; Plaut *et al.*, 2012). Multiple successive drought events are likely to pose a major threat to the survival of individuals of this functional type (Breshears *et al.*, 2009). This finding supports predictions obtained from modelling changes in species' climate envelopes that many proteoid species are vulnerable to extinction from changing climate (Hannah *et al.*, 2002, 2005; Midgley *et al.*, 2002; Midgley & Thuiller, 2010). Importantly, these results also point the way for future studies investigating the role of climate-change-type drought events in causing mortality in fynbos communities. We provide testable hypotheses for the likely mechanisms of mortality to be experienced by proteoids and ericoids in future drought events. Our results also highlight species that might be targeted for monitoring efforts in an effort to provide early warning that climate-change mortality is occurring. In particular, *M. densa*, *Aspalathus hirta* and *A. pachyloba* are all vulnerable to carbon starvation, while *E. monsoniana*, *M. hirtus* and *L. salignum* may be most likely to succumb to hydraulic failure. Although our model is unable to make robust predictions for restioid species, our results indicate that these species are likely to be affected by increasing temperatures, which will impact the availability of dew in mountain communities. Future research should aim to investigate this response more precisely.

Finally, our results show that urgent attention needs to be paid to carbon budgets in fynbos communities. Alarmingly, seven of the fourteen species included in our analysis were predicted to suffer carbon limitation during a drought. However, relatively few studies have investigated the carbon budgets of mountain fynbos species (van der Heyden & Lewis, 1989; von Willert *et al.*, 1989; Herppich *et al.*, 1994; West *et al.*, 2012) and fewer still have conducted long-term studies into the effects of drought. Whether carbon starvation *per se* poses a significant threat to plant species during drought is also a contentious issue (Körner, 2003; Adams *et al.*, 2009; Sala, 2009; McDowell & Sevanto, 2010; Sala *et al.*, 2010). Several tree species have been shown to increase their mobile carbon compounds under water-limiting conditions (Sala & Hoch, 2009) and to have significant carbon reserves even under drought-stressed conditions (Körner, 2003). Körner (2003) showed that Mediterranean shrubs

were more limited by declines in growth and demand than by carbon assimilation. These findings suggest that certain tree species may have adequate supplies of stored non-structural carbohydrates which they are able to mobilise during drought events. Despite this, evidence is also emerging that several species do in fact die as a direct (Sevanto *et al.*, 2013) or indirect (McDowell *et al.*, 2011; Plaut *et al.*, 2012) result of carbon starvation. In particular, multiple periods of limited leaf-level carbon assimilation have been shown to weaken plant defences and enhance the risk of mortality through pathogen infestation (Breshears *et al.*, 2005; Allen *et al.*, 2010; McDowell *et al.*, 2011; Plaut *et al.*, 2012). As a consequence, it is over long periods, with multiple drought events, that carbon limitation is likely to pose a major threat to the survival of individuals (Breshears *et al.*, 2009). Future studies in mountain fynbos communities should incorporate long-term monitoring over several drought periods into their study design; this recommendation echoes calls made by West et al. (2012).

Chapter Six: Hydraulic regulation strategies are critical for understanding plant response to drought in the Cape Floristic Region

> A tree is a complex organism shaped by millions of years of evolutionary trade-offs. Thus, how a tree dies during drought is likely to be a complex process. (Zeppel *et al.*, 2013)

This quote is an apt starting point for the synthesis of my dissertation. To begin with, it offers up several obvious lines of justification for the work that was done. Recent reports of increased and widespread plant mortality in response to regional drought events indicate that global climate change poses a threat to many plant species around the world (Breshears *et al.*, 2005, 2009; Allen *et al.*, 2010). The Cape Floristic Region (CFR), a global biodiversity hotspot, is no exception to this. Climate projections for the region include future declines in rainfall and increases in temperatures (Hewitson & Crane, 2006; Lumsden *et al.*, 2009). Many species within the region and, in particular, several members of the Proteaceae family have been flagged as vulnerable to range contraction as a result of future climate change (Midgley *et al.*, 2002, 2006; Hannah *et al.*, 2005; Bomhard *et al.*, 2005; Midgley & Thuiller, 2010). Drought-response studies are critically important for improving predictions for how communities are likely to be affected. Previous detailed examinations of the physiological processes occurring during dehydration have provided significant insights into potential mechanisms of mortality (Sala, 2009; McDowell & Sevanto, 2010; Anderegg *et al.*, 2012a; Sevanto *et al.*, 2013). These efforts have been focused on several species in particular, such as those of the piñon pine-juniper woodlands or the Douglas fir of North America (Sperry & Ikeda, 1997; West *et al.*, 2007a,b, 2008, 2012; McDowell *et al.*, 2008, 2013; Barnard *et al.*, 2011; Plaut *et al.*, 2012; Sevanto *et al.*, 2013).

Nevertheless, as the quote suggests, trees are indeed complex organisms and there is still much to learn. Varied responses within individual species, combined with the difficulty of describing precisely how individuals die during drought, ensures uncertainty in making future predictions of mortality events (Sala & Hoch, 2009; Sala, 2009; Sevanto *et al.*, 2013). The quote also highlights the most notable bias in our current understanding of plant response to drought: the predominance of investigations into tree species over other functional types in drought-response studies. The hydraulic framework in general has been dominated by trees or large woody shrubs. By ignoring graminoids and small shrubs, such as ericoids, we might be overlooking considerable complexity in the response of plants to drought. Here, I argue that this is indeed the case by highlighting several critical observations from the preceding

chapters. One of the primary objectives of this dissertation was to examine the relevance of hydraulic strategies in determining plant response to drought in highly speciose mountain fynbos communities.

Chapters Two and Three show the presence of highly contrasting hydraulic strategies in the CFR by quantifying detailed physiological responses of three species to major environmental drivers over several successive years. Chapter Two describes advances in the use of miniature external heat-ratio-method (HRM) sapflow gauges on fynbos species. These advances were necessary to establish that these gauges were suitable for quantifying transpiration of highly diverse functional types with varied stem morphologies. Significantly, novel findings in Chapter Two demonstrated that it was possible to capture almost continuous sapflow measurements from Restionaceae species. Continuous measurements provided the opportunity to quantify the dependence of species on varying or transient water sources shown in Chapter Three. This ability is particularly relevant in highly pulsed environments, such as the CFR, where periodic campaign measurements might inadequately capture response to ephemeral events. Chapter Three identified contrasting physiological responses to summer drought periods and the traits that predisposed species to those strategies.

We showed that *Protea repens* (L.) L. (Proteaceae) and *Erica monsoniana* L.f. (Ericaceae) adopt the classic isohydric and anisohydric strategies. These species also provide evidence in support of our hypothesis that deeper-rooted, isohydric species will be more sensitive to atmospheric vapour pressure deficits than shallow-rooted anisohydric species. We also showed that *E. monsoniana* is more likely to respond to changes in soil moisture and relies heavily on refilling after rainfall events. *Cannomois congesta* Mast. (Restionaceae)'s strategy was more difficult to characterise. Individuals of this species maintained predawn water potential at relatively high values, despite being shallow-rooted. They were also able to maintain high rates of transpiration, despite experiencing high loss of conductivity due to highly vulnerable xylem. We provide several lines of evidence suggesting that the ability to take up moisture from ephemeral sources, such as dew, allows *C. congesta* individuals to regularly refill. In particular, the observations of highly enriched moisture sources, consistently high predawn water potentials and rates of transpiration (Chapter Three) and the improved simulation of transpiration and water potential patterns with the inclusion of regular moisture inputs (Chapter Five) provide strong support for this argument. This is also consistent with the interpretation of previous hydraulic studies done on this functional type

(Marloth, 1903, 1905; West *et al.*, 2012). Since this response does not fall neatly within the isohydric-anisohydric paradigm, we suggest that it should be given a different term. Species that maintain a relatively consistent difference between predawn and midday water potential values have previously been referred to as isohydrodynamic (Franks *et al.*, 2007). However, we feel that this implies stomatal regulation of water potential, similar to isohydric regulation. Instead, we propose that the relatively anisohydric regulation of water potential by stomatal conductance in addition to regular refilling and therefore constant predawn water potential should be referred to as "anisodynamic". These results further emphasise the remarkable diversity of solutions to the problem of desiccation posed by long, hot and relatively dry summers present within the CFR (Specht & Moll, 1983; Yates *et al.*, 2010b; Skelton *et al.*, 2012; Pratt *et al.*, 2012).

As ever, within the diversity of functional traits we see the traces of millions of years of evolutionary pressure. Throughout the dissertation, I have incorporated functional traits into an understanding of how species are likely to respond to drought events. Functional traits allow complex, whole-plant responses to be understood. Our results showed the importance of examining the interactions between functional traits and physiological responses. Consistently with previous studies, we showed that species varied in the key functional traits affecting drought response, such as vulnerability to cavitation and rooting depth (Higgins *et al.*, 1987; Jacobsen *et al.*, 2007, 2009). Knowledge of these traits proved crucial to elucidating the full picture of species response. A primary goal of Chapter Four was to identify potential outcomes as determined by associations between traits and physiological responses. We were able to develop a predictive framework based on associations between key functional traits that enabled rapid, yet reliable, assessment of the vulnerability of diverse species. We then used this framework to predict likely mechanisms of mortality within mountain fynbos communities. Results indicated that ericoids are most vulnerable to a combination of hydraulic failure and carbon limitation, while restioids are vulnerable to hydraulic failure. Although proteoids were predicted to be the least vulnerable to hydraulic failure, they were predicted to experience some degree of carbon limitation. These results were consistent with our earlier results (Chapter Three). Further work, as outlined in Chapter Five, extended our predictive ability by establishing a model that simulated drought events and the physiological response of diverse species. The model was developed using biophysical properties of the soil-plant-atmosphere continuum (SPAC) and parameterised using key functional traits. The results enabled us to make predictions about the likely effect

of different drought events on species with different hydraulic strategies. In addition to providing testable hypotheses about trait combinations and pathways to mortality, the model returned predictions of how long different species might persist during a protracted drought. Results showed that restioids and ericoids are likely to experience hydraulic failure within three months of the onset of drought conditions. By contrast, deeper-rooted proteoids are only likely to experience hydraulic failure after several months without rainfall. Additionally, ericoids and proteoids were predicted to suffer carbon limitation. These results are consistent with those from previous chapters and emphasise the vulnerability of communities to future drought.

This study has shown the importance of detailed physiological knowledge in understanding and predicting the response to future drought in mountain fynbos communities. It provides several testable hypotheses as to which species or functional types are susceptible to drought mortality and the manner in which they are likely to die. Although response within functional types is somewhat varied, broad functional types work. A comparison of the responses of species from our study shows consistency with the responses of those shown in previous drought studies of fynbos (West *et al.*, 2012). In particular, the responses within families or functional types are remarkably consistent (West *et al.*, 2012). We posit that shallow-rooted, isohydric species are likely to be most susceptible to drought-induced mortality through a combination of hydraulic failure and carbon starvation (Chapters Three, Four and Five). This functional type is most commonly represented by ericoid species. Despite this, the ericoids of fynbos, which include the highly diverse and largely endemic *Erica*, have received little attention in previous climate-change risk assessments or climate-envelope modelling studies (Midgley *et al.*, 2002, 2006; Bomhard *et al.*, 2005; Midgley & Thuiller, 2010). The proteoid functional type is more likely to experience carbon limitation during protracted drought periods than hydraulic failure (Chapters Three, Four and Five). Our ability to make accurate predictions about the restioids remains limited despite several important advancements. For example, we were able to provide further evidence for the possible role of atmospheric moisture sources in the functionality of this group. Our results suggest that carbon limitation is unlikely to be a major factor in these species in the future, but that levels of hydraulic failure might increase under warmer conditions. This may be particularly significant if temperatures rise above those that promote the formation of dew.

Yet, with these predictions come some important caveats. We are currently unable to determine how long species can endure leaf-level carbon limitation before carbon starvation occurs. Thus, our ability to describe mortality events within mountain fynbos communities remains limited (Körner, 2003; Sala, 2009; Sala *et al.*, 2012). Although our study has highlighted the interdependency of carbon and water, it also shows the inadequacy of current understandings of carbon dynamics and allocation in fynbos species (Körner, 2003). If we are to improve our ability to predict the response of fynbos species, it is critical to obtain a better understanding of carbon dynamics. Future studies should urgently address this critical gap in our knowledge. We recommend conducting long-term, rainfall manipulation studies and measuring a range of carbon supplies and sinks. The goal of these should be to generate an improved understanding of whole plant carbon dynamics by monitoring measures such as leaf-level assimilation, metabolic demand, growth and reallocation of non-structural carbohydrate during drought events. Finally, we recommend long-term monitoring of the species and functional types highlighted in this thesis. In particular, ericoids and restioids deserve to be monitored in the future, since they appear to be particularly vulnerable to global climate-change-type events. Highly charismatic, economically important and ecologically significant *Erica* and restioid species abound within mountain fynbos communities and should be identified and targeted for monitoring. Some reports indicate that the impact of climate change is likely to be visible within the next fifty years (Midgley *et al.*, 2002; Hannah *et al.*, 2005; Bomhard *et al.*, 2005). If we care about preserving this remarkable flora, we should start gathering the knowledge required to make a difference immediately. With a better understanding of how species respond, we might be able to positively influence the future management of this flora and ensure that fynbos species continue to be shaped by evolutionary trade-offs for millions of years.

References

Ackerly DD. **2004**. Functional strategies of Chaparral shrubs in relation to seasonal water deficit and disturbance. *Ecological Monographs* **74**: 25–44.

Adams HD, Guardiola-Claramonte M, Barron-Gafford GA, Villegas JC, Breshears DD, Zou CB, Troch PA, Huxman TE. **2009**. Reply to Sala: Temperature sensitivity in drought-induced tree mortality hastens the need to further resolve a physiological model of death. *Proceedings of the National Academy of Sciences of the United States of America* **106**: E69–E69.

Adams HD, Macalady AK, Breshears DD, Allen CD, Stephenson NL, Saleska SR, Huxman TE, McDowell NG. **2010**. Climate-induced tree mortality: Earth system consequences. *Eos, Transactions American Geophysical Union* **91**: 153–154.

Agenbag L, Esler KJ, Midgley GF, Boucher C. **2008**. Diversity and species turnover on an altitudinal gradient in Western Cape , South Africa: baseline data for monitoring range shifts in response to climate change. *Bothalia* **191**: 161–191.

Allen CD, Macalady AK, Chenchouni H, Bachelet D, McDowell N, Vennetier M, Kitzberger T, Rigling A, Breshears DD, Hogg EH, *et al.* 2010. A global overview of drought and heat-induced tree mortality reveals emerging climate change risks for forests. *Forest Ecology and Management* **259**: 660–684.

Anderegg WRL, Berry JA, Field CB. **2012a**. Linking definitions, mechanisms, and modeling of drought-induced tree death. *Trends in plant science* **17**: 693–700.

Anderegg WRL, Berry JA, Smith DD, Sperry JS, Anderegg LDL, Field CB. **2012b**. The roles of hydraulic and carbon stress in a widespread climate-induced forest die-off. *Proceedings of the National Academy of Sciences of the United States of America* **109**: 233–237.

Anderegg WRL, Plavcová L, Anderegg LDL, Hacke UG, Berry JA, Field CB. **2013**. Drought's legacy: multiyear hydraulic deterioration underlies widespread aspen forest die-off and portends increased future risk. *Global Change Biology* **19**: 1188–96.

Araya YN, Silvertown J, Gowing DJ, McConway KJ, Linder HP, Midgley GF. **2011**. A fundamental, eco-hydrological basis for niche segregation in plant communities. *New Phytologist* **189**: 253–258.

Aston T. **2007**. Geohydrological characteristics of Table Mountain Group aquifer-fed seeps and the plant ecophysiological consequences. : 146.

Austin A, Yahdjian L, Stark J, Belnap J, Porporato A, Norton U, Ravetta D, Schaeffer S. **2004**. Water pulses and biogeochemical cycles in arid and semiarid ecosystems. *Oecologia* **141**: 221–235.

Barnard DM, Meinzer FC, Lachenbruch B, McCulloh KA, Johnson DM, Woodruff DR. **2011**. Climate-related trends in sapwood biophysical properties in two conifers: avoidance of

hydraulic dysfunction through coordinated adjustments in xylem efficiency, safety and capacitance. *Plant, Cell & Environment* **34**: 643–654.

Betts RA, Boucher O, Collins M, Cox PM, Falloon PD, Gedney N, Hemming DL, Huntingford C, Jones CD, Sexton DMH, *et al.* 2007. Projected increase in continental runoff due to plant responses to increasing carbon dioxide. *Nature* **448**: 1037–41.

Bhaskar R, Valiente-Banuet A, Ackerly DD. **2007**. Evolution of hydraulic traits in closely related species pairs from Mediterranean and nonMediterranean environments of North America. *New Phytologist* **176**: 718–726.

Blackman CJ, Brodribb TJ, Jordan GJ. **2009**. Leaf hydraulics and drought stress: response, recovery and survivorship in four woody temperate plant species. *Plant, Cell & Environment* **32**: 1584–1595.

Bomhard B, Richardson DM, Donaldson JS, Hughes GO, Midgley GF, Raimondo DC, Rebelo AG, Rouget M, Thuiller W. **2005**. Potential impacts of future land use and climate change on the Red List status of the Proteaceae in the Cape Floristic Region, South Africa. *Global Change Biology* **11**: 1452–1468.

Brand WA. **1996**. High precision isotope ratio monitoring techniques in mass spectrometry. *Journal of Mass Spectrometry* **31**: 225–235.

Breshears DD, Cobb NS, Rich PM, Price KP, Allen CD, Balice RG, Romme WH, Kastens JH, Floyd ML, Belnap J, *et al.* 2005. Regional vegetation die-off in response to global-change-type drought. *Proceedings of the National Academy of Sciences* **102**: 15144–15148.

Breshears DD, Myers OB, Meyer CW, Barnes FJ, Zou CB, Allen CD, McDowell NG, Pockman WT. **2009**. Tree die-off in response to global change-type drought: mortality insights from a decade of plant water potential measurements. *Frontiers in Ecology and the Environment* **7**: 185–189.

Brodribb TJ, Cochard H. **2009**. Hydraulic failure defines the recovery and point of death in water-stressed conifers. *Plant Physiology* **149**: 575–84.

Brodribb TJ, Holbrook NM. **2003**. Stomatal closure during leaf dehydration: Correlation with other leaf physiological traits. *Plant Physiology* **132**: 2166–2173.

Brodribb TJ, Jordan GJ. **2008**. Internal coordination between hydraulics and stomatal control in leaves. *Plant, Cell & Environment* **31**: 1557–1564.

Brodribb TJ, McAdam SAM. **2013**. Abscisic Acid mediates a divergence in the drought response of two conifers. *Plant Physiology* **162**: 1370–7.

Burgess SSO, Adams MA, Bleby TM. **2000**. Measurement of sap flow in roots of woody plants: a commentary. *Tree Physiology* **20**: 909–913.

Burgess SSO, Adams MA, Turner NC, Beverly CR, Ong CK, Khan AA, Bleby TM. **2001**. An improved heat pulse method to measure low and reverse rates of sap flow in woody plants. *Tree Physiology* **21**: 589–98.

Campbell GS. **1985**. *Soil physics with BASIC: transport models for soil-plant systems*. New York, N.Y.: Elsevier.

Campbell GS, Norman JM. **1998**. *An introduction to environmental biophysics*. New York, N.Y.: Springer.

Campbell BM, Werger MJA. **1988**. Plant form in the mountains of the Cape, South Africa. *Journal of Ecology* **76**: 637–653.

Chaves MM, Maroco JP, Pereira JS. **2003**. Understanding plant responses to drought — from genes to the whole plant. *Functional Plant Biology* **30**: 239–264.

Chaves MM, Pereira JS, Maroco JP, Rodrigues ML, Ricardo CPP, Osorio ML, Carvalho I, Faria T, Pinheiro C. **2002**. How plants cope with water stress in the field. Photosynthesis and growth. *Annals of Botany* **89**: 907–916.

Choat B. **2013**. Predicting thresholds of drought-induced mortality in woody plant species. *Tree Physiology* **33**: 669–671.

Choat B, Drayton WM, Brodersen C, Matthews MA, Shackel KA, Wada H, McElrone AJ. **2010**. Measurement of vulnerability to water stress-induced cavitation in grapevine: a comparison of four techniques applied to a long-vesseled species. *Plant, Cell & Environment* **33**: 1502–1512.

Choat B, Jansen S, Brodribb TJ, Cochard H, Delzon S, Bhaskar R, Bucci SJ, Feild TS, Gleason SM, Hacke UG, *et al.* 2012. Global convergence in the vulnerability of forests to drought. *Nature* **491**: 752–755.

Clark ID, Fritz P. **1997**. *Environmental isotopes in hydrogeology*. CRC Press.

Clearwater MJ, Luo Z, Mazzeo M, Dichio B. **2009**. An external heat pulse method for measurement of sap flow through fruit pedicels, leaf petioles and other small-diameter stems. *Plant, Cell & Environment* **32**: 1652–63.

Cleveland WS, Devlin SJ. **1988**. Locally weighted regression: an approach to regression analysis by local fitting. *Journal of American Statistical Association* **83**: 596–610.

Cochard H, Badel E, Herbette S, Delzon S, Choat B, Jansen S. **2013**. Methods for measuring plant vulnerability to cavitation: a critical review. *Journal of Experimental Botany* **64**: 4779–4791.

Cohen Y, Fuchs M. **1989**. Problems in calibrating the heat pulse method for measuring sap flow in the stem of trees and herbaceous plants. *Agronomie* **9**: 321–325.

Cohen Y, Li Y. **1996**. Validating sap flow measurement in field-grown sunflower and corn. *Journal of Experimental Botany* **47**: 1699–1707.

Cowling RM, Rundel PW, Lamont BB, Arroyo MK, Arianoutsou M. **1996**. Plant diversity in mediterranean-climate regions. *Trends in Ecology & Evolution* **11**: 362–366.

Cramer W, Bondeau A, Woodward FI, Prentice IC, Betts RA, Brovkin V, Cox PM, Fisher V, Foley JA, Friend AD, *et al.* 2001. Global response of terrestrial ecosystem structure and function to CO_2 and climate change: results from six dynamic global vegetation models. *Global Change Biology* **7**: 357–373.

Damour G, Simonneau T, Cochard H, Urban L. **2010**. An overview of models of stomatal conductance at the leaf level. *Plant, Cell & Environment* **33**: 1419–1438.

Díaz S, Cabido M. **2001**. *Vive la différence*: plant functional diversity matters to ecosystem processes. *Trends in Ecology & Evolution* **16**: 646–655.

Dobson AJ, Barnett AG. **2008**. *An Introduction to Generalized Linear Models, Third Edition*. CRC Press.

Domec J-C, Gartner BL. **2001**. Cavitation and water storage capacity in bole xylem segments of mature and young Douglas-fir trees. *Trees* **15**: 204–214.

Donovan LA, Richards JH, Linton MJ. **2003**. Magnitude and mechanisms of disequilibrium between predawn plant and soil water potentials. *Ecology* **84**: 463–470.

Edwards WRN, Becker P, Eermak J. **1996**. A unified nomenclature for sap flow measurements. *Tree Physiology* **17**: 65–67.

Ewers BE, Oren R. **2000**. Analyses of assumptions and errors in the calculation of stomatal conductance from sap flux measurements. *Tree Physiology* **20**: 579–589.

Ewers BE, Oren R, Sperry JS. **2000**. Influence of nutrient versus water supply on hydraulic architecture and water balance in *Pinus taeda*. *Plant, Cell & Environment* **23**: 1055–1066.

Farquhar GD, Sharkey TD. **1982**. Stomatal Conductance and Photosynthesis. *Annual Review of Plant Physiology* **33**: 317–345.

Field CB, Barros VC, Mastrandrea MD, Mach KJ, Abdrabo MA-K, Adger WN, Anokhin YA, Anisimov OA, Arent DJ, Barnett J. **2014**. *Climate Change 2014: Impacts, Adaptation, and Vulnerability*.

Foden W, Midgley GF, Hughes G, Bond WJ, Thuiller W, Hoffman MT, Kaleme P, Underhill LG, Rebelo A, Hannah L. **2007**. A changing climate is eroding the geographical range of the Namib Desert tree *Aloe* through population declines and dispersal lags. *Diversity and Distributions* **13**: 645–653.

Franks PJ, Drake PL, Froend RH. **2007**. Anisohydric but isohydrodynamic: seasonally constant plant water potential gradient explained by a stomatal control mechanism incorporating variable plant hydraulic conductance. *Plant, Cell & Environment* **30**: 19–30.

Froux F, Ducrey M, Dreyer E, Huc R. **2005**. Vulnerability to embolism differs in roots and shoots and among three Mediterranean conifers: consequences for stomatal regulation of water loss? *Trees* **19**: 137–144.

Goldblatt P, Manning JC. **2002**. Plant diversity of the Cape region of Southern Africa. *Annals of the Missouri Botanical Garden* **89**: 281–302.

Guyot G, Scoffoni C, Sack L. **2012**. Combined impacts of irradiance and dehydration on leaf hydraulic conductance: insights into vulnerability and stomatal control. *Plant, Cell & Environment* **35**: 857–71.

Hacke UG, Sperry JS. **2001**. Functional and ecological xylem anatomy. *Perspectives in Plant Ecology, Evolution and Systematics* **4**: 97–115.

Hacke UG, Sperry JS, Pockman WT, Davis SD, McCulloh KA. **2001**. Trends in wood density and structure are linked to prevention of xylem implosion by negative pressure. *Oecologia* **126**: 457–461.

Hannah L, Midgley GF, Hughes G, Bomhard B. **2005**. The view from the Cape: extinction risk, protected areas, and climate change. *BioScience* **55**: 231–242.

Hannah L, Midgley GF, Lovejoy T, Bond WJ, Bush M, Lovett JC, Scott D, Woodward FI. **2002**. Conservation of biodiversity in a changing climate. *Conservation Biology* **16**: 264–268.

Hartmann H. **2011**. Will a 385 million year-struggle for light become a struggle for water and for carbon? - How trees may cope with more frequent climate change-type drought events. *Global Change Biology* **17**: 642–655.

Herppich M, Herppich WB, von Willert DJ. **1994**. Influence of drought, rain and artificial irrigation on photosynthesis, gas exchange and water relations of the fynbos plant *Protea acaulos* at the end of the dry season. *Botanica Acta* **107**: 440–450.

Hewitson BC, Crane RG. **2006**. Consensus between GCM climate change projections with empirical downscaling: precipitation downscaling over South Africa. *International Journal of Climatology* **26**: 1315–1337.

Van der Heyden F, Lewis OAM. **1989**. Seasonal variation in photosynthetic capacity with respect to plant water status of five species of the mediterranean climate region of South Africa. *South African Journal of Botany* **55**: 509–515.

Van der Heyden F, Lewis OAM. **1990**. Environmental control of photosynthetic gas exchange characteristics of fynbos species representing three growth forms. *South African Journal of Botany* **56**: 654–658.

Higgins KB, Lamb AJ, van Wilgen BW. **1987**. Root systems of selected plant species in mesic mountain fynbos in the Jonkershoek Valley, south-western Cape Province. *South African Journal of Botany* **3**: 249–257.

Hijmans RJ, Graham CH. **2006**. The ability of climate envelope models to predict the effect of climate change on species distributions. *Global Change Biology* **12**: 2272–2281.

Hoffman MT, Carrick PJ, Gillson L, West AG. **2009**. Drought, climate change and vegetation response in the succulent karoo, South Africa. *South African Journal of Science* **105**: 54–60.

Jackson RB, Sperry JS, Dawson TE. **2000**. Root water uptake and transport: using physiological predictions. *Trends in Plant Science* **5**: 482–488.

Jacobsen AL, Agenbag L, Esler KJ, Pratt RB, Ewers FW, David SD. **2007**. Xylem density, biomechanics and anatomical traits correlate with water stress in 17 evergreen shrub species of the Mediterranean-type climate region of South Africa. *Journal of Ecology* **95**: 171–183.

Jacobsen AL, Esler KJ, Pratt RB, Ewers FW. **2009**. Water stress tolerance of shrubs in Mediterranean-type climate regions: Convergence of fynbos and succulent karoo communities with California shrub communities. *American Journal of Botany* **96**: 1445–53.

Jarvis PG. **1976**. The interpretation of the variations in leaf water potential and stomatal conductance found in canopies in the field. *Philosophical transactions of the Royal Society of London* **273**: 593–610.

Johnson DM, McCulloh KA, Meinzer FC, Woodruff DR, Eissenstat DM. **2011**. Hydraulic patterns and safety margins, from stem to stomata, in three eastern U.S. tree species. *Tree Physiology* **31**: 659–668.

Jones HG, Sutherland RA. **1991**. Stomatal control of xylem embolism. *Plant, Cell & Environment* **14**: 607–612.

Körner C. **2003**. Carbon limitation in trees. *Ecology* **91**: 4–17.

Kume T, Onozawa Y, Komatsu H, Tsuruta K, Shinohara Y, Umebayashi T, Otsuki K. **2010**. Stand-scale transpiration estimates in a Moso bamboo forest: (I) Applicability of sap flux measurements. *Forest Ecology and Management* **260**: 1287–1294.

Lambers H, Chapin III FS, Pons TL. **2008**. *Plant Physiological Ecology*. New York, N.Y.: Springer.

Linder HP. **2003**. The radiation of the Cape flora, southern Africa. *Biological Reviews of the Cambridge Philosophical Society* **78**: 597–638.

Lumsden TG, Schulze RE, Hewitson BC. **2009**. Evaluation of potential changes in hydrologically relevant statistics of rainfall in Southern Africa under conditions of climate change. *Water SA* **35**: 649–656.

Madurapperuma WS, Bleby TM, Burgess SSO. **2009**. Evaluation of sap flow methods to determine water use by cultivated palms. *Environmental and Experimental Botany* **66**: 372–380.

Maherali H, Moura CF, Caldeira MC, Willson CJ, Jackson RB. **2006**. Functional coordination between leaf gas exchange and vulnerability to xylem cavitation in temperate forest trees. *Plant, Cell & Environment* **29**: 571–583.

Maherali H, Pockman WT, Jackson RB. **2004**. Adaptive variation in the vulnerability of woody plants to xylem cavitation. *Ecology* **85**: 2184–2199.

Marloth R. **1903**. Results of experiments on Table Mountain for ascertaining the amount of moisture deposited from the south east clouds. *Transactions of the South African Philosophical Society* **14**: 403–408.

Marloth R. **1905**. Results of further experiments on Table Mountain for ascertaining the amount of precipitation deposited from southeast clouds. *Transactions of the South African Philosophical Society* **16**: 97–105.

Marshall DC. **1958**. Measurement of sap flow in conifers by heat transport. *Plant Physiology* **33**: 385–396.

McDonald PG, Fonseca CR, Overton JM, Westoby M. **2003**. Leaf-size divergence along rainfall and soil-nutrient gradients: is the method of size reduction common among clades? *Functional Ecology* **17**: 50–57.

McDowell NG. **2011**. Mechanisms linking drought, hydraulics, carbon metabolism, and vegetation mortality. *Plant Physiology* **155**: 1051–1059.

McDowell NG, Beerling DJ, Breshears DD, Fisher RA, Raffa KF, Stitt M. **2011**. The interdependence of mechanisms underlying climate-driven vegetation mortality. *Trends in Ecology & Evolution* **26**: 523–532.

McDowell NG, Fisher RA, Xu C, Domec J-C, Holtta T, Mackay DS, Sperry JS, Boutz A, Dickman L, Gehres N, *et al.* 2013. Tansley review. Evaluating theories of drought-induced vegetation mortality using a multimodel – experiment framework. *New Phytologist* **200**: 304–321.

McDowell NG, Pockman WT, Allen CD, Breshears DD, Cobb NS, Kolb T, Plaut J, Sperry JS, West AG, Williams DG, *et al.* 2008. Mechanisms of plant survival and mortality during drought: why do some plants survive while others succumb to drought? *New Phytologist* **178**: 719–739.

McDowell NG, Sevanto S. **2010**. The mechanisms of carbon starvation: how, when, or does it even occur at all? *New Phytologist* **186**: 267–270.

McGill BJ, Enquist BJ, Weiher E, Westoby M. **2006**. Rebuilding community ecology from functional traits. *Trends in Ecology & Evolution* **21**: 178–85.

Meinzer FC, Johnson DM, Lachenbruch B, McCulloh KA, Woodruff DR. **2009**. Xylem hydraulic safety margins in woody plants: coordination of stomatal control of xylem tension with hydraulic capacitance. *Functional Ecology* **23**: 922–930.

Meinzer FC, Mcculloh KA. **2013**. Xylem recovery from drought-induced embolism: where is the hydraulic point of no return? *Tree Physiology* **33**: 331–334.

Melcher PJ, Goldstein G, Meinzer FC, Yount DE, Jones TJ, Holbrook NM, Huang CX. **2001**. Water relations of coastal and estuarine *Rhizophora mangle*: xylem pressure potential and dynamics of embolism formation and repair. *Oecologia* **126**: 182–192.

Midgley GF, Hannah L, Millar D, Rutherford MC, Powrie LW. **2002**. Assessing the vulnerability of species richness to anthropogenic climate change in a biodiversity hotspot. *Global Ecology and Biogeography* **11**: 445–451.

Midgley G, Hughes G, Thuiller W, Drew G, Foden W. **2005**. *Assessment of potential climate change impacts on Namibia's floristic diversity, ecosystem structure and function*. Cape Town.

Midgley GF, Hughes GO, Thuiller W, Rebelo AG. **2006**. Migration rate limitations on climate change-induced range shifts in Cape Proteaceae. *Diversity and Distributions* **12**: 555–562.

Midgley GF, Thuiller W. **2010**. Potential responses of terrestrial biodiversity in Southern Africa to anthropogenic climate change. *Regional Environmental Change* **11**: 127–135.

Miller PC, Miller JM, Miller PM. **1983**. Seasonal progression of plant water relations in fynbos in the western Cape Province, South Africa. *Oecologia* **56**: 392–396.

Milton SJ, Dean WRJ, Marincowitz CP, Kerley GIH. **1995**. Effects of the 1990/91 drought on rangeland in the Steytlerville Karoo. *South African Journal of Science* **91**: 74:84.

Mitchell PJ, O'Grady AP, Tissue DT, White DA, Ottenschlaeger ML, Pinkard EA. **2012**. Drought response strategies define the relative contributions of hydraulic dysfunction and carbohydrate depletion during tree mortality. *New Phytologist* **197**: 862–872.

Mitchell PJ, O'Grady AP, Tissue DT, Worledge D, Pinkard EA. **2014**. Co-ordination of growth, gas exchange and hydraulics define the carbon safety margin in tree species with contrasting drought strategies. *Tree Physiology* **34**: 443–458.

Mitchell PJ, Veneklaas EJ, Lambers H, Burgess SSO. **2008**. Leaf water relations during summer water deficit: differential responses in turgor maintenance and variation in leaf structure among different plant communities in south-western Australia. *Plant, Cell & Environment* **31**: 1791–802.

Monteith JL. **1995**. A reinterpretation of stomatal responses to humidity. *Plant, Cell & Environment* **18**: 357–364.

Nagel JF. **1956**. Fog precipitation on Table Mountain. *Quarterly Journal of the Royal Meteorological Society* **82**: 452–460.

Nardini A, Lo Gullo M a., Trifilò P, Salleo S. **2014**. The challenge of the Mediterranean climate to plant hydraulics: Responses and adaptations. *Environmental and Experimental Botany* **103**: 68–79.

Oren R, Sperry JS, Katul GG, Pataki DE, Ewers BE, Phillips N, Schafer KVR. **1999**. Survey and synthesis of intra- and interspecific variation in stomatal sensitivity to vapour pressure deficit. *Plant, Cell & Environment* **22**: 1515–1526.

Pammenter NW, Vander Willigen C. **1998**. A mathematical and statistical analysis of the curves illustrating vulnerability of xylem to cavitation. *Tree Physiology* **18**: 589–593.

Pearson RG, Dawson TP. **2003**. Predicting the impacts of climate change on the distribution of species: are bioclimate envelope models useful? *Global Ecology and Biogeography* **12**: 361–371.

Pivovaroff AL, Sack L, Santiago LS. **2014**. Coordination of stem and leaf hydraulic conductance in southern California shrubs: a test of the hydraulic segmentation hypothesis. *New Phytologist* **203**: 842–850.

Plaut JA, Yepez EA, Hill J, Pangle R, Sperry JS, Pockman WT, McDowell NG. **2012**. Hydraulic limits preceding mortality in a piñon-juniper woodland under experimental drought. *Plant, Cell & Environment* **35**: 1601–1617.

Poot P, Veneklaas EJ. **2012**. Species distribution and crown decline are associated with contrasting water relations in four common sympatric eucalypt species in southwestern Australia. *Plant and Soil* **364**: 409–423.

Pratt RB, Jacobsen AL, Ewers FW, Davis SD. **2007**. Relationships among xylem transport, biomechanics and storage in stems and roots of nine Rhamnaceae species of the California chaparral. *New Phytologist* **174**: 787–98.

Pratt RB, Jacobsen AL, Jacobs SM, Esler KJ. **2012**. Xylem transport safety and efficiency differ among Fynbos shrub life history types and between two sites differing in mean rainfall. *International Journal of Plant Sciences* **173**: 474–483.

Quinn GP, Keough MJ. **2002**. *Experimental design and data analysis for biologists*. New York, N.Y.: Cambridge University Press.

R Development Core Team. **2013**. R: A language and environment for statistical computing.

Reich PB. **2014**. The world-wide "fast-slow" plant economics spectrum: a traits manifesto (H Cornelissen, Ed.). *Journal of Ecology* **102**: 275–301.

Rockwell FE, Wheeler JK, Holbrook NM. **2014**. Cavitation and its discontents. *Plant Physiology*.

Roddy A, Dawson TE. **2012**. Determining the water flow dynamics during flowering using miniature sap flow sensors. *Acta Horticulturae* **951**: 47–53.

Sala A. **2009**. Lack of direct evidence for the carbon-starvation hypothesis to explain drought-induced mortality in trees. *Proceedings of the National Academy of Sciences of the United States of America* **106**: E68.

Sala A, Hoch G. **2009**. Height-related growth declines in ponderosa pine are not due to carbon limitation. *Plant, Cell & Environment* **32**: 22–30.

Sala A, Piper F, Hoch G. **2010**. Physiological mechanisms of drought-induced tree mortality are far from being resolved. *New Phytologist* **186**: 274–281.

Sala A, Woodruff DR, Meinzer FC. **2012**. Carbon dynamics in trees: feast or famine? *Tree Physiology* **32**: 764–775.

Salleo S, Lo Gullo MA, Trifilo P, Nardini A. **2004**. New evidence for a role of vessel-associated cells and phloem in the rapid xylem refilling of cavitated stems of *Laurus nobilis* L. *Plant, Cell & Environment* **27**: 1065–1076.

Scheiter S, Higgins SI. **2009**. Impacts of climate change on the vegetation of Africa: an adaptive dynamic vegetation modelling approach. *Global Change Biology* **15**: 2224–2246.

Scoffoni C, McKown AD, Rawls M, Sack L. **2012**. Dynamics of leaf hydraulic conductance with water status: quantification and analysis of species differences under steady state. *Journal of Experimental Botany* **63**: 643–58.

Sevanto S, McDowell NG, Dickman LT, Pangle R, Pockman WT. **2013**. How do trees die? A test of the hydraulic failure and carbon starvation hypotheses. *Plant, Cell & Environment* **37**: 153–161.

Silvertown J, Araya YN, Linder HP, Gowing DJ. **2012**. Experimental investigation of the origin of fynbos plant community structure after fire. *Annals of Botany* **110**: 1377–1383.

Silvertown J, Dodd ME, Gowing DJG, Mountford JO. **1999**. Hydrologically defined niches reveal a basis for species richness in plant communities. *Nature* **400**: 61–63.

Skelton RP, Midgley JJ, Nyaga JM, Johnson SD, Cramer MD. **2012**. Is leaf pubescence of Cape Proteaceae a xeromorphic or radiation-protective trait? *Australian Journal of Botany* **60**: 104–113.

Skelton RP, West AG, Dawson TE, Leonard JM. **2013**. External heat-pulse method allows comparative sapflow measurements in diverse functional types in a Mediterranean-type shrubland in South Africa. *Functional Plant Biology* **40**: 1076–1087.

Sparks JP, Black RA. **1999**. Regulation of water loss in populations of *Populus trichocarpa*: the role of stomatal control in preventing xylem cavitation. *Tree Physiology* **19**: 453–459.

Specht RL, Moll EJ. **1983**. Mediterranean-type heathlands and sclerophyllous shrublands of the world: An overview. In: Kruger F, Mitchell D, Jarvis JM, eds. Ecological Studies. Mediterranean-Type Ecosystems. Springer Berlin Heidelberg, 41–65.

Sperry JS. **2000**. Hydraulic constraints on plant gas exchange. *Agricultural and Forest Meteorology* **104**: 13–23.

Sperry J. **2013**. Cutting-edge research or cutting-edge artefact? An overdue control experiment complicates the xylem refilling story. *Plant, Cell & Environment* **11**: 1916–1918.

Sperry JS, Adler FR, Campbell GS, Comstock JP. **1998**. Limitation of plant water use by rhizosphere and xylem conductance: results from a model. *Plant, Cell & Environment* **21**: 347–359.

Sperry JS, Christman MA, Torres-Ruiz JM, Taneda H, Smith DD. **2012**. Vulnerability curves by centrifugation: is there an open vessel artefact, and are "r" shaped curves necessarily invalid? *Plant, Cell & Environment* **35**: 601–610.

Sperry JS, Hacke UG, Oren R, Comstock JP. **2002**. Water deficits and hydraulic limits to leaf water supply. *Plant, Cell & Environment* **25**: 251–263.

Sperry JS, Ikeda T. **1997**. Xylem cavitation in roots and stems of Douglas-fir and white fir. *Tree Physiology* **17**: 275–280.

Sperry JS, Pockman WT. **1993**. The effect of reduced hydraulic conductance on stomatal conductance and xylem cavitation. *Journal of Experimental Botany* **44**: 1075–1082.

Sperry JS, Saliendra NZ. **1994**. Intra- and inter-plant variation in xyiem cavitation in *Betula occidentalis*. *Plant, Cell & Environment* **17**: 1233–1241.

Sperry JS, Stiller V, Hacke UG. **2003**. Xylem hydraulics and the soil-plant-atmosphere continuum: opportunities and unresolved issues. *Agronomy Journal* **95**: 1362–1370.

Stiller V, Sperry JS, Lafitte R. **2005**. Embolized conduits of rice (*Oryza sativa*, Poaceae) refill despite negative xylem pressure. *American Journal of Botany* **92**: 1970–1974.

Tardieu F, Simonneau T. **1998**. Variability among species of stomatal control under fluctuating soil water status and evaporative demand: modelling isohydric and anisohydric behaviours. *Journal of Experimental Botany* **49**: 419–432.

Thomas CD, Cameron A, Green RE, Bakkenes M, Beaumont LJ, Collingham YC, Erasmus BFN, de Siqueira MF, Grainger A, Hannah L, *et al.* 2004. Extinction risk from climate change. *Nature* **427**: 145–148.

Thuiller W, Albert C, Araújo MB, Berry PM, Cabeza M, Guisan A, Hickler T, Midgley GF, Paterson J, Schurr FM, *et al.* 2008. Predicting global change impacts on plant species' distributions: Future challenges. *Perspectives in Plant Ecology, Evolution and Systematics* **9**: 137–152.

Thuiller W, Midgley GF, Rouget M, Cowling RM. **2006**. Predicting patterns of plant species richness in megadiverse South Africa. *Ecography* **29**: 733–744.

Tyree MT, Cochard H, Cruiziat P, Sinclair B, Ameglio T. **1993**. Drought-induced leaf shedding in walnut: evidence for vulnerability segmentation. *Plant, Cell & Environment* **16**: 879–882.

Tyree MT, Ewers FW. **1991**. Tansley review no. 34. The hydraulic architecture of trees and other woody plants. *New Phytologist* **119**: 345–360.

Tyree MT, Sperry JS. **1988**. Do woody plants operate near the point of catastrophic xylem dysfunction caused by dynamic water stress? Answers from a model. *Plant Physiology* **88**: 574–580.

Tyree MT, Sperry JS. **1989**. Vulnerability of xylem to cavitation and embolism. *Annual Reviews of Plant Physiology and Plant Molecular Biology* **40**: 19–38.

Urli M, Porté AJ, Cochard H, Guengant Y, Burlett R, Delzon S. **2013**. Xylem embolism threshold for catastrophic hydraulic failure in angiosperm trees. *Tree Physiology* **33**: 672–683.

Vandegehuchte MW, Steppe K. **2012a**. A triple-probe heat-pulse method for measurement of thermal diffusivity in trees. *Agricultural and Forest Meteorology* **160**: 90–99.

Vandegehuchte MW, Steppe K. **2012b**. Sapflow+: a four-needle heat-pulse sap flow sensor enabling nonempirical sap flux density and water content measurements. *New Phytologist* **196**: 306–317.

Vilagrosa A, Hernández EI, Luis VC, Cochard H, Pausas JG. **2014**. Physiological differences explain the co-existence of different regeneration strategies in Mediterranean ecosystems. *New Phytologist* **201**: 1277:1288.

Wang Q, Fleisher DH, Timlin D, Reddy VR, Chun JA. **2012**. Quantifying the measurement errors in a portable open gas-exchange system and their effects on the parameterization of Farquhar *et al*. model for C_3 leaves. *Photosynthetica* **50**: 223–238.

Van der Werf A, Poorter H, Lambers H. **1994**. Respiration as dependent on a species' inherent growth rate and on the nitrogen supply to the plant. In: Roy J, Garnier E, eds. A whole-plant perspective of carbon-nitrogen interactions. The Hague: SPB Academic Publishing, 61–77.

West AG, Dawson TE, February EC, Midgley GF, Bond WJ, Aston TL. **2012**. Diverse functional responses to drought in a Mediterranean-type shrubland in South Africa. *New Phytologist* **195**: 396–407.

West AG, Hultine KR, Burtch KG, Ehleringer JR. **2007a**. Seasonal variations in moisture use in a piñon-juniper woodland. *Oecologia* **153**: 787–798.

West AG, Hultine KR, Jackson TL, Ehleringer JR. **2007b**. Differential summer water use by *Pinus edulis* and *Juniperus osteosperma* reflects contrasting hydraulic characteristics. *Tree Physiology* **27**: 1711–1720.

West AG, Hultine KR, Sperry JS, Bush SE, Ehleringer JR. **2008**. Transpiration and hydraulic strategies in a piñon-juniper woodland. *Ecological Applications* **18**: 911–927.

West AG, Patrickson SJ, Ehleringer JR. **2006**. Water extraction times for plant and soil materials used in stable isotope analysis. *Rapid communications in mass spectrometry* **20**: 1317–1321.

Wheeler JK. **2014**. Water transport, embolism recovery and water storage in trees. *PhD Thesis*: 130.

Wheeler JK, Huggett BA, Tofte AN, Rockwell FE, Holbrook NM. **2013**. Cutting xylem under tension or supersaturated with gas can generate PLC and the appearance of rapid recovery from embolism. *Plant, Cell & Environment* **36**: 1938–1949.

Von Willert DJ, Herppich M, Miller JM. **1989**. Photosynthetic characteristics and leaf water relations of mountain fynbos vegetation in the Cedarberg area (South Africa). *South African Journal of Botany* **55**: 288–298.

De Wit MJ, Stankiewicz J. **2006**. Changes in surface water supply across Africa with predicted climate change. *Science* **311**: 1917–1921.

Wong SC, Cowan IR, Farquhar GD. **1979**. Stomatal conductance correlates with photosynthetic capacity. *Nature* **282**: 424–426.

Wullschleger SD, Meinzer FC, Vertessy RA. **1998**. A review of whole-plant water use studies in trees. *Tree Physiology* **18**: 499–512.

Yates CJ, Elith J, Latimer AM, Le Maitre D, Midgley GF, Schurr FM, West AG. **2010a**. Projecting climate change impacts on species distributions in megadiverse South African Cape and Southwest Australian Floristic Regions: Opportunities and challenges. *Austral Ecology* **35**: 374–391.

Yates M, Verboom GA, Rebelo AG, Cramer MD. **2010b**. Ecophysiological significance of leaf size variation in Proteaceae from the Cape Floristic Region. *Functional Ecology* **24**: 485–492.

Zeppel MJB, Anderegg WRL, Adams HD. **2013**. Forest mortality due to drought: latest insights, evidence and unresolved questions on physiological pathways and consequences of tree death. *New Phytologist* **197**: 372–374.

Zeppel MJB, Macinnis-Ng C, Palmer A, Taylor D, Whitley R, Fuentes S, Yunusa I, Williams M, Eamus D. **2008**. An analysis of the sensitivity of sap flux to soil and plant variables assessed for an Australian woodland using a soil–plant–atmosphere model. *Functional Plant Biology* **35**: 509–520.

Zimmermann MH. **1983**. *Xylem structure and the ascent of sap*. Berlin: Springer-Verlag.